Spatially coherent oscillations in neural fields with inhibition and adaptation. I. One-dimensional domains

Stefanos E. Folias *

Department of Mathematics & Statistics, University of Alaska Anchorage, Anchorage, Alaska 99508, USA

(Received 13 October 2024; revised 18 September 2025; accepted 11 November 2025; published 8 January 2026)

We study Hopf bifurcation of stationary activity bumps to localized, spatially coherent oscillations in a family of elementary neural field models involving nonlocal synaptic excitation and inhibition with Heaviside firing rate nonlinearity and local linear adaption, both with and without a localized input inhomogeneity, on the one-dimensional spatial domain $(-\infty, \infty)$, including cases of interacting pairs of neural fields. (We treat the same neural fields on two-dimensional spatial domain $\mathbb{R}^2$ separately.) A main focus is to categorize how the underlying symmetries of the nonlinear operators in this family of equations give rise to a related set of spatially coherent time-periodic solutions that bifurcate via Hopf bifurcation with respect to different spatial eigenmodes, each with different spatial structures being selected as a result of the relative balance of synaptic inhibition to excitation. A general framework is constructed to analyze stationary bump solutions in a neural field model containing N neural fields with M linear gating variables that modulate different neural fields. Under a basic set of symmetry assumptions on the synaptic weight functions and the input homogeneity, we show that all such neural fields have two broad classes of eigenmodes with either even or odd spatial symmetry. When these eigenmodes destabilize via Hopf bifurcation, it leads to various types of spatially coherent, time-periodic oscillations that can take the form of breathing bumps or *breathers* that expand and contract and sloshing bumps or *sloshers* which move side-to-side. Analytical treatments combined with numerical simulations provide a more complete picture of the emergence of these periodic activity patterns and novel secondary bifurcations are found to occur, including torus, period-doubled, and Rossler band-like dynamics. Interacting pairs of neural fields that support bumps, breathers, and sloshers can lead to novel spatially coherent oscillations with different patterns of synchrony and spatial positioning depending on the type of synaptic interactions between the neural fields including novel in-phase and antiphase breathers and sloshers. A novel transition from a slosher to a spatially localized, traveling periodic wave is also found. The approach is extended to the case of multibump solutions and bifurcations leading to various multibump breathers and sloshers are observed.

DOI: 10.1103/zd32-vxww

I. INTRODUCTION

Neural field equations are nonlocal partial integrodifferential equations that describe the average activity in large populations of neurons on spatial domains, or domains in feature space, and are capable of a diverse range of spatiotemporal behavior on one-dimensional domains, including stationary, traveling, and oscillatory localized bump solutions [1–52]. Inherent in the improvement of modeling equations for physical phenomena, such as activity in the brain [53–69], is a deeper understanding of the basic underlying spatiotemporal dynamics supported by these neural field equations and its relationship to model parameters. We investigate the response in the activity of various networks of neuronal populations that support stationary localized bump and breather solutions, both in the presence of a sustained, localized input inhomogeneity and in the input-free case. The localized input inhomogeneity could represent a diverse set of phenomena, including a sensory input to the layer, input from another brain region to the layer, a locally depolarized or hyperpolarized region within the layer, an external input due to an electrode or other device, etc. We are interested in sustained responses of activity and whether they will be modulated by an oscillation.

The objective of this paper is threefold. First, it compares results for linear stability and Hopf bifurcation of stationary bumps across a family of elementary neural fields and the dependence on network parameters. Second, it classifies the spatial structure of the eigenmodes and demonstrates its relation to the spatiotemporal structure of the time-periodic solutions emerging in the Hopf bifurcation and model parameters. Third, in a large class of neural fields obeying symmetry assumptions on the synaptic weight functions and inputs, it shows that the linearization about an even-symmetric stationary bump yields two broad classes of eigenfunctions with even or odd symmetry. Bifurcations with respect to these different eigenmodes thereby lead to two different classes of spatially localized, time-periodic oscillations termed *breathers* and *sloshers* as they exhibit either *expanding-and-contracting* or *side-to-side* motions. The analysis is extended to the case of N neural fields with M gating variables, including multibump solutions.

The family of elementary neural fields incorporates different forms of the fundamental types of excitatory and inhibitory synaptic inputs as well as an adaptation gating

*Contact author: sfolias@alaska.edu

variable or negative feedback mechanism, which can model the process of spike-rate adaptation observed in neurons in cortex that decrease their firing rates after sustained firing. Adaptation serves as a concrete case for incorporating gating variables in the stability analysis for the generalization to more varied neural fields. It also compares two different dynamic mechanisms, nonlocal synaptic interactions and local negative feedback, that are capable of producing Hopf bifurcations of bumps. Interacting neural fields may represent interacting populations of neurons nearby or across in a layer, between different layers, between different brain regions, etc.

We demonstrate a variety of novel types of activity patterns, including bifurcations to multibump breathers as well as single bump breathers with variable activity arising from secondary bifurcations either to dynamics on a torus, period doubling with mixed breathing and sloshing behavior, or a period-doubling cascade leading to Rossler-like dynamics. We show a novel transition from a stationary bump or multibump to a spatially localized traveling periodic wave pinned to the input as a parameter is varied. Evidence of a Hopf-Hopf nonlinear mode interaction was sought, without success, between the breather and slosher eigenmodes in the presence of an input homogeneity as the analog to the drift-Hopf bifurcation found in the input-free case [51].

The paper is organized as follows. In Sec. II we outline a family of elementary neural fields depicted in Fig. 1 and studied herein. In Sec. III we construct a general vectorized neural field model to analyze any configuration of N interacting neural fields with M gating variables and proceed to establish existence and stability conditions for the coupled neural fields in the general case, including construction of the eigenfunctions. In Sec. IV we analyze the $(N \times M)$ vectorized system in the special case that the synaptic weight functions and the input inhomogeneity are even-symmetric about the same common center and show the eigenfunctions of the linearization about a stationary bump fall in to two broad classes of either even or odd spatial symmetry about the common center. In Sec. V we analyze the family of elementary neural fields, outline the existence and stability results for stationary bumps, obtain conditions for which different spatial eigenmodes destabilize in a Hopf bifurcation, and discuss the relationship to the spatiotemporal structure of the emergent time-periodic solution. In Sec. VI we extend the analysis to the case of multibump solutions and their Hopf bifurcation to oscillatory multibumps.

II. ELEMENTARY NEURAL FIELD MODELS

The neural field models studied in this paper are models that involve different network topologies containing the two fundamental types of excitatory and inhibitory synaptic inputs generated either by separate populations of neurons or an effective mix in a single population of neurons. We also incorporate a local linear negative feedback mechanism in the form of an adaptation gating variable that models spike rate adaptation as a concrete example. The synaptic connectivity assumed in the analysis is based on short range connections found in regions of the cortex but can be generalized to other types of connectivity. Each neural field is capable of supporting stationary bumps that undergo Hopf bifurcation to time-oscillatory solutions. These fundamental building blocks can be used to build more complex neural field models.

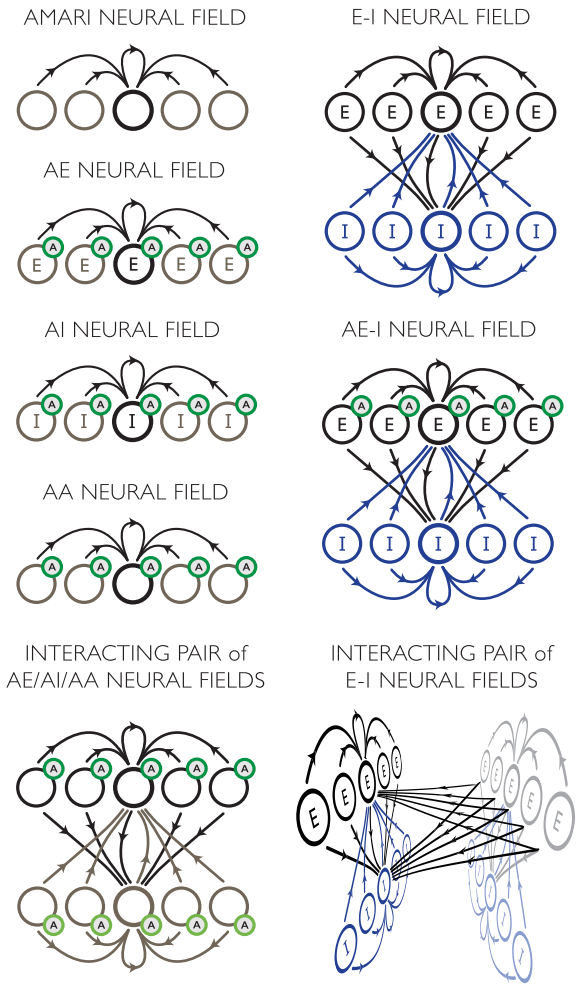

FIG. 1. Synaptic connectivity patterns for the neural fields studied in this paper. AE neural field represents a population of excitatory neurons whose activity is modulated by an adaptation variable. Similarly, AI and AA represent an inhibitory population and Amari neural field modulated by adaptation. The Amari neural field is an effective mix of excitation and inhibition in a single population using a Mexican hat weight function. The E-I neural field is a two-population neural field with distinct populations of excitatory and inhibitory neurons. The AE-I neural field is an E-I neural field where the E population is modulated by an adaptation variable. Interacting pairs of neural fields are formed from these fundamental neural fields. In the interacting pair of E-I neural fields, the interlayer connections are symmetric though only one set is shown. Interlayer connections project from the E population only to model long-range excitatory connections in cortex.

We define the symbol $w * f[u]$ for a nonlinear spatial convolution of a solution $u(x,t)$ over $(-\infty,\infty)$, where

$$(w_{jk} * f[u])(x) = \int_{\mathbb{R}} w_{jk}(\|x-y\|) f(u(y,t)) dy \qquad (1)$$

represents the total synaptic input *from* the neurons in population k *to* the neurons in population j where $w_{jk}(x)$ is the synaptic weight function. The firing rate nonlinearity

$f(u)$, generally sigmoidal in form, is taken to be a Heaviside function $f[u] = H(u - \theta)$ with threshold θ, as introduced by Amari [2] for analytic tractability. $I(x)$ is a stationary, localized (Gaussian-like) input homogeneity.

A. Amari neural field

$$\frac{\partial u}{\partial t} + u = w * f[u] + I(x). \tag{2}$$

The simplest neural field supporting a stationary bump is the *Amari neural field* representing a single neuronal population in which the net synaptic input can be net excitatory or inhibitory, typically in the shape of a Mexican hat (locally excitatory, laterally inhibitory) [2]. Stationary bumps occur for other classes of synaptic weight function w in this model, including a case with midrange excitation and both local and long-range inhibition [19]. Though the Amari neural field is not discussed here, we note that Hopf bifurcation of stationary bumps do occur in the case of synaptic delays as analyzed in Ref. [45].

B. AE, AI, or AA neural field

$$\begin{aligned} \frac{\partial u}{\partial t} + u &= w * f[u] - \beta n + I(x), \\ \frac{1}{\alpha}\frac{\partial n}{\partial t} + n &= u. \end{aligned} \tag{3}$$

We take $f[u] = H(u - \theta)$, and θ is a constant threshold. The AE *neural field* represents a layer of coupled excitatory (E) neurons ($u = u_e$) with positive coupling strength ($w(x) > 0$) subject to linear adaptation (A) in the form of the local negative feedback term $-\beta n$, where n is a gating-like variable governed by linear dynamics introduced by Pinto & Ermentrout [6,10]. The AI *neural field* is a layer of coupled inhibitory (I) neurons ($u = u_i$) with negative synaptic coupling strength ($w(x) < 0$). Other choices of $w(x)$ lead to different neural field models. If $w(x)$ is a Mexican hat weight function (locally excitatory, laterally inhibitory), this represents the Amari neural field with a layer of neurons ($u = u$) whose firing rate is modulated by a gating variable, which we denote as the AA *neural field* for *adapting Amari* neural field.

C. E-I neural field

$$\begin{aligned} \frac{\partial u_e}{\partial t} + u_e &= w_{ee} * f_e[u_e] - w_{ei} * f_i[u_i] + I_e(x), \\ \tau\frac{\partial u_i}{\partial t} + u_i &= w_{ie} * f_e[u_e] - w_{ii} * f_i[u_i] + I_i(x), \end{aligned} \tag{4}$$

where we take $f_e[u] = H(u - \theta_e)$, $f_i[u] = H(u - \theta_i)$, and θ_e and θ_i are constant thresholds. The E-I *neural field* is a variation on the original Wilson-Cowan neural field [1]. We consider the formulation with all Heaviside nonlinearities introduced in Ref. [24]. An alternative formulation was considered in Ref. [11]. The synaptic weight functions w_{jk} are purely positive and the excitatory or inhibitory synaptic currents are determined by the sign in the equations. Note that, under certain assumptions, an E-I neural field can be directly reduced to the Amari neural field [11].

D. AE-I neural field

$$\begin{aligned} \frac{\partial u_e}{\partial t} + u_e &= w_{ee} * f_e[u_e] - w_{ei} * f_i[u_i] - \beta n_e + I_e, \\ \tau\frac{\partial u_i}{\partial t} + u_i &= w_{ie} * f_e[u_e] - w_{ii} * f_i[u_i] + I_i, \\ \frac{1}{\alpha}\frac{\partial n_e}{\partial t} + n_e &= u_e, \end{aligned} \tag{5}$$

where we take $f_e[u] = H(u - \theta_e)$, $f_i[u] = H(u - \theta_i)$, and θ_e and θ_i are constant thresholds. The AE-I *neural field* is the natural combination of two population E-I neural field where the E-population is additionally subject to linear adaptation (A) introduced in Refs. [31,32]. This model could reflect, for example, spike-rate adaptation observed in excitatory neurons coupled to inhibitory interneurons in neocortex.

E. Interacting pair of AE/AI/AA neural fields

An interacting pair of Amari neural fields with symmetric local and symmetric or asymmetric interlayer connections was introduced and analyzed in Refs. [40,41]. Here we introduce two forms of interacting pairs of AA/AE/AI neural fields with the addition of adaptation variables n_1 and n_2: (*i*) a *symmetric case* where the two neural fields are identical in synaptic weight functions, inputs, and parameters, but are allowed to evolve independently and (*ii*) an *asymmetric case* where the temporal dynamics are identical but all synaptic weight functions, nonlinear thresholds, and inputs are allowed to differ.

Case I: Symmetric case

$$\begin{aligned} \frac{\partial u_1}{\partial t} + u_1 &= w_{\rm loc} * f[u_1] + w_{\rm lay} * f[u_2] - \beta n_1 + I(x), \\ \frac{\partial u_2}{\partial t} + u_2 &= w_{\rm loc} * f[u_2] + w_{\rm lay} * f[u_1] - \beta n_2 + I(x), \\ \frac{1}{\alpha}\frac{\partial n_1}{\partial t} + n_1 &= u_1, \\ \frac{1}{\alpha}\frac{\partial n_2}{\partial t} + n_2 &= u_2, \end{aligned} \tag{6}$$

where in our treatment $f[u] = H(u - \theta)$ and θ is a constant threshold. The synaptic weight function $w_{\rm loc}$ represents the local connection within each population, whereas $w_{\rm lay}$ represents the interlayer synaptic connections from one population to the other. In this case, both weight functions are identical for each population.

Case II: Asymmetric case

$$\begin{aligned}
\frac{\partial u_1}{\partial t} + u_1 &= w_{11}^{\text{loc}} * f_1[u_1] + w_{12}^{\text{lay}} * f_2[u_2] - \beta n_1 + I_1,\\
\frac{\partial u_2}{\partial t} + u_2 &= w_{22}^{\text{loc}} * f_2[u_2] + w_{21}^{\text{lay}} * f_1[u_1] - \beta n_2 + I_2,\\
\frac{1}{\alpha}\frac{\partial n_1}{\partial t} + n_1 &= u_1,\\
\frac{1}{\alpha}\frac{\partial n_2}{\partial t} + n_2 &= u_2,
\end{aligned} \tag{7}$$

where we take $f_1[u] = H(u - \theta_1)$ and $f_2[u] = H(u - \theta_2)$, and θ_1 and θ_2 are constant thresholds. In this case both the local and interlayer synaptic weight functions are allowed to be different. We still assume the weight functions themselves are even-symmetric and translation-invariant, though asymmetric synaptic weight functions have been investigated in the AE neural field [30]. Note that the case of differing α_1, α_2 and β_1, β_2 may also be treated but the stability analysis is more complicated. Here our focus is more on the asymmetry in the synaptic connections in the two populations rather than differences in the temporal dynamics.

F. Interacting pair of E-I neural fields

$$\begin{aligned}
\frac{\partial u_e}{\partial t} + u_e &= w_{ee}^{\text{loc}} * f_e[u_e] - w_{ei}^{\text{loc}} * f_i[u_i] + w_{ee}^{\text{lay}} * f_e[v_e] + I_e,\\
\tau\frac{\partial u_i}{\partial t} + u_i &= w_{ie}^{\text{loc}} * f_e[u_e] - w_{ii}^{\text{loc}} * f_i[u_i] + w_{ie}^{\text{lay}} * f_e[v_e] + I_i,\\
\frac{\partial v_e}{\partial t} + v_e &= w_{ee}^{\text{loc}} * f_e[v_e] - w_{ei}^{\text{loc}} * f_i[v_i] + w_{ee}^{\text{lay}} * f_e[u_e] + I_e,\\
\tau\frac{\partial v_i}{\partial t} + v_i &= w_{ie}^{\text{loc}} * f_e[v_e] - w_{ii}^{\text{loc}} * f_i[v_i] + w_{ie}^{\text{lay}} * f_e[u_e] + I_i,
\end{aligned} \tag{8}$$

where we take $f_e[u] = H(u - \theta_e)$, $f_i[u] = H(u - \theta_i)$, and θ_e and θ_i are constant thresholds. This neural field was introduced by Folias and Ermentrout in Ref. [41]. For simplicity we assume the two E-I neural fields are identical with symmetric connections. The interlayer connections between the two E-I neural fields are projecting from the E cells only to reflect the excitatory long-range connections in the neocortex. Inhibitory interlayer connections naturally could be introduced but are not considered here.

Of the neural fields listed here, stability and Hopf bifurcation of stationary bumps have been previously be examined by us in the AE/AA neural field in Refs. [18,39], in the E-I neural field in the absence of inputs by Blomquist *et al.* [24] and in the case of input inhomogenieties by us briefly in Ref. [51] and herein, and in the dual E-I neural field in the absence of inputs by us in Ref. [41]. Additionally we cast existence and stability conditions in a systematic notation so that the conditions in different models can be directly compared, and we fully categorize the spatial structure of the eigenmodes to investigate the various emergent solutions resulting from Hopf bifurcation of different eigenmodes.

III. ANALYSIS OF STATIONARY BUMPS

A. Notation

We define notation to move between vector and scalar notation for different steps of the analysis. The notation

$$\mathbf{u} = [u_j]$$

for $j = 1, \ldots, N$ will denote an N-dimensional vector whose jth element is the expression u_j which is a neural field or a gating variable v_j. Subsequently, the notation

$$(\mathbf{u})_j$$

is used to refer to jth element of any defined vector $\mathbf{u}$. The notation

$$\mathbf{M} = [\mathrm{M}_{jk}]$$

for $j = 1, \ldots, M$, $k = 1, \ldots, N$ denotes an $(M \times N)$ matrix with element jk of the matrix given by expression M_{jk}. Similarly,

$$(\mathbf{M})_{jk}$$

refers to element jk of the matrix $\mathbf{M}$.

B. Structure of the neural fields on $(-\infty, \infty)$

We construct a vector formulation for a family of N neural fields with M linear gating variables each coupled only one neural field (each neural field may couple to more than one gating variable). The existence and stability of a stationary bump in this vector formulation is based upon the type of analysis that has appeared in various studies (e.g., see Refs. [2,11,18,24]).

We consider two forms of a general neural field equation for N coupled neuronal populations of the form

$$\frac{\partial \mathbf{u}}{\partial t} = \mathbf{A}\mathbf{u} + \mathbf{W} * \mathbf{H}[\mathbf{u} - \theta] + \mathbf{I}(x), \tag{9}$$

where the vector $\mathbf{u} = [u_j]$ represents a vector of N neural fields $u_1, u_2, \ldots, u_N$ all defined along a universal spatial coordinate x and time t.

We also consider neural field equations with N neural fields with M additional linear auxiliary or gating variables v_j

$$\begin{aligned}
\frac{\partial \mathbf{u}}{\partial t} &= \mathbf{A}\mathbf{u} + \mathbf{B}\mathbf{v} + \mathbf{W} * \mathbf{H}[\mathbf{u} - \theta] + \mathbf{I}(x),\\
\frac{\partial \mathbf{v}}{\partial t} &= \mathbf{C}\mathbf{u} + \mathbf{D}\mathbf{v},
\end{aligned} \tag{10}$$

where $\mathbf{u} = [u_j]$ is a vector of N neural fields $u_1, u_2, \ldots, u_N$ and $\mathbf{v} = [v_k]$ is a vector of M linear gating variables $v_1, \ldots, v_M$ each defined along the universal spatial coordinate x and time t.

Different neural fields u_j are assumed to interact only through nonlinear synaptic interactions and may be coupled to more than one gating variable. Each gating variable is assumed to be coupled to one neural field only and evolve according to linear dynamics. These assumptions imply $\mathbf{A}$ is an $(N \times N)$ *diagonal* matrix, $\mathbf{D}$ is an $(M \times M)$ *diagonal* matrix, $\mathbf{B}$ is an $(N \times M)$ matrix, and $\mathbf{C}$ is an $(M \times N)$ matrix which are assumed to be constant. Both $\mathbf{B}$ and $\mathbf{C}^{\mathrm{T}}$ have one nonzero entry in each column in the same location so nonzero

entry jk of $\mathbf{B}$ aligns with nonzero entry kj in $\mathbf{C}$. This implies $\mathbf{BD}^{-1}\mathbf{C}$ is *diagonal* whenever $\mathbf{D}$ is invertible since its nonzero elements occur when multiplying nonzero element jk of $\mathbf{B}$ with corresponding nonzero element kj of $\mathbf{C}$ which produces element jj on the diagonal, given that $\mathbf{D}^{-1}$ is diagonal. We shall assume $\mathbf{A}$, $\mathbf{D}$, and $(\mathbf{A}-\mathbf{BD}^{-1}\mathbf{C})$ are invertible.

$\mathbf{I}(x)=[I_j(x)]$ represents a localized excitatory input inhomogeneity which, for each neural field u_j, is assumed to be a Gaussian-like and even-symmetric about some point $x_{c,j}$ in the universal coordinate system. A special case we consider is where the input in each population is centered about 0 or a common center x_c. For concreteness we take $I_j(x)=I_\circ^j e^{-(x/\sigma_j)^2}$ or a translate. The case $\mathbf{I}(x)=\mathbf{0}$ represents the associated *input-free* neural field.

The convolution $\mathbf{W}*\mathbf{H}[\mathbf{u}-\theta]$ is defined as

$$\mathbf{W}*\mathbf{H}[\mathbf{u}-\theta] = \int_{\mathbb{R}} \mathbf{W}(x-x')\,\mathbf{H}[\mathbf{u}(x',t)-\theta]\,dx',$$

where the vector function defined by

$$\mathbf{H}[\mathbf{u}-\theta]=\begin{bmatrix} H(u_1-\theta_1)\\ H(u_2-\theta_2)\\ \vdots\\ H(u_N-\theta_N)\end{bmatrix}$$

is a vector of Heaviside firing rate nonlinearities over the N populations u_j with thresholds θ_j (where $\theta=[\theta_j]$).

We define the syanptic kernel matrix $\mathbf{W}(x)$ as the $(N\times N)$ matrix of synaptic weight functions $w_{jk}(x)$ from neuronal populations k to populations j:

$$\mathbf{W}(x)=[w_{jk}(x)]=\begin{bmatrix} w_{11}(x) & \cdots & w_{1N}(x)\\ \vdots & \ddots & \\ w_{N1}(x) & & w_{NN}(x)\end{bmatrix}. \tag{11}$$

The first index j denotes the post-synaptic population that receives the synaptic input, while the second index k denotes the pre-synaptic population that induces the synaptic currents. In Secs. III and IV, we shall assume that the *sign* that determines whether the interaction between population j and k is purely *excitatory* or purely *inhibitory* is contained in the definition of the synaptic weight function w_{jk} itself. In Secs. II and V, purely inhibitory synaptic connections are represented by positive weight functions, premultiplied with a $-$ sign. A *Mexican hat* weight function can be formulated by subtracting two positive weight functions with different parameters to generate a mixture of excitation and inhibition in the following form $w_M(x)=w(x;\bar{w}_e,\sigma_e)-w(x;\bar{w}_i,\sigma_i)$ [2].

C. Existence of a stationary bump

We consider stationary bump solutions of neural field equations (9) and (10). A stationary bump is any such solution where there is at most a single localized interval of activity in the entire domain of each population.

In the case ($\mathbf{v}=\mathbf{0}$) of no gating or auxiliary variables, a stationary solution to the neural field equations for N coupled neuronal populations satisfies the equation

$$\mathbf{0} = \mathbf{Au}+\mathbf{W}*\mathbf{H}[\mathbf{u}-\theta]+\mathbf{I}(x). \tag{12}$$

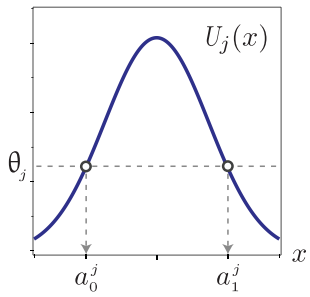

FIG. 2. Stationary bump profile $U_j(x)$ with threshold points $x=a_0^j$ and a_1^j in the jth neural field u_j.

In the case ($\mathbf{v}\neq\mathbf{0}$) where (linear) gating or auxiliary variables are present, a stationary solution satisfies

$$\begin{aligned}\mathbf{0} &= \mathbf{Au}+\mathbf{Bv}+\mathbf{W}*\mathbf{H}[\mathbf{u}-\theta]+\mathbf{I}(x),\\ \mathbf{0} &= \mathbf{Cu}+\mathbf{Dv}.\end{aligned} \tag{13}$$

Provided $\mathbf{D}$ is invertible, the pair of vector equations (13) can be reduced to the same form as Eq. (12) by solving for $\mathbf{v}=-\mathbf{D}^{-1}\mathbf{Cu}$ and defining matrix $\widetilde{\mathbf{A}}=\mathbf{A}-\mathbf{BD}^{-1}\mathbf{C}$ to arrive at

$$\mathbf{0} = \widetilde{\mathbf{A}}\mathbf{u}+\mathbf{W}*\mathbf{H}[\mathbf{u}-\theta]+\mathbf{I}(x). \tag{14}$$

Equation (14) has the same form as Eq. (12). Both $\widetilde{\mathbf{A}}$ in Eq. (14) and $\mathbf{A}$ in Eq. (12) are *diagonal* under our assumptions on the matrices. We express $\widetilde{\mathbf{A}}$ in terms of its diagonal elements $\widetilde{A}_{jj}$ by writing $\widetilde{\mathbf{A}}=\mathsf{diag}(\widetilde{A}_{11},\ldots,\widetilde{A}_{NN})$.

We assume a solution in the form of a localized stationary bump $\mathbf{u}(x,t)=\mathbf{U}(x)=[U_j(x)]$ by requiring the bump profile $U_j(x)$ in each neural field j be superthreshold over a single interval (a_0^j,a_1^j) for each $j=1,\ldots,N$. The intervals need not be centered around the same point (see, for example, the stationary *allotopic* bump in Ref. [41]).

We assume each $U_j(x)$ is bounded on $(-\infty,\infty)$ and satisfies the following threshold conditions (see Fig. 2):

$$\begin{aligned} &U_j(x)>\theta_j, \quad x\in(a_0^j,a_1^j), \qquad a_0^j<a_1^j,\\ &U_j(x)=\theta_j, \quad x=a_0^j,a_1^j,\\ &U_j(x)<\theta_j, \quad \text{otherwise},\\ &U_j(x)\to 0, \quad \text{as } x\to\pm\infty.\end{aligned}$$

The convolution $\mathbf{W}*\mathbf{H}[\mathbf{u}-\theta]$ can be expressed as the vector function $\mathcal{W}(x;\boldsymbol{a}_0,\boldsymbol{a}_1)$ where

$$\mathbf{W}*\mathbf{H}[\mathbf{u}-\theta]=\mathcal{W}=[\mathcal{W}_j],$$

and $\mathcal{W}_j$ is given by

$$\begin{aligned}\mathcal{W}_j(x;\boldsymbol{a}_0,\boldsymbol{a}_1) &= \sum_{k=1}^{N}\int_{a_0^k}^{a_1^k} w_{jk}(x-y)\,dy\\ &= \sum_{k=1}^{N}\big(W_{jk}(x-a_0^k)-W_{jk}(x-a_1^k)\big),\end{aligned}$$

where $\boldsymbol{a}_0=[a_0^j]$ and $\boldsymbol{a}_1=[a_1^j]$ for $j=1,\ldots,N$ and

$$W_{jk}(x)=\int_0^x w_{jk}(y)\,dy.$$

Next, provided $\mathbf{A}$ in Eq. (12) or $\widetilde{\mathbf{A}}$ in Eq. (14) is invertible, each Eq. (12) or Eq. (14) may be solved for $\mathbf{u}$ for the profile of a stationary bump.

A stationary bump, when no linear gating variables are present, can then be expressed as

$$\mathbf{u}(x,t) = \mathbf{U}(x) = \mathbf{A}^{-1}(\mathcal{W}(x;\boldsymbol{a}_0,\boldsymbol{a}_1) + \mathbf{I}(x)), \tag{15}$$

or, when linear gating variables are present, as

$$\begin{aligned}\mathbf{u}(x,t) &= \mathbf{U}(x) = \widetilde{\mathbf{A}}^{-1}(\mathcal{W}(x;\boldsymbol{a}_0,\boldsymbol{a}_1) + \mathbf{I}(x)),\\ \mathbf{v}(x,t) &= \mathbf{V}(x) = -\mathbf{D}^{-1}\mathbf{C}\,\mathbf{U}(x),\end{aligned} \tag{16}$$

where $\widetilde{\mathbf{A}} = \mathbf{A} - \mathbf{B}\mathbf{D}^{-1}\mathbf{C}$ which is diagonal.

The unknown bump threshold points $\boldsymbol{a}_0, \boldsymbol{a}_1$ with scalar components a_0^j, a_1^j for $j = 1,\ldots,N$ are determined by requiring the bump profile $U_j(x)$ for each population j to satisfy its left and right threshold conditions $U_j(a_l^j) = \theta_j$ for $l = 0, 1$ which can be expressed as the nonlinear system of $2N$ equations

$$\begin{aligned}U_j\big(a_0^j\big) &\equiv \frac{1}{\widetilde{A}_{jj}}\left(\mathcal{W}_j\big(a_0^j;\boldsymbol{a}_0,\boldsymbol{a}_1\big) + I_j\big(a_0^j\big)\right) = \theta_j,\\ U_j\big(a_1^j\big) &\equiv \frac{1}{\widetilde{A}_{jj}}\left(\mathcal{W}_j\big(a_1^j;\boldsymbol{a}_0,\boldsymbol{a}_1\big) + I_j\big(a_1^j\big)\right) = \theta_j,\end{aligned} \tag{17}$$

where $\widetilde{\mathbf{A}}^{-1} = \mathsf{diag}(\widetilde{A}_{11}^{-1},\ldots,\widetilde{A}_{NN}^{-1})$ reducing to $\widetilde{\mathbf{A}}^{-1} = \mathbf{A}^{-1}$ in the case of no gating variables. Equation (17) represents a system of $2N$ nonlinear equations in $2N$ variables a_l^j for $j = 1,\ldots,N$ and $l = 0, 1$.

The stationary bump solution is $\mathbf{U} = [U_j]$ where the jth component can be expressed as

$$U_j(x) = \frac{1}{\widetilde{A}_{jj}}\left[\sum_{k=1}^{N}\left(W_{jk}\big(x - a_0^k\big) - W_{jk}\big(x - a_1^k\big)\right) + I_j(x)\right].$$

In the special case that the bump is *even-symmetric* about a common location $x = x_c$ in all populations, then the locations of the vectors of left and right threshold points for neural field $j = 1,\ldots,N$ can be expressed as

$$\boldsymbol{a}_0 = [x_c - a^j], \quad \boldsymbol{a}_1 = [x_c + a^j],$$

where a^j is the bump half-width in the jth neural field.

Note that, at times these existence equations produce spurious solutions that cross threshold more than two times and violate the assumed threshold conditions for a stationary bump; consequently any solution of the existence equations must be verified that it yields a stationary bump solution that properly obeys the threshold crossings, otherwise it does not correspond to a solution.

D. Stability analysis and spatial dependence of the eigenfunctions of the linearization

To investigate the stability of a stationary bump $\mathbf{U}(x,t)$, Eqs. (9) and (10) are linearized about the stationary solution $(\mathbf{U},\mathbf{V})$, by introducing the time-dependent perturbations

$$\begin{aligned}\mathbf{u}(x,t) &= \mathbf{U}(x) + \widetilde{\boldsymbol{\varphi}}(x,t),\\ \mathbf{v}(x,t) &= \mathbf{V}(x) + \widetilde{\boldsymbol{\psi}}(x,t),\end{aligned}$$

and expanding to first order in $\widetilde{\boldsymbol{\varphi}}, \widetilde{\boldsymbol{\psi}}$ which leads to the linear system of integrodifferential equations

$$\begin{aligned}\frac{\partial}{\partial t}\widetilde{\boldsymbol{\varphi}} &= \mathbf{A}\widetilde{\boldsymbol{\varphi}} + \mathbf{B}\widetilde{\boldsymbol{\psi}} + \mathbf{N}\widetilde{\boldsymbol{\varphi}},\\ \frac{\partial}{\partial t}\widetilde{\boldsymbol{\psi}} &= \mathbf{C}\widetilde{\boldsymbol{\varphi}} + \mathbf{D}\widetilde{\boldsymbol{\psi}},\end{aligned} \tag{18}$$

where $\mathbf{N}$ is a nonlocal compact linear operator given by

$$\begin{aligned}\mathbf{N}\boldsymbol{\varphi} &= \mathbf{W} * [\boldsymbol{\delta}(\mathbf{U} - \boldsymbol{\theta})\boldsymbol{\varphi}]\\ &= \int_{\mathbb{R}} \mathbf{W}(x-y)\,\boldsymbol{\delta}(\mathbf{U}(y) - \boldsymbol{\theta})\,\boldsymbol{\varphi}(y)\,dy.\end{aligned}$$

$\mathbf{W}$ is the matrix of synaptic weight functions in Eq. (11) and $\boldsymbol{\delta}(\mathbf{U} - \boldsymbol{\theta})\boldsymbol{\varphi}$ is the vector of δ functions over the N neural fields φ_j with threshold θ_j and bump profile $U_j(x)$:

$$\boldsymbol{\delta}(\mathbf{U} - \boldsymbol{\theta})\boldsymbol{\varphi} = \begin{bmatrix}\delta(U_1 - \theta_1)\,\varphi_1\\ \delta(U_2 - \theta_2)\,\varphi_2\\ \vdots\\ \delta(U_N - \theta_N)\,\varphi_N\end{bmatrix}.$$

Setting $\widetilde{\boldsymbol{\varphi}}(x,t) = \boldsymbol{\varphi}(x)e^{\lambda t}$ and $\widetilde{\boldsymbol{\psi}}(x,t) = \boldsymbol{\psi}(x)e^{\lambda t}$ in Eq. (18) results in the *spectral problem*

$$\begin{aligned}\lambda\,\boldsymbol{\varphi} &= \mathbf{A}\boldsymbol{\varphi} + \mathbf{B}\boldsymbol{\psi} + \mathbf{N}\boldsymbol{\varphi},\\ \lambda\,\boldsymbol{\psi} &= \mathbf{C}\boldsymbol{\varphi} + \mathbf{D}\boldsymbol{\psi}.\end{aligned} \tag{19}$$

Provided that $(\lambda\mathbf{I} - \mathbf{D})$ is invertible, the function $\boldsymbol{\psi}$ is determined uniquely by $\boldsymbol{\varphi}$ according to

$$\boldsymbol{\psi} = (\lambda\mathbf{I} - \mathbf{D})^{-1}\mathbf{C}\boldsymbol{\varphi},$$

thereby reducing Eq. (19) to the *reduced spectral problem*

$$\lambda\,\boldsymbol{\varphi} = (\mathbf{L}(\lambda) + \mathbf{N})\boldsymbol{\varphi}, \tag{20}$$

where matrix operator $\mathbf{L}(\lambda) = \mathbf{A} + \mathbf{B}(\lambda\mathbf{I} - \mathbf{D})^{-1}\mathbf{C}$ depends on the spectral parameter λ. When gating variables are not present, $\mathbf{L}(\lambda)$ reduces to $\mathbf{L}(\lambda) = \mathbf{A}$.

For $\mathbf{A}, \mathbf{B}, \mathbf{C}, \mathbf{D}$ satisfying the assumptions in Sec. III B, it follows that $\mathbf{L}(\lambda)$ is *diagonal* assuming $(\lambda\mathbf{I} - \mathbf{D})$ is invertible. To reference the elements of $\mathbf{L}(\lambda)$ we define

$$\mathbf{L}(\lambda) = \mathsf{diag}(\ell_{11}(\lambda), \ell_{22}(\lambda), \ldots, \ell_{NN}(\lambda)).$$

We view the nonlocal operator $\mathbf{N}$ acting on the vector function $\boldsymbol{\varphi}(x)$ in terms of operators $\mathcal{N}_{jk}$,

$$\mathbf{N} = [\mathcal{N}_{jk}],$$

each acting on its scalar component $\varphi_k(x)$ according to

$$\begin{aligned}\mathcal{N}_{jk}\,\varphi_k &= w_{jk} * [H'(U_k - \theta_k)\,\varphi_k]\\ &= \int_{-\infty}^{\infty} w_{jk}(x-\eta)\,\delta(U_k(\eta) - \theta_k)\,\varphi_k(\eta)\,d\eta\\ &= \mathcal{M}_{jk}\big(x;a_0^k\big)\,\varphi_k\big(a_0^k\big) + \mathcal{M}_{jk}\big(x;a_1^k\big)\,\varphi_k\big(a_1^k\big),\end{aligned}$$

where

$$\mathcal{M}_{jk}\big(x;a_l^k\big) = \frac{w_{jk}\big(x - a_l^k\big)}{\big|U_k'\big(a_l^k\big)\big|}$$

and

$$U_k'(x) = \frac{1}{\widetilde{A}_{jj}}\left[\sum_{k=1}^{N}\left[w_{jk}\left(x-a_0^k\right)-w_{jk}\left(x-a_1^k\right)\right]+I_j'(x)\right].$$

If we define the $2N$-dimensional constant vector $\mathbf{\Phi}$ below for the special nonlocal values $\varphi_j(a_l^j)$,

$$\mathbf{\Phi} = \left(\varphi_1\left(a_0^1\right),\ldots,\varphi_N\left(a_0^N\right),\varphi_1\left(a_1^1\right),\ldots,\varphi_N\left(a_1^N\right)\right)^{\mathrm{T}}, \quad (21)$$

we can express $\mathbf{N}\boldsymbol{\varphi}$ in terms of the $(N\times 2N)$ matrix $\boldsymbol{\mathcal{M}}(x)$ where

$$\mathbf{N}\boldsymbol{\varphi}(x) = \boldsymbol{\mathcal{M}}(x)\,\mathbf{\Phi}, \qquad \begin{aligned}\boldsymbol{\mathcal{M}}(x) &= [\,\boldsymbol{\mathcal{M}}_0(x) \quad \boldsymbol{\mathcal{M}}_1(x)],\\ \boldsymbol{\mathcal{M}}_l(x) &= \left[\,\mathcal{M}_{jk}\left(x;a_l^k\right)\right].\end{aligned}$$

$\boldsymbol{\mathcal{M}}_l(x)$ is an $(N\times N)$ matrix, $j,k=1,\ldots,N$, and $l=0,1$.

1. Essential spectrum

$\mathbf{N}$ is a compact operator. The essential spectra of $(\mathbf{L}+\mathbf{N})$ and $\mathbf{L}$ are the same, since $\mathbf{L}+\mathbf{N}$ is a compact perturbation of $\mathbf{L}$, and comprise the finite set of values

$$\sigma_{\mathsf{ess}} = \left\{\lambda_i^{\mathsf{ess}}\right\}_{i=1}^{Q},$$

which is the set of all solutions $\lambda=\lambda_i^{\mathsf{ess}}$ to the equation

$$\prod_{j=1}^{N}(\ell_{jj}(\lambda)-\lambda)=0,$$

where $\ell_{jj}(\lambda)$ are the diagonal elements of $\mathbf{L}(\lambda)$. Operator $(\mathbf{L}-\lambda\mathbf{I})$ has an infinite-dimensional kernel at each λ_i^{ess}. Since $(\mathbf{L}+\mathbf{N})$ and $\mathbf{L}$ are closed operators and λ_i^{ess} are isolated points with infinite geometric multiplicity, then λ_i^{ess} belong to the essential spectrum of $\mathbf{L}$ and $(\mathbf{L}+\mathbf{N})$ [70]. The essential spectrum lies in the open left-half complex plane whenever $\mathcal{R}\mathsf{e}\,\{\lambda_i^{\mathsf{ess}}\}<0$ for all $i=1,\ldots,Q$.

2. Point spectrum

We rewrite the spectral problem Eq. (20) using $\mathbf{N}\boldsymbol{\varphi}=\boldsymbol{\mathcal{M}}(x)\mathbf{\Phi}$ to express it as

$$(\lambda\mathbf{I}-\mathbf{L}(\lambda))\boldsymbol{\varphi}(x)=\boldsymbol{\mathcal{M}}(x)\mathbf{\Phi}. \quad (22)$$

Since the diagonal matrix $(\lambda\mathbf{I}-\mathbf{L}(\lambda))$ is invertible whenever $\lambda\notin\sigma_{\mathsf{ess}}$, Eq. (22) generates nontrivial solutions whenever the vector of special nonlocal values $\mathbf{\Phi}$ is nonzero. The eigenfunctions over space are determined by the special nonlocal values $\mathbf{\Phi}$ of the eigenfunctions at the threshold points. A self-consistency or compatibility condition for the vector of special nonlocal values $\mathbf{\Phi}$ is constructed by setting $x=a_0^j,a_1^j$ in the jth entry of the vector equation (22) stated as

$$(\lambda-\ell_{jj}(\lambda))\varphi_j(x)=\sum_{l=0}^{1}\sum_{k=1}^{N}\mathcal{M}_{jk}\left(x;a_l^k\right)\varphi_k\left(a_l^k\right),$$

to obtain the following compatibility condition for the existence of threshold points $x=a_0^j,a_1^j$ of the bump

$$\begin{aligned}(\lambda-\ell_{jj}(\lambda))\varphi_j\left(a_0^j\right)&=\sum_{l=0}^{1}\sum_{k=1}^{N}\mathcal{M}_{jk}\left(a_0^j;a_l^k\right)\varphi_k\left(a_l^k\right),\\ (\lambda-\ell_{jj}(\lambda))\varphi_j\left(a_1^j\right)&=\sum_{l=0}^{1}\sum_{k=1}^{N}\mathcal{M}_{jk}\left(a_1^j;a_l^k\right)\varphi_k\left(a_l^k\right).\end{aligned} \quad (23)$$

Compatibility condition (23) is expressed compactly as

$$(\lambda\mathbf{I}-\widetilde{\mathbf{L}}(\lambda))\mathbf{\Phi}=\mathbf{M}\mathbf{\Phi}, \quad (24)$$

where $\widetilde{\mathbf{L}}(\lambda)$ is a $(2N\times 2N)$ matrix (that can depend on spectral parameter λ if gating variables are present)

$$\widetilde{\mathbf{L}}(\lambda)=\begin{bmatrix}\mathbf{L}(\lambda) & \mathbf{0}\\ \mathbf{0} & \mathbf{L}(\lambda)\end{bmatrix}.$$

$\mathbf{M}$ is the $(2N\times 2N)$ matrix composed as a (2×2) block matrix with $(N\times N)$ submatrices $\mathbf{M}_{pq}$, where

$$\mathbf{M}=\begin{bmatrix}\mathbf{M}_{00} & \mathbf{M}_{01}\\ \mathbf{M}_{10} & \mathbf{M}_{11}\end{bmatrix}, \quad \mathbf{M}_{pq}=\left[\mathcal{M}_{jk}\left(a_p^j;a_q^k\right)\right],$$

$$\mathcal{M}_{jk}\left(a_p^j;a_q^k\right)=\frac{w_{jk}\left(a_p^j-a_q^k\right)}{\left|U_k'\left(a_q^k\right)\right|},$$

where $p,q=0,1$ and $j,k=1,\ldots,N$.

Rewriting *compatibility condition* (24) for the vector of special nonlocal values $\mathbf{\Phi}$ as

$$(\lambda\mathbf{I}-\widetilde{\mathbf{L}}(\lambda)-\mathbf{M})\mathbf{\Phi}=\mathbf{0}. \quad (25)$$

Nontrivial solutions to Eq. (25) exists, and hence eigenfunctions to spectral problem Eq. (19) exist, whenever $\mathsf{det}(\lambda\mathbf{I}-\widetilde{\mathbf{L}}(\lambda)-\mathbf{M})=0$ on the set of $\lambda\notin\sigma_{\mathsf{ess}}$.

Consequently, an *Evans function* $\mathcal{E}(\lambda)$ for the stationary bump $(\mathbf{U}(x),\mathbf{V}(x))$ is

$$\mathcal{E}(\lambda)=\mathsf{det}(\lambda\mathbf{I}-\widetilde{\mathbf{L}}(\lambda)-\mathbf{M}) \quad (26)$$

for $\lambda\notin\sigma_{\mathsf{ess}}$. The *zero set* of the Evans function represents the set of all eigenvalues of $(\mathbf{L}(\lambda)-\mathbf{N})$ in this region.

3. Eigenfunctions

From Eq. (22), an eigenfunction corresponding to eigenvalue λ can be expressed as

$$\begin{aligned}\boldsymbol{\varphi}(x)&=(\lambda\mathbf{I}-\mathbf{L}(\lambda))^{-1}\boldsymbol{\mathcal{M}}(x)\,\mathbf{\Phi},\\ \boldsymbol{\psi}(x)&=(\lambda\mathbf{I}-\mathbf{D})^{-1}\mathbf{C}\,\boldsymbol{\varphi}(x).\end{aligned}$$

Note that $(\lambda\mathbf{I}-\mathbf{L}(\lambda))$ is invertible since $\lambda\notin\sigma_{\mathsf{ess}}$. The jth element of $\boldsymbol{\varphi}(x)=[\varphi_j(x)]$ can be expressed as

$$\varphi_j(x)=\frac{1}{(\lambda-\ell_{jj}(\lambda))}\sum_{l=0}^{1}\sum_{k=1}^{N}\mathcal{M}_{jk}\left(x;a_l^k\right)\varphi_k\left(a_l^k\right)$$

$$\overset{\mathsf{OR}}{=}\ \varphi_k\left(a_r^j\right)\frac{\sum_{l=0}^{1}\sum_{k=1}^{N}\mathcal{M}_{jk}\left(x;a_l^k\right)\varphi_k\left(a_l^k\right)}{\sum_{l=0}^{1}\sum_{k=1}^{N}\mathcal{M}_{jk}\left(a_r^j;a_l^k\right)\varphi_k\left(a_l^k\right)}$$

for $r=0,1$ and $j=0,1,\ldots,N$ using Eq. (23).

IV. SPATIAL STRUCTURE OF THE EIGENFUNCTIONS FOR NEURAL FIELDS WITH EVEN SYMMETRY

When even symmetry is present in the synaptic weight functions $w_{jk}(x)$ and the inputs $I_j(x)$ (when present), and, moreover, the stationary bump in each population k shares a common center x_c then we show that the spatial structure of operator $\mathbf{L}+\mathbf{N}$ in general can be decomposed into two components with either even or odd symmetry that give rise to eigenfunctions with even or odd spatial symmetry. As these assumptions underlie the specific neural fields investigated in this paper in Secs. II and V the following applies to all of them.

Structure of M for even-symmetric U(x), W(x)

Claim: If $w_{jk}(x)$, $I_j(x)$, and $U_j(x)$ are even-symmetric about a common center x_c for all $j,k=1,\ldots,N$, then

$$\mathbf{M}_{00}=\mathbf{M}_{11}\equiv\boldsymbol{\Omega}\qquad\text{and}\qquad\mathbf{M}_{01}=\mathbf{M}_{10}\equiv\boldsymbol{\Sigma},$$

so $\mathbf{M}$ reduces to the form

$$\mathbf{M}=\begin{bmatrix}\mathbf{M}_{00}&\mathbf{M}_{01}\\ \mathbf{M}_{01}&\mathbf{M}_{00}\end{bmatrix}=\begin{bmatrix}\boldsymbol{\Omega}&\boldsymbol{\Sigma}\\ \boldsymbol{\Sigma}&\boldsymbol{\Omega}\end{bmatrix}.$$

To see why this is true, if the bump $U_k(x)$ in each population k is even-symmetric about a common center $x=x_c$, then $|U_k'(a_0^k)|=|U_k'(a_1^k)|$ and $|a_0^j-a_0^k|=|a_1^j-a_1^k|$ and $|a_0^j-a_1^k|=|a_1^j-a_0^k|$ for $j,k=1,\ldots,N$, Consequently, by the even symmetry of w_{jk}, it follows that for all j,k,

$$\frac{w_{jk}\big(a_0^j-a_0^k\big)}{\big|U_k'\big(a_0^k\big)\big|}=\frac{w_{jk}\big(a_1^j-a_1^k\big)}{\big|U_k'\big(a_1^k\big)\big|},$$

which means for all j,k,

$$\mathcal{M}_{jk}\big(a_0^j;a_0^k\big)=\mathcal{M}_{jk}\big(a_1^j;a_1^k\big),\quad\Rightarrow\quad\mathbf{M}_{00}=\mathbf{M}_{11}.$$

Similarly,

$$\frac{w_{jk}\big(a_0^j-a_1^k\big)}{\big|U_k'\big(a_1^k\big)\big|}=\frac{w_{jk}\big(a_1^j-a_0^k\big)}{\big|U_k'\big(a_0^k\big)\big|},$$

for all j,k, which means

$$\mathcal{M}_{jk}\big(a_0^j;a_1^k\big)=\mathcal{M}_{jk}\big(a_1^j;a_0^k\big)\quad\Rightarrow\quad\mathbf{M}_{01}=\mathbf{M}_{10}.$$

■

By a similarity transformation for $\mathbf{M}$, we may express

$$\mathbf{Q}^{-1}\mathbf{M}\mathbf{Q}=\begin{bmatrix}\mathbf{M}_\oplus&\mathbf{0}\\ \mathbf{0}&\mathbf{M}_\ominus\end{bmatrix}\qquad\mathbf{Q}=\begin{bmatrix}\mathbf{I}_N&\mathbf{I}_N\\ \mathbf{I}_N&-\mathbf{I}_N\end{bmatrix}$$
$$\mathbf{M}_\oplus=\boldsymbol{\Omega}+\boldsymbol{\Sigma},$$
$$\mathbf{M}_\ominus=\boldsymbol{\Omega}-\boldsymbol{\Sigma},$$

where $\mathbf{I}_N$ is the $(N\times N)$ identity matrix. Moreover, $\widetilde{\mathbf{L}}(\lambda)$ is similar to itself under this similarity transformation, so $\widetilde{\mathbf{L}}(\lambda)=\mathbf{Q}^{-1}\widetilde{\mathbf{L}}(\lambda)\mathbf{Q}$ and we can conclude that

$$\mathbf{Q}^{-1}(\widetilde{\mathbf{L}}(\lambda)+\mathbf{M})\mathbf{Q}=\begin{bmatrix}\mathbf{L}(\lambda)+\mathbf{M}_\oplus&\mathbf{0}\\ \mathbf{0}&\mathbf{L}(\lambda)+\mathbf{M}_\ominus\end{bmatrix}.\quad(27)$$

Consequently, we can express the Evans function $\mathcal{E}(\lambda)$ as the product (*eigenvalues* comprise the zero set of $\mathcal{E}(\lambda)$)

$$\mathcal{E}(\lambda)=\mathsf{det}(\lambda\mathbf{I}-\mathbf{L}(\lambda)-\mathbf{M}_\oplus)\cdot\mathsf{det}(\lambda\mathbf{I}-\mathbf{L}(\lambda)-\mathbf{M}_\ominus).\quad(28)$$

An eigenfunction $\boldsymbol{\varphi}(x)$ corresponding to an eigenvalue λ can be expressed as

$$\boldsymbol{\varphi}(x)=(\lambda\mathbf{I}-\mathbf{L}(\lambda))^{-1}\mathbf{N}\boldsymbol{\varphi}(x),\quad(29)$$

where

$$\mathbf{N}\boldsymbol{\varphi}(x)=\boldsymbol{\mathcal{M}}(x)\boldsymbol{\Phi}=\boldsymbol{\mathcal{M}}_0(x)\boldsymbol{\Phi}_0+\boldsymbol{\mathcal{M}}_1(x)\boldsymbol{\Phi}_1,\qquad\boldsymbol{\Phi}=\begin{bmatrix}\boldsymbol{\Phi}_0\\ \boldsymbol{\Phi}_1\end{bmatrix},$$

the $2N$-vector $\boldsymbol{\Phi}$ is expressed in terms of two N-vectors $\boldsymbol{\Phi}_0=[\varphi_j(a_0^j)]$ and $\boldsymbol{\Phi}_1=[\varphi_j(a_1^j)]$ where $j=1,\ldots,N$ and

$$\boldsymbol{\mathcal{M}}(x)=[\,\boldsymbol{\mathcal{M}}_0(x)\quad\boldsymbol{\mathcal{M}}_1(x)]$$

is a block matrix formed from two $(N\times N)$ submatrices where

$$\boldsymbol{\mathcal{M}}_0(x)=\big[\mathcal{M}_{jk}\big(x;a_0^k\big)\big]\quad\boldsymbol{\mathcal{M}}_1(x)=\big[\mathcal{M}_{jk}\big(x;a_1^k\big)\big],$$

where $j,k=1,\ldots,N$.

Based on the similarity transformation (27), nontrivial solutions $\boldsymbol{\Phi}$ of the compatibility condition have one of the following two forms where $\boldsymbol{\phi}$ is an N-vector

$$\boldsymbol{\Phi}^\oplus=\begin{bmatrix}\boldsymbol{\Phi}_0^\oplus\\ \boldsymbol{\Phi}_1^\oplus\end{bmatrix}=\begin{bmatrix}\boldsymbol{\phi}\\ \boldsymbol{\phi}\end{bmatrix}\quad\text{or}\quad\boldsymbol{\Phi}^\ominus=\begin{bmatrix}\boldsymbol{\Phi}_0^\ominus\\ \boldsymbol{\Phi}_1^\ominus\end{bmatrix}=\begin{bmatrix}\boldsymbol{\phi}\\ -\boldsymbol{\phi}\end{bmatrix}.$$

Note that the matrix function $\boldsymbol{\mathcal{M}}_1(x)$ is a reflection of $\boldsymbol{\mathcal{M}}_0(x)$ across $x=x_c$ which is the common center point of the stationary bump, i.e.,

$$\boldsymbol{\mathcal{M}}_1(-(x-x_c))=\boldsymbol{\mathcal{M}}_0(x-x_c).$$

In the $\oplus$ case, $\mathbf{N}\boldsymbol{\varphi}(x)$ is *even-symmetric* about $x=x_c$

$$\mathbf{N}\boldsymbol{\varphi}(x)=(\boldsymbol{\mathcal{M}}_0(x)+\boldsymbol{\mathcal{M}}_1(x))\,\boldsymbol{\phi},$$

and in the $\ominus$ case, $\mathbf{N}\boldsymbol{\varphi}(x)$ is *odd-symmetric* about $x=x_c$

$$\mathbf{N}\boldsymbol{\varphi}(x)=(\boldsymbol{\mathcal{M}}_0(x)-\boldsymbol{\mathcal{M}}_1(x))\,\boldsymbol{\phi}.$$

If we define diagonal matrix $\mathcal{D}=(\lambda\mathbf{I}-\mathbf{L}(\lambda))^{-1}$, then from Eq. (20) eigenfunctions are given by one of the two forms

$$\boldsymbol{\varphi}^\oplus(x)=\mathcal{D}\,(\boldsymbol{\mathcal{M}}_0(x)+\boldsymbol{\mathcal{M}}_1(x))\,\boldsymbol{\phi},$$
$$\boldsymbol{\varphi}^\ominus(x)=\mathcal{D}\,(\boldsymbol{\mathcal{M}}_0(x)-\boldsymbol{\mathcal{M}}_1(x))\,\boldsymbol{\phi}.$$

If we define the matrix functions

$$\text{从}(x)\equiv(\boldsymbol{\mathcal{M}}_0(x)+\boldsymbol{\mathcal{M}}_1(x))=[\text{从}_{jk}(x)],$$
$$\text{爻}(x)\equiv(\boldsymbol{\mathcal{M}}_0(x)-\boldsymbol{\mathcal{M}}_1(x))=[\text{爻}_{jk}(x)],$$

then the elements may be expressed as

$$\text{从}_{jk}(x)=\frac{w_{jk}\big(x-a_0^k\big)}{\big|U_k'\big(a_0^k\big)\big|}+\frac{w_{jk}\big(x-a_1^k\big)}{\big|U_k'\big(a_1^k\big)\big|},$$
$$\text{爻}_{jk}(x)=\frac{w_{jk}\big(x-a_0^k\big)}{\big|U_k'\big(a_0^k\big)\big|}-\frac{w_{jk}\big(x-a_1^k\big)}{\big|U_k'\big(a_1^k\big)\big|}.\quad(30)$$

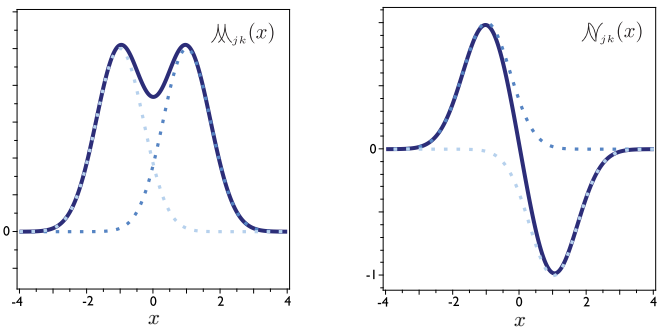

FIG. 3. Graphs of $\mathcal{W}_{jk}(x)$ and $\mathcal{N}_{jk}(x)$ in the case of Gaussian weight functions $w_{jk}(x)$ which form the sum $\oplus$ and difference $\ominus$ eigenmodes for the linearization about an even symmetric stationary bump in neural fields with even symmetric weight functions w_{jk} and inputs I_j.

The component functions $\mathcal{W}_{jk}(x)$ are even-symmetric and $\mathcal{N}_{jk}(x)$ are odd-symmetric functions about $x = x_c$, the center of the bump. Consequently, $\mathcal{W}(x)$ and $\mathcal{N}(x)$ are even and odd functions about $x = x_c$, respectively. Thus the eigenfunctions corresponding to eigenvalues λ associated with $\mathbf{M}_\oplus$ and $\mathbf{M}_\ominus$ modes can be expressed as

$$\boldsymbol{\varphi}^{\oplus}(x) = \mathcal{D}\,\mathcal{W}(x)\boldsymbol{\phi}, \qquad \boldsymbol{\varphi}^{\ominus}(x) = \mathcal{D}\,\mathcal{N}(x)\boldsymbol{\phi}.$$

Note that the symbols $\mathcal{W}$ and $\mathcal{N}$ are chosen to caricature the general shape of the component functions of the matrices $(\boldsymbol{\mathcal{M}}_0(x) + \boldsymbol{\mathcal{M}}_1(x))$ and $(\boldsymbol{\mathcal{M}}_0(x) - \boldsymbol{\mathcal{M}}_1(x))$ which take on the characteristic form of the following figures:

$$\mathcal{W} \quad \mathcal{N},$$

when w is the exponential weight function $e^{-|x|}$; if w is a Gaussian, then the sharp corners become smooth as in Fig. 3.

V. EXISTENCE AND STABILITY OF BUMPS IN ELEMENTARY NEURAL FIELDS ON $(-\infty, \infty)$

The stationary bump solution for each neural field described in this section is expressed in terms of the integral

$$W(x) = \int_0^x w(y)\,dy$$

of the synaptic weight functions w_{jk} for each model as denoted by various subscripts. For concrete calculations and simulations, positive synaptic weight functions are taken to be either $\frac{1}{\sqrt{\pi}\sigma}\overline{w}e^{-(x/\sigma)^2}$ or $\frac{1}{2\sigma}\overline{w}e^{-|x|/\sigma}$ and in the AE/AI/AA model $w(x) = w_e(x) - w_i(x)$ where excitatory and inhibitory components $w_e(x)$ and $w_i(x)$ are positive weight functions.

In all cases a stationary bump solution is a bounded solution $U_j(x)$ on $(-\infty, \infty)$ in which there is a bump in each neural field variable, indexed by j, that is centered about the origin in the universal coordinate system and satisfies the threshold conditions $U_j(\pm a_j) = \theta_j$ with $U_j(x) > \theta_j$, for $x \in (-a_j, a_j)$. Stationary bumps more generally could be formed from bumps in each neural field centered around a different point (as in Sec. III).

Spectral stability of the stationary bump is analyzed and, in all models, the essential spectrum σ_{ess} was determined to be negative and not a cause of instability. Stability of the stationary bump is thereby determined by the eigenvalues in the point spectrum and eigenvalues and eigenfunctions are constructed.

A stationary bump is *linearly stable* if all eigenvalues have negative real part except the generic, single 0 eigenvalue associated with translation invariance of stationary solutions in neural fields with translation symmetry. This is valid for the neural fields in this section in the absence of any input inhomogeneity and the translation mode in this case cannot destabilize in a Hopf bifurcation except possibly in the AE-I model. When input inhomogeneities are introduced, the translation symmetry is broken and the translation eigenmode generically has nonzero eigenvalues that may become complex and lead to a Hopf bifurcation of the translation mode. This results in side-to-side periodic oscillations that we have termed *sloshers* due to their back-and-forth sloshing behavior in contrast with the expanding-contracting periodic oscillations of the breathing bumps or *breathers* [39].

A. AE, AI, and AA neural fields

A stationary bump solution to neural field equation (3) is given by $(u(x,t), n(x,t)) = (U(x), N(x))$, where

$$(1+\beta)U(x) = W(x+a) - W(x-a) + I(x),$$
$$N(x) = U(x),$$

where a is determined by the threshold condition

$$W(2a) + I(a) = \theta(1+\beta),$$

provided $U(x)$ obeys the threshold behavior on $(-\infty, \infty)$.

Perturbations $(\widetilde{\varphi}(x,t), \widetilde{\psi}(x,t))$ of the stationary bump $(U(x), N(x))$ evolve according to

$$\frac{\partial\widetilde{\varphi}}{\partial t} + \widetilde{\varphi} = \mathcal{N}\widetilde{\varphi} - \beta\widetilde{\psi},$$
$$\frac{1}{\alpha}\frac{\partial\widetilde{\psi}}{\partial t} + \widetilde{\psi} = \widetilde{\varphi}. \tag{31}$$

Setting $(\widetilde{\varphi}, \widetilde{\psi}) = \boldsymbol{\varphi}(x)e^{\lambda t}$ yields the spectral problem for λ and $\boldsymbol{\varphi}(x) = (\varphi(x), \psi(x))^{\mathrm{T}}$,

$$-\varphi + \mathcal{N}\varphi - \beta\psi = \lambda\varphi,$$
$$\alpha\varphi - \alpha\psi = \lambda\psi. \tag{32}$$

Solving for ψ leads to the reduced spectral problem

$$-\varphi + \mathcal{N}\varphi = \left(\lambda + \frac{\alpha\beta}{\lambda+\alpha}\right)\varphi. \tag{33}$$

The compatibility equation determining both the eigenvalues and special nonlocal values of the eigenfunctions at the threshold points is

$$(\mathbf{M}_{\mathrm{AE}} - \mathbf{I})\boldsymbol{\phi} = \left(\lambda + \frac{\alpha\beta}{\lambda+\alpha}\right)\boldsymbol{\phi}, \tag{34}$$

where

$$\mathbf{M}_{\mathrm{AE}} = \begin{bmatrix} \mathcal{M}(0) & \mathcal{M}(2a) \\ \mathcal{M}(2a) & \mathcal{M}(0) \end{bmatrix}, \quad \boldsymbol{\phi} = \begin{pmatrix} \varphi(+a) \\ \varphi(-a) \end{pmatrix}$$

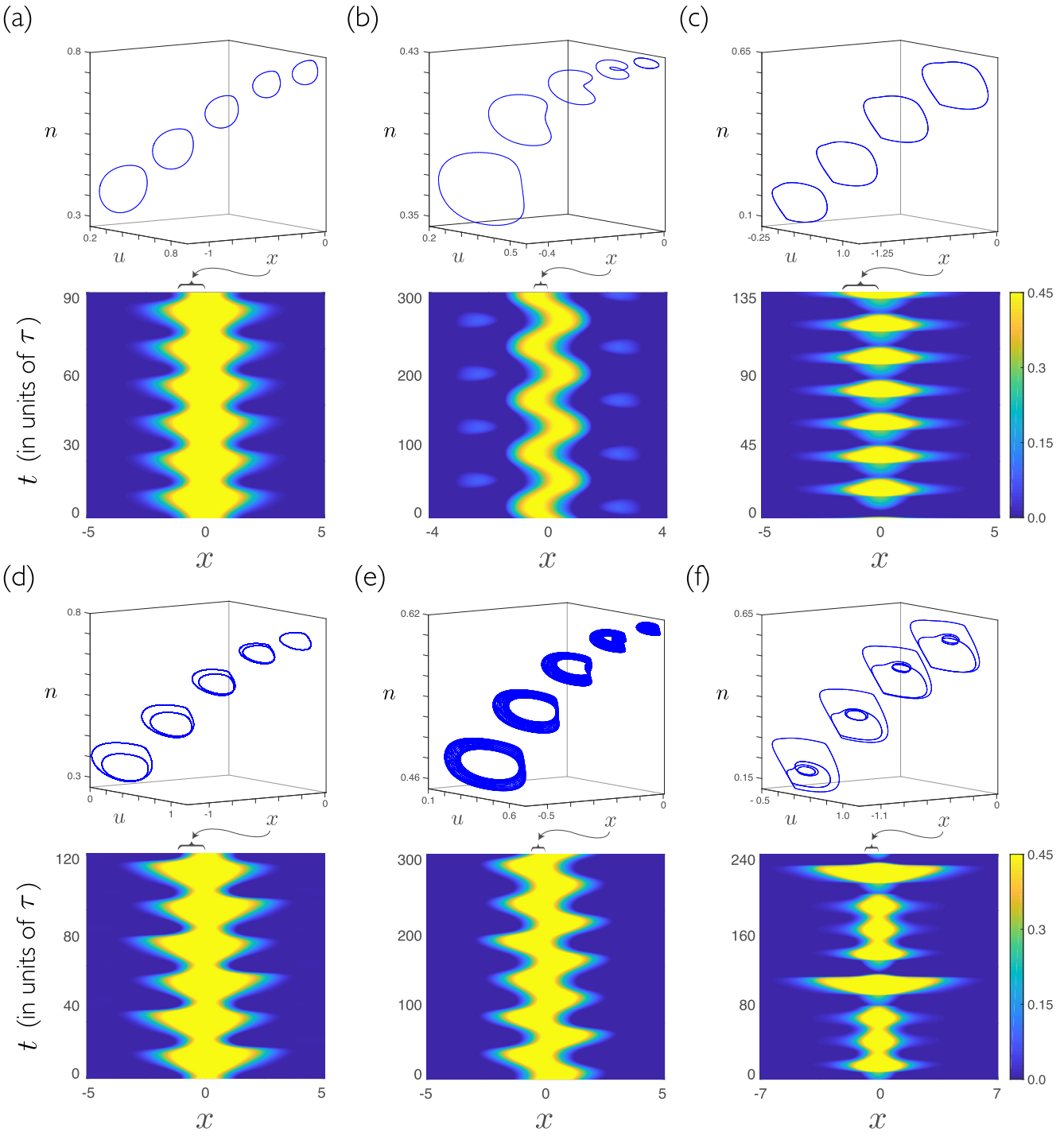

FIG. 4. Various types of spatially coherent localized oscillations in the AE/AI/AA neural field. Each figure is composed of a (lower graph) space-time plot of the neural activity variable $u(x,t)$, and (upper graph) plots of the orbit of $u(x_o,t)$ in the (u,n)-phase plane plotted at different spatial locations x near $x=0$ to illustrate the nonlinear dynamics through a projection. (a) *Breather* resulting from destabilizing the $\oplus$ eigenmode with the orbit as a limit cycle. (b) *Slosher* resulting from destabilizing the $\ominus$ eigenmode with orbit as a limit cycle; note the orbit has a period-doubled structure moving from the lateral region to $x=0$. (c) Intermixed localized super/subthreshold activity driven by the input inhomogeneity $I(x)$, akin to large amplitude relaxation oscillations and different from a breather. (d) Period doubling (secondary bifurcation) occurring on an even-symmetric breather giving rise to a period-2 orbit that exhibits a breather with a *side-to-side* or *sloshing* modulation. (e) Secondary bifurcation to a torus exhibiting a slosher with more variable activity in time. (f) Mixed-mode oscillations that alternate between superthreshold breathing oscillations and a relaxation oscillation intermixed with periods of subthreshold activity. This activity occurs just beyond a secondary bifurcation point (purportedly subcritical) with the breathing activity appearing to correspond to the orbit passing in the vicinity of the unstable limit cycle (breather).

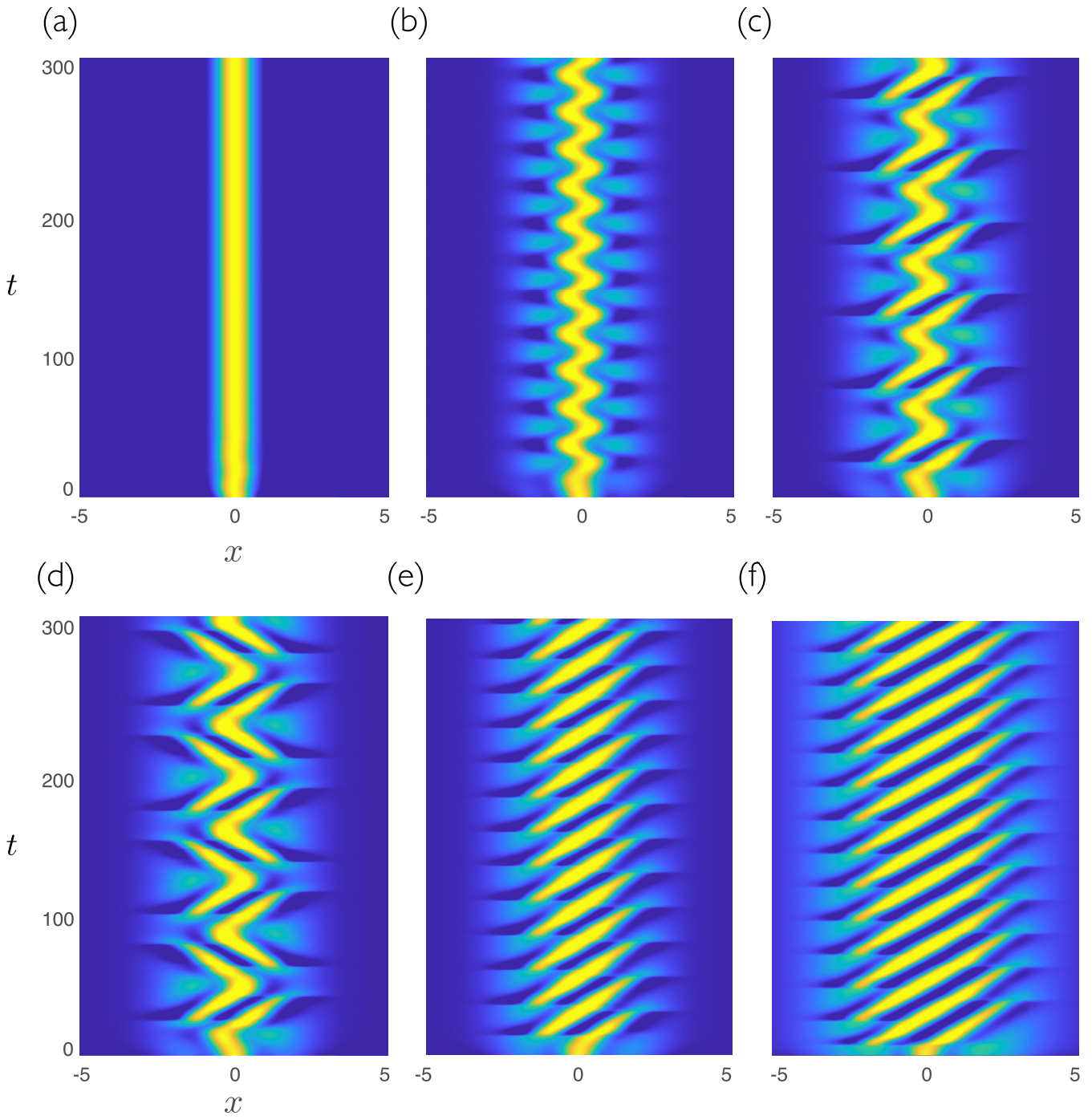

FIG. 5. Transition between different spatial patterns in the AA neural field as the input space constant σ (measure of spatial extent of elevated input) is increased: (a) at $\sigma = 0.98$, a stable stationary bump, (b) at $\sigma = 1.5$, a stable sloshing bump, (c) at $\sigma = 1.75$, a mixed wave pattern, (d) at $\sigma = 1.9$, a mixed wave pattern, (e) at $\sigma = 2.0$, a localized periodic traveling wave, (f) at $\sigma = 3.0$, a localized periodic traveling wave. As the input widens further, the region of localized periodic traveling waves continues to widen. The (supercritical) Hopf bifurcation point occurs approximately at $\sigma = 1.0$. Other parameters are $I_0 = 1$, $\alpha = 0.1$, $\beta = 1$, $\theta = 0.3$, $\overline{w}_e = 1.5$, $\overline{w}_i = 2.5$, $\sigma_e = 0.5$, $\sigma_i = 1$ and the weight functions are Gaussian. Warmer shades indicate superthreshold values of the activity $u(x, t)$ whereas cooler shades indicate subthreshold values.

and $\mathcal{M}(x) = w(x)/|U'(a)|$. The matrix $\mathbf{M}_{\rm AE}$ is symmetric and is diagonalized by the similarity transformation

$$\mathbf{Q}^{-1}\,\mathbf{M}_{\rm AE}\,\mathbf{Q} = \mathbf{\Lambda}_{\rm AE} \equiv \begin{bmatrix} \mathcal{M}^{\oplus} & 0 \\ 0 & \mathcal{M}^{\ominus} \end{bmatrix}, \quad \mathbf{Q} = \begin{bmatrix} 1 & 1 \\ 1 & -1 \end{bmatrix},$$

where $\mathcal{M}^{\oplus\ominus} = \mathcal{M}(0) \pm \mathcal{M}(2a)$. Equation (34) can be written as

$$(\mathbf{M}_{\rm AE} - \mu(\lambda)\mathbf{I})\boldsymbol{\phi} = 0, \tag{35}$$

where $\mu(\lambda) = 1 + \lambda + \frac{\alpha\beta}{\lambda+\alpha}$. Nontrivial $\boldsymbol{\phi}$ exist when

$$\det(\mathbf{M}_{\rm AE} - \mu(\lambda)\mathbf{I}) = 0.$$

Solving for μ and then λ in terms of μ we obtain

$$\lambda^{\oplus} = -\Gamma \pm \sqrt{\Gamma^2 - \Delta} \qquad \Gamma = \tfrac{1}{2}(1+\alpha-\mu^{\oplus}),$$
$$\mu^{\oplus} = \mathcal{M}^{\oplus} = \mathcal{M}(0) \pm \mathcal{M}(2a) \qquad \Delta = \alpha(1+\beta-\mu^{\oplus}).$$

Solving Eq. (35) for the vector of special nonlocal values we obtain the form $\boldsymbol{\phi}^{\oplus} = (\varphi(-a), \varphi(a))^{\mathrm{T}} = (1, \pm 1)^{\mathrm{T}}$ where the $\pm$ corresponds to the different spatial modes $\mathcal{M}^{\oplus}$. The spatial eigenfunctions $\boldsymbol{\varphi}^{\oplus}(x)$ for the sum $\oplus$ and difference $\ominus$ eigenmodes are given by

$$\boldsymbol{\varphi}^{\oplus}(x) = \begin{pmatrix} \varphi(x) \\ \psi(x) \end{pmatrix} = \begin{pmatrix} 1 \\ \frac{\alpha}{\lambda+\alpha} \end{pmatrix} \mathcal{M}^{\oplus}(x;a),$$
$$\mathcal{M}^{\oplus}(x;a) = \Omega^{\oplus}(x;a)/|U'(a)|,$$
$$\Omega^{\oplus}(x;a) = w(x-a) \pm w(x+a).$$

At a Hopf bifurcation point the Hopf frequency is

$$\omega_H = \mathsf{Im}\{\lambda\} = \sqrt{\alpha(\beta-\alpha)}.$$

Determining whether the $\oplus$ or $\ominus$ eigenmodes destabilizes in a Hopf bifurcation of a stationary bump depends on the real part of the complex eigenvalues for the two modes and leads to the following condition. The $\oplus$ gives rise to expanding-contracting *breathers* and the $\ominus$ mode gives rise to side-to-side *sloshers*. See Fig. 4 for examples of breathers and sloshers including secondary bifurcations. Figure 5 depicts a novel transition from a slosher to a localized periodic traveling wave.

1. Condition for Hopf bifurcation of $\oplus$ or $\ominus$ mode

In the absence of an input ($I = 0$), difference mode $\ominus$ has a persistent 0 eigenvalue associated with translation invariance of the stationary bump and a second real eigenvalue. A drift bifurcation of the difference mode $\ominus$ occurs when $\alpha = \beta$ leading to traveling bump solutions. In the case $\alpha > \beta$, the sum mode $\oplus$ can only destabilize in a saddle-node bifurcation (see Fig. 6 and Table I).

In the presence of an input inhomogeneity ($I(x) \neq 0$), the eigenvalues are nonzero generically and both $\oplus$ and $\ominus$ eigenmodes may have complex eigenvalues. Below we state a condition determining which mode destabilizes first, assuming all eigenvalues are complex.

The $\oplus$ mode destabilizes first in a Hopf bifurcation if

$$w(2a) > 0$$

at the Hopf bifurcation point whereas the $\ominus$ mode destabilizes first in a Hopf bifurcation when

$$w(2a) < 0.$$

The $\oplus$ gives rise to expanding-contracting breathers and the $\ominus$ mode gives rise to side-to-side sloshers.

For $\alpha < \beta$, the condition for a Hopf bifurcation of a stable bump can be expressed in terms of the gradient of the input $I(a)$. A bump is stable if $|I'(a)|$ satisfies

$$|I'(a)| > D^{\mathrm{H}}(a)$$
$$= \begin{cases} D^{\mathrm{H}}_{\oplus}(a) \equiv \left(\frac{\beta-\alpha}{1+\alpha}\right)\Omega^{\oplus}(a;a) + 2w(2a), & w(2a) \geqslant 0, \\ D^{\mathrm{H}}_{\ominus}(a) \equiv \left(\frac{\beta-\alpha}{1+\alpha}\right)\Omega^{\ominus}(a;a), & w(2a) < 0, \end{cases}$$

with the Hopf bifurcation occurring at $|I'(a)| = D^{\mathrm{H}}(a)$. See Table I for the case $\alpha > \beta$. For the general forms of the synaptic weight function $w(x)$ depicted in Fig. 6, we state conditions for stability and bifurcations of stationary bumps in Table I.

We mention that a condition determining whether the bifurcation is supercritical or subcritical is given by the relevant coefficient in the normal form for the Hopf bifurcation which is calculated for this neural field in Ref. [39].

B. E-I neural field

A stationary bump solution to neural field equation (4) is given by $(u_e(x,t), u_i(x,t)) = (U_e(x), U_i(x))$, where

$$U_e(x) = [W_{ee}(x+a_e) - W_{ee}(x-a_e)] - [W_{ei}(x+a_i) - W_{ei}(x-a_i)] + I_e(x),$$
$$U_i(x) = [W_{ie}(x+a_e) - W_{ie}(x-a_e)] - [W_{ii}(x+a_i) - W_{ii}(x-a_i)] + I_i(x),$$

where a_e and a_i satisfy the threshold conditions

$$W_{ee}(2a_e) - W_{ei}(a_e+a_i) + W_{ei}(a_e-a_i) + I_e(a_e) = \theta_e,$$
$$W_{ie}(a_i+a_e) - W_{ie}(a_i-a_e) - W_{ii}(2a_i) + I_i(a_i) = \theta_i,$$

provided the threshold behavior is obeyed on $(-\infty, \infty)$.

Perturbations $(\widetilde{\varphi}_e(x,t), \widetilde{\varphi}_i(x,t))$ of the stationary bump $(U_e(x), U_i(x))$ evolve according to

$$\frac{\partial \widetilde{\varphi}_e}{\partial t} + \widetilde{\varphi}_e = \mathcal{N}_{ee}\,\widetilde{\varphi}_e - \mathcal{N}_{ei}\,\widetilde{\varphi}_i,$$
$$\tau\frac{\partial \widetilde{\varphi}_i}{\partial t} + \widetilde{\varphi}_i = \mathcal{N}_{ie}\,\widetilde{\varphi}_e - \mathcal{N}_{ii}\,\widetilde{\varphi}_i. \tag{36}$$

Setting $(\widetilde{\varphi}_e, \widetilde{\varphi}_i) = \boldsymbol{\varphi}(x)e^{\lambda t}$ yields the spectral problem for λ and $\boldsymbol{\varphi}(x) = (\varphi_e(x), \varphi_i(x))^{\mathrm{T}}$,

$$-\varphi_e + \mathcal{N}_{ee}\,\varphi_e - \mathcal{N}_{ei}\,\varphi_i = \lambda\varphi_e,$$
$$-\frac{1}{\tau}\varphi_i + \frac{1}{\tau}\mathcal{N}_{ie}\,\varphi_e - \frac{1}{\tau}\mathcal{N}_{ii}\,\varphi_i = \lambda\varphi_i. \tag{37}$$

The compatibility equation determining the eigenvalues and special nonlocal values of the eigenfunctions at threshold points a_e and a_i is

$$(\mathbf{M}_{\mathrm{EI}} - \mathbf{I}_{\mathrm{EI}})\boldsymbol{\phi} = \lambda\,\boldsymbol{\phi}, \tag{38}$$

where $\mathbf{I}_{\mathrm{EI}} = \mathsf{diag}\,(1,\ 1,\ \tau^{-1},\ \tau^{-1})$, $a_{e\pm i} = a_e \pm a_i$,

$$\mathbf{M}_{\mathrm{EI}} = \begin{bmatrix} \mathcal{M}_{ee}(0) & \mathcal{M}_{ee}(2a_e) & -\mathcal{M}_{ei}(a_{e-i}) & -\mathcal{M}_{ei}(a_{e+i}) \\ \mathcal{M}_{ee}(2a_e) & \mathcal{M}_{ee}(0) & -\mathcal{M}_{ei}(a_{e+i}) & -\mathcal{M}_{ei}(a_{e-i}) \\ \frac{1}{\tau}\mathcal{M}_{ie}(a_{e-i}) & \frac{1}{\tau}\mathcal{M}_{ie}(a_{e+i}) & -\frac{1}{\tau}\mathcal{M}_{ii}(0) & -\frac{1}{\tau}\mathcal{M}_{ii}(2a_i) \\ \frac{1}{\tau}\mathcal{M}_{ie}(a_{e+i}) & \frac{1}{\tau}\mathcal{M}_{ie}(a_{e-i}) & -\frac{1}{\tau}\mathcal{M}_{ii}(2a_i) & -\frac{1}{\tau}\mathcal{M}_{ii}(0) \end{bmatrix},$$

$$\mathcal{M}_{jk}(x) = \frac{w_{jk}(x)}{|U_k'(a_k)|}, \qquad \boldsymbol{\phi} = \begin{pmatrix} \varphi_e(+a_e) \\ \varphi_e(-a_e) \\ \varphi_i(+a_i) \\ \varphi_i(-a_i) \end{pmatrix}.$$

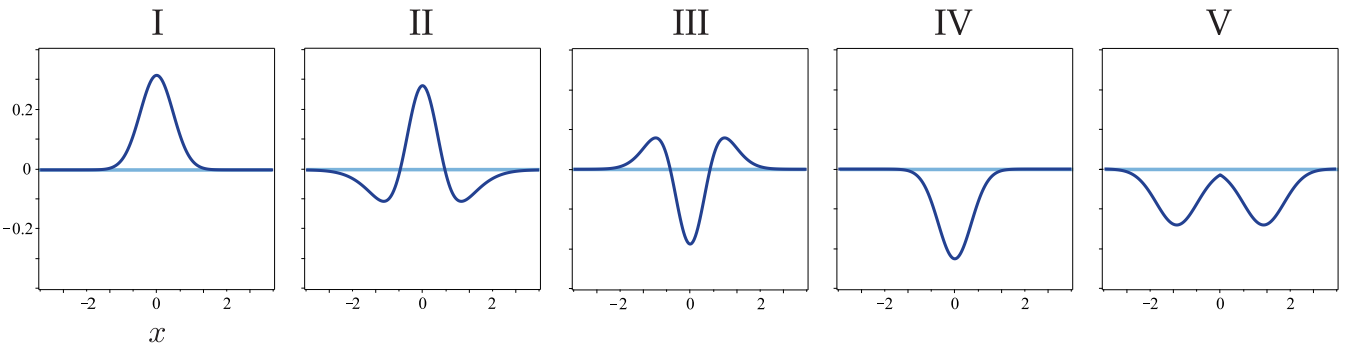

FIG. 6. Different forms of the synaptic weight function $w(x)$ in the AE/AI/AA neural field. I. purely exciatory (AE), II. Mexican hat (AA), III. inverted Mexican hat, IV. purely inhibitory (AI), V. bimodal inhibitory (AI).

The following similarity transform yields

$$\mathbf{Q}^{-1}\mathbf{M}_{\mathrm{EI}}\mathbf{Q} = \mathbf{\Lambda}_{\mathrm{EI}} \equiv \begin{bmatrix} \mathbf{\Lambda}_{\mathrm{EI}}^{\oplus} & 0 \\ 0 & \mathbf{\Lambda}_{\mathrm{EI}}^{\ominus} \end{bmatrix},$$

$$\mathbf{Q} = \begin{bmatrix} 1 & 0 & 1 & 0 \\ 1 & 0 & -1 & 0 \\ 0 & 1 & 0 & 1 \\ 0 & 1 & 0 & -1 \end{bmatrix}$$

$$\mathbf{\Lambda}_{\mathrm{EI}}^{\oplus} = \begin{bmatrix} \mathcal{M}_{ee}^{\oplus}(a_e;a_e) & -\mathcal{M}_{ei}^{\oplus}(a_e;a_i) \\ \frac{1}{\tau}\mathcal{M}_{ie}^{\oplus}(a_i;a_e) & -\frac{1}{\tau}\mathcal{M}_{ii}^{\oplus}(a_i;a_i) \end{bmatrix},$$

$$\mathcal{M}_{ee}^{\oplus}(a_e;a_e) = \mathcal{M}_{ee}(0) \pm \mathcal{M}_{ee}(2a_e),$$
$$\mathcal{M}_{ei}^{\oplus}(a_e;a_i) = \mathcal{M}_{ei}(a_e - a_i) \pm \mathcal{M}_{ei}(a_e + a_i),$$
$$\mathcal{M}_{ie}^{\oplus}(a_i;a_e) = \mathcal{M}_{ie}(a_e - a_i) \pm \mathcal{M}_{ie}(a_e + a_i),$$
$$\mathcal{M}_{ii}^{\oplus}(a_i;a_i) = \mathcal{M}_{ii}(0) \pm \mathcal{M}_{ii}(2a_i).$$

Compatibility equation (38) can be rewritten as

$$(\mathbf{M}_{\mathrm{EI}} - \mathbf{D}(\lambda))\boldsymbol{\phi} = 0, \tag{39}$$

where $\mathbf{D}(\lambda) = \mathrm{diag}\,(1+\lambda, 1+\lambda, \frac{1}{\tau}+\lambda, \frac{1}{\tau}+\lambda)$. Nontrivial solutions $\boldsymbol{\phi}$ to Eq. (39) exist and yield eigenfunctions when

$$\det(\mathbf{M}_{\mathrm{EI}} - \mathbf{D}(\lambda)) = \det\left(\mathbf{\Lambda}_{\mathrm{EI}}^{\oplus} - \widetilde{\mathbf{D}}(\lambda)\right) \cdot \det\left(\mathbf{\Lambda}_{\mathrm{EI}}^{\ominus} - \widetilde{\mathbf{D}}(\lambda)\right) = 0,$$

where $\widetilde{\mathbf{D}} = \mathrm{diag}\,(1+\lambda, \frac{1}{\tau}+\lambda)$.

Solving for the eigenvalues λ we obtain

$$\lambda^{\oplus} = \left[\frac{\mathcal{M}_{ee}^{\oplus} - 1}{2} - \frac{\mathcal{M}_{ii}^{\oplus} + 1}{2\tau}\right] \pm \sqrt{\left[\frac{\mathcal{M}_{ee}^{\oplus} - 1}{2} + \frac{\mathcal{M}_{ii}^{\oplus} + 1}{2\tau}\right]^2 - \frac{\mathcal{M}_{ei}^{\oplus}\mathcal{M}_{ie}^{\oplus}}{\tau}},$$

TABLE I. Each cell of the table describes the conditions for stability and bifurcations of any even-symmetric stationary bumps that may exist for the AE/AI/AA neural field with the synaptic connectivity given by the synaptic weight function $w(x)$ depicted in Fig. 6 with the corresponding Roman numerals listed. STABLE/UNSTABLE indicates any bumps that may exist are stable/unstable throughout the case; NO BUMPS indicates that the neural field models do not support stationary bumps when $I(x) = 0$; otherwise, the sufficient condition for stability is provided for any bump with halfwidth a that may exist within the region. Only Hopf, drift, and fold/saddle-node bifurcations of stable stationary bumps occurring in the models are listed. SN indicates a fold/saddle-node bifurcation; HOPF indicates a Hopf bifurcation and the associated mode destabilizing in the bifurcation is indicated by the critical gradient $D_{\oplus}^{\mathrm{H}}$ or $D_{\ominus}^{\mathrm{H}}$; DRIFT indicates a drift (pitchfork) bifurcation associated with translation mode $\ominus$ which gives rise to traveling bumps. Note that in Case III (inverted Mexican hat) with input $I(a) > 0$, a bump can only destabilize via the sum $\oplus$ mode in a Hopf bifurcation as $D_{\ominus}^{\mathrm{H}}(a) < |I'(a)|$ is always satisfied (since $w(0) < w(2a)$) and, if $w(2a) > 0$, a saddle-node bifurcation occurs prior to a Hopf bifurcation if $w(0) < \gamma w(2a)$ where $\gamma = (2 + 3\alpha - \beta)/(\beta - \alpha)$.

Stability and bifurcations of stable stationary bumps in the AE/AI/AA neural field				
	$I(x) = 0$		$I(x) > 0$	
	$\alpha > \beta$	$\alpha < \beta$	$\alpha > \beta$	$\alpha < \beta$
I	UNSTABLE	UNSTABLE	STABLE IF $2w(2a) < \lvert I'(a)\rvert$	STABLE IF $D_{\oplus}^{\mathrm{H}}(a) < \lvert I'(a)\rvert$, **HOPF** AT $D_{\oplus}^{\mathrm{H}}(a) = \lvert I'(a)\rvert$
II	STABLE (**SN**): $w(2a) < 0$ (=)	**DRIFT** AT: $\alpha = \beta$	**SN** AT $2w(2a) = \lvert I'(a)\rvert$	STABLE IF $D^{\mathrm{H}}(a) < \lvert I'(a)\rvert$, **HOPF** AT $D^{\mathrm{H}}(a) = \lvert I'(a)\rvert$
III	UNSTABLE			$D^{\mathrm{H}} = D_{\oplus}^{\mathrm{H}}$ IF $w(2a) > 0$, $D^{\mathrm{H}} = D_{\ominus}^{\mathrm{H}}$ IF $w(2a) < 0$
IV	NO BUMPS	NO BUMPS	STABLE	STABLE
V				STABLE IF $D_{\ominus}^{\mathrm{H}}(a) < \lvert I'(a)\rvert$, **HOPF** AT $D_{\ominus}^{\mathrm{H}}(a) = \lvert I'(a)\rvert$

where $\mathcal{M}^{\oplus}_{jk} = \mathcal{M}^{\oplus}_{jk}(a_j; a_k)$. From Eq. (39) the vector of special nonlocal values for the eigenfunction is $\boldsymbol{\phi} = (\varphi_e(a_e), \varphi_e(-a_e), \varphi_i(a_i), \varphi_i(-a_i))^{\mathrm{T}} = (1, \pm 1, \nu^{\oplus}, \pm\nu^{\oplus})^{\mathrm{T}}$ where

$$\nu^{\oplus} = \frac{\lambda^{\oplus} + 1 - \mathcal{M}^{\oplus}_{ee}(a_e; a_e)}{-\mathcal{M}^{\oplus}_{ei}(a_e; a_i)}$$

$$= \frac{\left[\frac{\mathcal{M}^{\oplus}_{ee}-1}{2} + \frac{\mathcal{M}^{\oplus}_{ii}+1}{2\tau}\right] \pm \sqrt{\left[\frac{\mathcal{M}^{\oplus}_{ee}-1}{2} + \frac{\mathcal{M}^{\oplus}_{ii}+1}{2\tau}\right]^2 - \frac{\mathcal{M}^{\oplus}_{ei}\mathcal{M}^{\oplus}_{ie}}{\tau}}}{-\mathcal{M}^{\oplus}_{ei}}.$$

The spatial eigenfunctions $\boldsymbol{\varphi}(x)$ are given by

$$\boldsymbol{\varphi}^{\oplus}(x) = \begin{pmatrix} \varphi_e \\ \varphi_i \end{pmatrix} = \begin{pmatrix} \frac{1}{\lambda^{\oplus}+1}\left[\mathcal{M}^{\oplus}_{ee}(x; a_e) - \nu^{\oplus}\mathcal{M}^{\oplus}_{ei}(x; a_i)\right] \\ \frac{1}{\tau\lambda^{\oplus}+1}\left[\mathcal{M}^{\oplus}_{ie}(x; a_e) - \nu^{\oplus}\mathcal{M}^{\oplus}_{ii}(x; a_i)\right] \end{pmatrix},$$

$$\mathcal{M}^{\oplus}_{jk}(x; a_k) = \Omega^{\oplus}_{jk}(x; a_k)/|U_k'(a_k)|,$$

$$\Omega^{\oplus}_{jk}(x; a_k) = w_{jk}(x - a_k) \pm w_{jk}(x + a_k).$$

At a Hopf bifurcation point the Hopf frequency is

$$\omega_H = \mathrm{Im}\{\lambda^{\oplus}\} = \sqrt{\frac{-\left(\mathcal{M}^{\oplus}_{ee} - 1\right)\left(\mathcal{M}^{\oplus}_{ii} + 1\right) + \mathcal{M}^{\oplus}_{ei}\mathcal{M}^{\oplus}_{ie}}{\tau}},$$

where $(\mathcal{M}^{\oplus}_{ee} - 1) = (\mathcal{M}^{\oplus}_{ii} + 1)/\tau$.

Determining which of the $\oplus$ or $\ominus$ eigenmode destabilizes in a Hopf bifurcation of a stationary bump depends on the real part of the eigenvalues for the two modes and leads to the following condition.

1. Condition for Hopf bifurcation of $\oplus$ or $\ominus$ mode

In the absence of any input ($I_e = I_i = 0$), the difference mode $\ominus$ has one persistent 0 eigenvalue reflecting the translation invariance of the stationary bump and a second real eigenvalue. In this case, only the $\oplus$ mode can destabilize in a Hopf bifurcation. In the presence of an input inhomogeneity where $I_e(x) \neq 0$ and/or $I_i(x) \neq 0$, the eigenvalues are nonzero generically, and both $\oplus$ and $\ominus$ eigenmodes may have complex eigenvalues.

Below we describe a condition for determining which mode $\oplus$ or $\ominus$ destabilizes first, assuming all eigenmodes are complex, by identifying a dominate eigenvalue with the larger real part of two pairs of complex eigenvalues.

The $\oplus$ mode destabilizes first in a Hopf bifurcation if

$$\frac{w_{ee}(2a_e)}{|U_e'(a_e)|} > \frac{w_{ii}(2a_i)}{\tau|U_i'(a_i)|}$$

at the bifurcation point (assuming complex) whereas the $\ominus$ mode destabilizes first in a Hopf bifurcation when

$$\frac{w_{ii}(2a_i)}{\tau|U_i'(a_i)|} > \frac{w_{ee}(2a_e)}{|U_e'(a_e)|}.$$

The sum $\oplus$ mode gives rise to expanding-contracting breathers and the $\ominus$ mode leads to side-to-side sloshers.

2. Drift and Hopf bifurcation for $I(x) = 0$

In the case of no input inhomogeneity ($I(x) = 0$), a drift bifurcation of a stationary bump can occur giving rise to traveling bump solutions. A drift bifurcation is a pitchfork bifurcation occurring on the translation mode ($\ominus$) in the presence of the persistent 0 eigenvalue associated with translation invariance of the neural field. Although drift bifurcations of a bump could occur through different parameter values, we have shown in Ref. [51] that stationary bumps always destabilize in a drift bifurcation at a critical value $\tau^{\mathcal{D}}_{\mathrm{crit}}$ of the relative time constant τ given by

$$\tau^{\mathcal{D}}_{\mathrm{crit}} = \frac{1 + \mathcal{M}^{\ominus}_{ii}(a_i; a_i)}{-1 + \mathcal{M}^{\ominus}_{ee}(a_e; a_e)}.$$

When the $\oplus$ eigenmode has complex eigenvalues, it destabilizes in a Hopf bifurcation at a critical value of τ,

$$\tau^{\mathcal{H}}_{\mathrm{crit}} = \frac{1 + \mathcal{M}^{\oplus}_{ii}(a_i; a_i)}{-1 + \mathcal{M}^{\oplus}_{ee}(a_e; a_e)}.$$

Moreover, it is possible to have a mode interaction (whereby the eigenmodes interact via nonlinear terms) between a drift bifurcation and a Hopf bifurcation leading to a codimension 2 drift-Hopf bifurcation that serves as an organizing center for both stationary and traveling bumps and breathers in the E-I neural field as depicted in Fig. 7 where $\mathcal{X}$ is the drift-Hopf bifurcation point [51].

C. AE-I neural field

A stationary bump solution to neural field equation (5) is $(u_e(x,t), u_i(x,t), n_e(x,t)) = (U_e(x), U_i(x), N_e(x))$, where

$$\begin{aligned}(1+\beta)U_e(x) &= [W_{ee}(x + a_e) - W_{ee}(x - a_e)] \\ &\quad - [W_{ei}(x + a_i) - W_{ei}(x - a_i)] + I_e(x), \\ U_i(x) &= [W_{ie}(x + a_e) - W_{ie}(x - a_e)] \\ &\quad - [W_{ii}(x + a_i) - W_{ii}(x - a_i)] + I_i(x), \\ N_e(x) &= U_e(x),\end{aligned}$$

and where a_e and a_i satisfy the threshold conditions

$$\begin{aligned}W_{ee}(2a_e) - W_{ei}(a_e + a_i) + W_{ei}(a_e - a_i) + I_e(a_e) &= \widetilde{\theta}_e, \\ W_{ie}(a_i + a_e) - W_{ie}(a_i - a_e) - W_{ii}(2a_i) + I_i(a_i) &= \theta_i,\end{aligned}$$

where $\widetilde{\theta}_e = \theta_e(1 + \beta)$, provided the threshold behavior is obeyed on $(-\infty, \infty)$.

Perturbations $(\widetilde{\varphi}_e(x,t), \widetilde{\varphi}_i(x,t), \widetilde{\psi}_e(x,t))$ of the stationary bump $(U_e(x), U_i(x), N_e(x))$ evolve according to

$$\begin{aligned}\frac{\partial\widetilde{\varphi}_e}{\partial t} + \widetilde{\varphi}_e &= \mathcal{N}_{ee}\,\widetilde{\varphi}_e - \mathcal{N}_{ei}\,\widetilde{\varphi}_i - \beta\widetilde{\psi}_e, \\ \tau\frac{\partial\widetilde{\varphi}_i}{\partial t} + \widetilde{\varphi}_i &= \mathcal{N}_{ie}\,\widetilde{\varphi}_e - \mathcal{N}_{ii}\,\widetilde{\varphi}_i, \\ \frac{1}{\alpha}\frac{\partial\widetilde{\psi}_e}{\partial t} + \widetilde{\psi}_e &= \widetilde{\varphi}_e. \end{aligned} \tag{40}$$

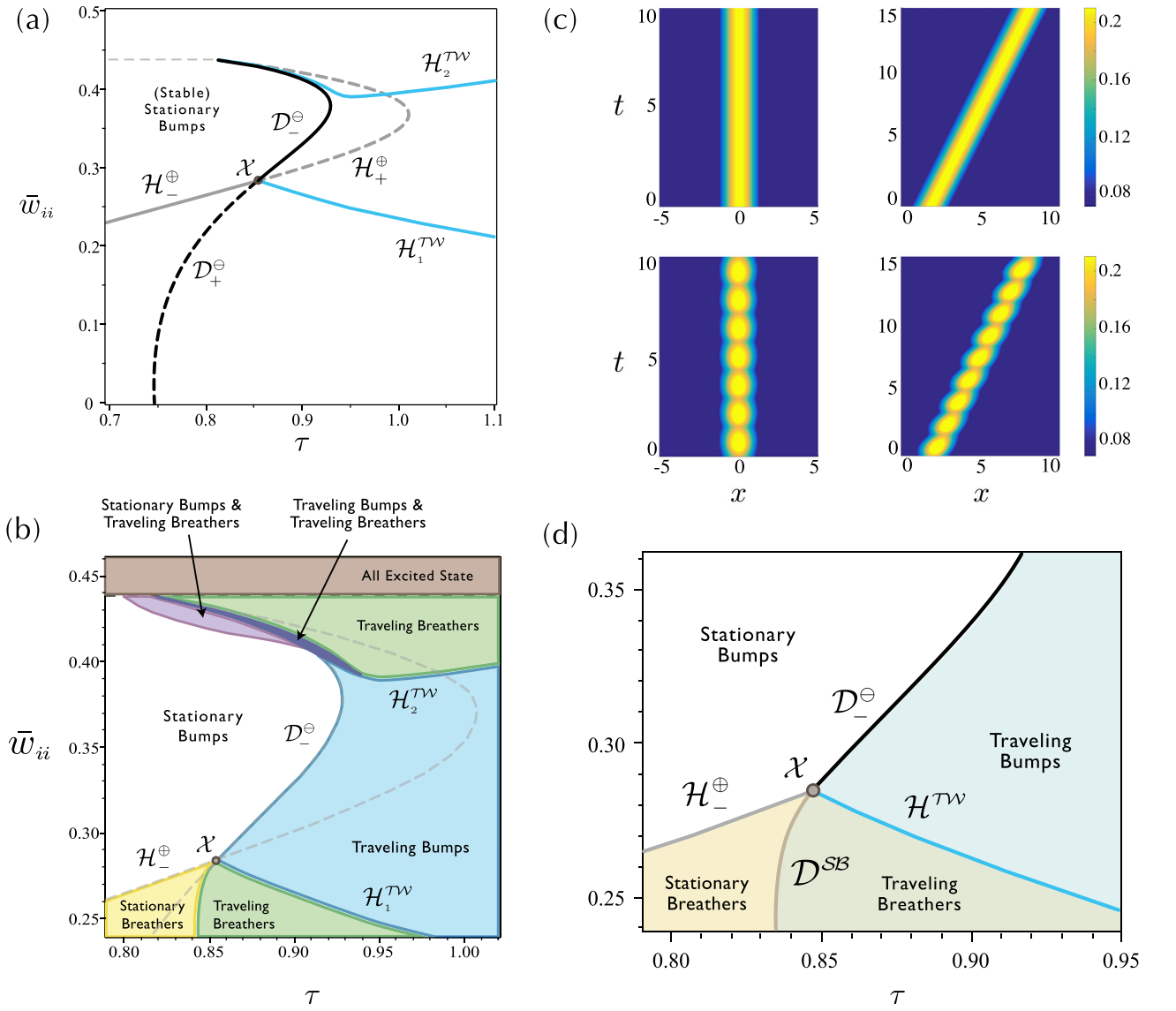

FIG. 7. Bumps and breathers in a E-I neural field in the absence of any input ($I_e(x) = I_i(x) = 0$), adapted from Ref. [51]. (a) In a parameter region in the E-I neural field ($\bar{w}_{ii}$ is the I-to-I synaptic strength) stationary bumps can destabilize either in a Hopf bifurcation along curve $\mathcal{H}_-^{\oplus}$, giving rise to stable stationary breathers, or a drift bifurcation along curve $\mathcal{D}_-^{\ominus}$, giving rise to stable traveling bump solutions. (b) Different regions indicate the stable attractors that occur in numerical simulations. The stable traveling bumps in the blue region destabilize in a Hopf bifurcation along curves $\mathcal{H}_{1,2}^{TW}$, giving rise to traveling breather solutions. (c) Space-time plots of the various stationary and traveling bump and breather solutions (excitatory variable $u_e(x,t)$ only). (d) To describe the stable attracting solutions around $\mathcal{X}$, a diagram for a hypothetical codim 2 bifurcation with a mode interaction occurring between the difference $\lambda^{\ominus}$-eigenmode (drift instability) and the sum $\lambda^{\oplus}$-eigenmode (Hopf instability). $\mathcal{H}_-^{\oplus}$ is a curve of Hopf bifurcations of stationary bumps, $\mathcal{D}_-^{\ominus}$ is a curve of drift bifurcations of stationary bumps, $\mathcal{H}^{TW}$ is a curve of Hopf bifurcations of traveling bumps, and $\mathcal{D}^{\mathcal{SB}}$ is a curve of drift bifurcations of stationary breathers. $\mathcal{H}_+^{\oplus}$, $\mathcal{D}_-^{\ominus}$ and $\mathcal{H}^{TW}$ are calculated from analytical results. Curve $\mathcal{D}^{\mathcal{SB}}$ is a proposed curve of drift bifurcations of stationary breathers based upon numerical simulations [51]. Curve $\mathcal{D}^{\mathcal{SB}}$ was recently verified and constructed via numerical continuation [52].

Setting $(\widetilde{\varphi}_e, \widetilde{\varphi}_i, \widetilde{\psi}_e) = \boldsymbol{\varphi}(x)e^{\lambda t}$ results in the spectral problem for λ and $\boldsymbol{\varphi}(x) = (\varphi_e(x), \varphi_i(x), \psi_e(x))^{\mathrm{T}}$,

$$\begin{aligned} -\varphi_e + \mathcal{N}_{ee}\,\varphi_e - \mathcal{N}_{ei}\,\varphi_i - \beta\psi_e &= \lambda\varphi_e, \\ -\frac{1}{\tau}\varphi_i + \frac{1}{\tau}\mathcal{N}_{ie}\,\varphi_e - \frac{1}{\tau}\mathcal{N}_{ii}\,\varphi_i &= \lambda\varphi_i, \\ \alpha\varphi_e - \alpha\psi_e &= \lambda\psi_e. \end{aligned} \tag{41}$$

The compatibility equation determining the eigenvalues and special nonlocal values of the eigenfunctions at threshold points a_e and a_i where $\psi_e(x) = (\frac{\alpha}{\lambda+\alpha})\varphi_e(x)$ is

$$(\mathbf{M}_{\mathrm{EI}} - \mathbf{I}_{\mathrm{EI}})\boldsymbol{\phi} = \begin{bmatrix} \lambda + \frac{\alpha\beta}{\lambda+\alpha} & 0 & 0 & 0 \\ 0 & \lambda + \frac{\alpha\beta}{\lambda+\alpha} & 0 & 0 \\ 0 & 0 & \lambda & 0 \\ 0 & 0 & 0 & \lambda \end{bmatrix} \boldsymbol{\phi}, \tag{42}$$

where $\mathbf{I}_{\rm EI} = \mathsf{diag}\,(1,\ 1,\ \tau^{-1},\ \tau^{-1})$, $a_{e\pm i} = a_e \pm a_i$,

$$\mathbf{M}_{\rm EI} = \begin{bmatrix} \mathcal{M}_{ee}(0) & \mathcal{M}_{ee}(2a_e) & -\mathcal{M}_{ei}(a_{e-i}) & -\mathcal{M}_{ei}(a_{e+i}) \\ \mathcal{M}_{ee}(2a_e) & \mathcal{M}_{ee}(0) & -\mathcal{M}_{ei}(a_{e+i}) & -\mathcal{M}_{ei}(a_{e-i}) \\ \frac{1}{\tau}\mathcal{M}_{ie}(a_{e-i}) & \frac{1}{\tau}\mathcal{M}_{ie}(a_{e+i}) & -\frac{1}{\tau}\mathcal{M}_{ii}(0) & -\frac{1}{\tau}\mathcal{M}_{ii}(2a_i) \\ \frac{1}{\tau}\mathcal{M}_{ie}(a_{e+i}) & \frac{1}{\tau}\mathcal{M}_{ie}(a_{e-i}) & -\frac{1}{\tau}\mathcal{M}_{ii}(2a_i) & -\frac{1}{\tau}\mathcal{M}_{ii}(0) \end{bmatrix},$$

$$\mathcal{M}_{jk}(x) = \frac{w_{jk}(x)}{|U_k'(a_k)|}, \quad \boldsymbol{\phi} = \begin{pmatrix} \varphi_e(+a_e) \\ \varphi_e(-a_e) \\ \varphi_i(+a_i) \\ \varphi_i(-a_i) \end{pmatrix}.$$

The following similarity transform yields

$$\mathbf{Q}^{-1}\mathbf{M}_{\rm EI}\mathbf{Q} = \mathbf{\Lambda}_{\rm EI} \equiv \begin{bmatrix} \mathbf{\Lambda}_{\rm EI}^{\oplus} & 0 \\ 0 & \mathbf{\Lambda}_{\rm EI}^{\ominus} \end{bmatrix},$$

$$\mathbf{Q} = \begin{bmatrix} 1 & 0 & 1 & 0 \\ 1 & 0 & -1 & 0 \\ 0 & 1 & 0 & 1 \\ 0 & 1 & 0 & -1 \end{bmatrix},$$

where

$$\mathbf{\Lambda}_{\rm EI}^{\pm} = \begin{bmatrix} \mathcal{M}_{ee}^{\pm}(a_e;a_e) & -\mathcal{M}_{ei}^{\pm}(a_e;a_i) \\ \frac{1}{\tau}\mathcal{M}_{ie}^{\pm}(a_i;a_e) & -\frac{1}{\tau}\mathcal{M}_{ii}^{\pm}(a_i;a_i) \end{bmatrix},$$

and $\mathcal{M}_{jk}^{\pm}(x;a_k) = \mathcal{M}_{jk}(x-a_k) \pm \mathcal{M}_{jk}(x+a_k)$.

Compatibility equation (42) can be rewritten as

$$(\mathbf{M}_{\rm EI} - \mathbf{D}(\lambda))\boldsymbol{\phi} = 0, \tag{43}$$

with $\mathbf{D}(\lambda) = \mathsf{diag}\,(1+\lambda+\frac{\alpha\beta}{\lambda+\alpha}, 1+\lambda+\frac{\alpha\beta}{\lambda+\alpha}, \frac{1}{\tau}+\lambda, \frac{1}{\tau}+\lambda)$. Nontrivial solutions $\boldsymbol{\phi}$ to Eq. (43) exist and yield eigenfunctions when

$$\begin{aligned}\det(\mathbf{M}_{\rm EI} - \mathbf{D}(\lambda)) &= \det\left(\mathbf{\Lambda}_{\rm EI}^{\oplus} - \widetilde{\mathbf{D}}(\lambda)\right)\cdot\det\left(\mathbf{\Lambda}_{\rm EI}^{\ominus} - \widetilde{\mathbf{D}}(\lambda)\right) \\ &= 0,\end{aligned}$$

where $\widetilde{\mathbf{D}}(\lambda) = \mathsf{diag}\,(1+\lambda+\frac{\alpha\beta}{\lambda+\alpha}, \frac{1}{\tau}+\lambda)$.

Two triads of eigenvalues satisfy the following pair ($\pm$) of cubic equations

$$\tau\lambda^3 + \Gamma^{\pm}\lambda^2 + \Delta^{\pm}\lambda + \mathrm{E}^{\pm} = 0,$$

where the coefficients are given by

$$\begin{aligned}\Gamma^{\pm} &= \tau\left[\alpha+1-\mathcal{M}_{ee}^{\pm}(a_e;a_e)\right] + \left[1+\mathcal{M}_{ii}^{\pm}(a_i;a_i)\right], \\ \Delta^{\pm} &= \left[\alpha+1-\mathcal{M}_{ee}^{\pm}(a_e;a_e)\right]\left[\tau\alpha+1+\mathcal{M}_{ii}^{\pm}(a_i;a_i)\right] \\ &\quad + \mathcal{M}_{ei}^{\pm}(a_e;a_i)\mathcal{M}_{ie}^{\pm}(a_i;a_e) + \tau\alpha(\beta-\alpha), \\ \mathrm{E}^{\pm} &= \alpha\left[\beta+1-\mathcal{M}_{ee}^{\pm}(a_e;a_e)\right]\left[1+\mathcal{M}_{ii}^{\pm}(a_i;a_i)\right] \\ &\quad + \alpha\left[\mathcal{M}_{ei}^{\pm}(a_e;a_i)\mathcal{M}_{ie}^{\pm}(a_i;a_e)\right].\end{aligned}$$

Solving Eq. (39) for the vector of special nonlocal values $\boldsymbol{\phi} = (\varphi_e(a_e), \varphi_e(-a_e), \varphi_i(a_i), \varphi_i(-a_i))^{\rm T} = (1, \pm 1, \nu^{\pm}, \pm\nu^{\pm})^{\rm T}$ we obtain

$$\nu^{\pm} = \frac{\lambda + \frac{\alpha}{\lambda+\alpha} + 1 - \mathcal{M}_{ee}^{\pm}(a_e;a_e)}{-\mathcal{M}_{ei}^{\pm}(a_e;a_i)}.$$

The spatial eigenfunctions $\boldsymbol{\varphi}(x)$ are given by

$$\boldsymbol{\varphi}(x) = \begin{pmatrix} \varphi_e \\ \varphi_i \\ \psi_e \end{pmatrix} = \begin{pmatrix} \frac{1}{\mu(\lambda^{\pm})}\left[\mathcal{M}_{ee}^{\pm}(x;a_e) - \nu^{\pm}\mathcal{M}_{ei}^{\pm}(x;a_i)\right] \\ \frac{1}{\tau\lambda^{\pm}+1}\left[\mathcal{M}_{ie}^{\pm}(x;a_e) - \nu^{\pm}\mathcal{M}_{ii}^{\pm}(x;a_i)\right] \\ \frac{\alpha}{\lambda^{\pm}+\alpha}\varphi_e(x) \end{pmatrix}$$

where

$$\begin{aligned}\mu(\lambda) &= \lambda + 1 + \frac{\alpha\beta}{\lambda+\alpha} \\ \mathcal{M}_{jk}^{\pm}(x;a_k) &= \Omega_{jk}^{\pm}(x;a_k)/|U_k'(a_k)| \\ \Omega_{jk}^{\pm}(x;a_k) &= w_{jk}(x-a_k) \pm w_{jk}(x+a_k).\end{aligned}$$

The $\oplus$ mode gives rise to expanding-contracting breathers and the $\ominus$ mode leads to side-to-side sloshers. See Fig. 8 for an example of a breather in the AE-I neural field that undergoes a period-doubling cascade to a breather that exhibits Rossler-band-like dynamics in a projection.

D. Interacting pair of AE/AI/AA neural fields

Case I: Symmetric case

A stationary bump solution to neural field equation (6) with the same widths a in each population can be expressed as $(u_1, u_2, n_1, n_2) = (U(x), V(x), N(x), M(x))$, where

$$\begin{aligned}(1+\beta)U(x) &= [W_{\rm loc}(x+a) - W_{\rm loc}(x-a)] \\ &\quad + [W_{\rm lay}(x+a) - W_{\rm lay}(x-a)] + I(x), \\ V(x) &= U(x), \\ N(x) &= U(x), \\ M(x) &= U(x),\end{aligned}$$

where a satisfies the threshold condition

$$W_{\rm loc}(2a) + W_{\rm lay}(2a) + I(a) = \theta(1+\beta),$$

provided the threshold behavior is obeyed on $(-\infty, \infty)$.

We note that it is possible to have a solution with a different size stationary bump in each population or a stationary bump in only one neural field only.

Perturbations $(\widetilde{\varphi}_1, \widetilde{\varphi}_2, \widetilde{\psi}_1, \widetilde{\psi}_2)(x,t)$ of the stationary bump $(U(x), V(x), N(x), M(x))$ evolve according to

$$\begin{aligned}\frac{\partial\widetilde{\varphi}_1}{\partial t} + \widetilde{\varphi}_1 &= \mathcal{N}_{\rm loc}\,\widetilde{\varphi}_1 + \mathcal{N}_{\rm lay}\,\widetilde{\varphi}_2 - \beta\widetilde{\psi}_1, \\ \frac{\partial\widetilde{\varphi}_2}{\partial t} + \widetilde{\varphi}_2 &= \mathcal{N}_{\rm loc}\,\widetilde{\varphi}_2 + \mathcal{N}_{\rm lay}\,\widetilde{\varphi}_1 - \beta\widetilde{\psi}_2, \\ \frac{1}{\alpha}\frac{\partial\widetilde{\psi}_1}{\partial t} + \widetilde{\psi}_1 &= \widetilde{\varphi}_1, \\ \frac{1}{\alpha}\frac{\partial\widetilde{\psi}_2}{\partial t} + \widetilde{\psi}_2 &= \widetilde{\varphi}_2.\end{aligned} \tag{44}$$

Setting $(\widetilde{\varphi}_1, \widetilde{\varphi}_2, \widetilde{\psi}_1, \widetilde{\psi}_2) = \boldsymbol{\varphi}(x)e^{\lambda t}$ results in the spectral problem for λ and $\boldsymbol{\varphi}(x) = (\varphi_1(x), \varphi_2(x), \psi_1(x), \psi_2(x))^{\rm T}$,

$$\begin{aligned}-\varphi_1 + \mathcal{N}_{\rm loc}\,\varphi_1 + \mathcal{N}_{\rm lay}\,\varphi_2 - \beta\psi_1 &= \lambda\varphi_1, \\ -\varphi_2 + \mathcal{N}_{\rm loc}\,\varphi_2 + \mathcal{N}_{\rm lay}\,\varphi_1 - \beta\psi_2 &= \lambda\varphi_2, \\ \alpha\varphi_1 - \alpha\psi_1 &= \lambda\psi_1, \\ \alpha\varphi_2 - \alpha\psi_2 &= \lambda\psi_2.\end{aligned} \tag{45}$$

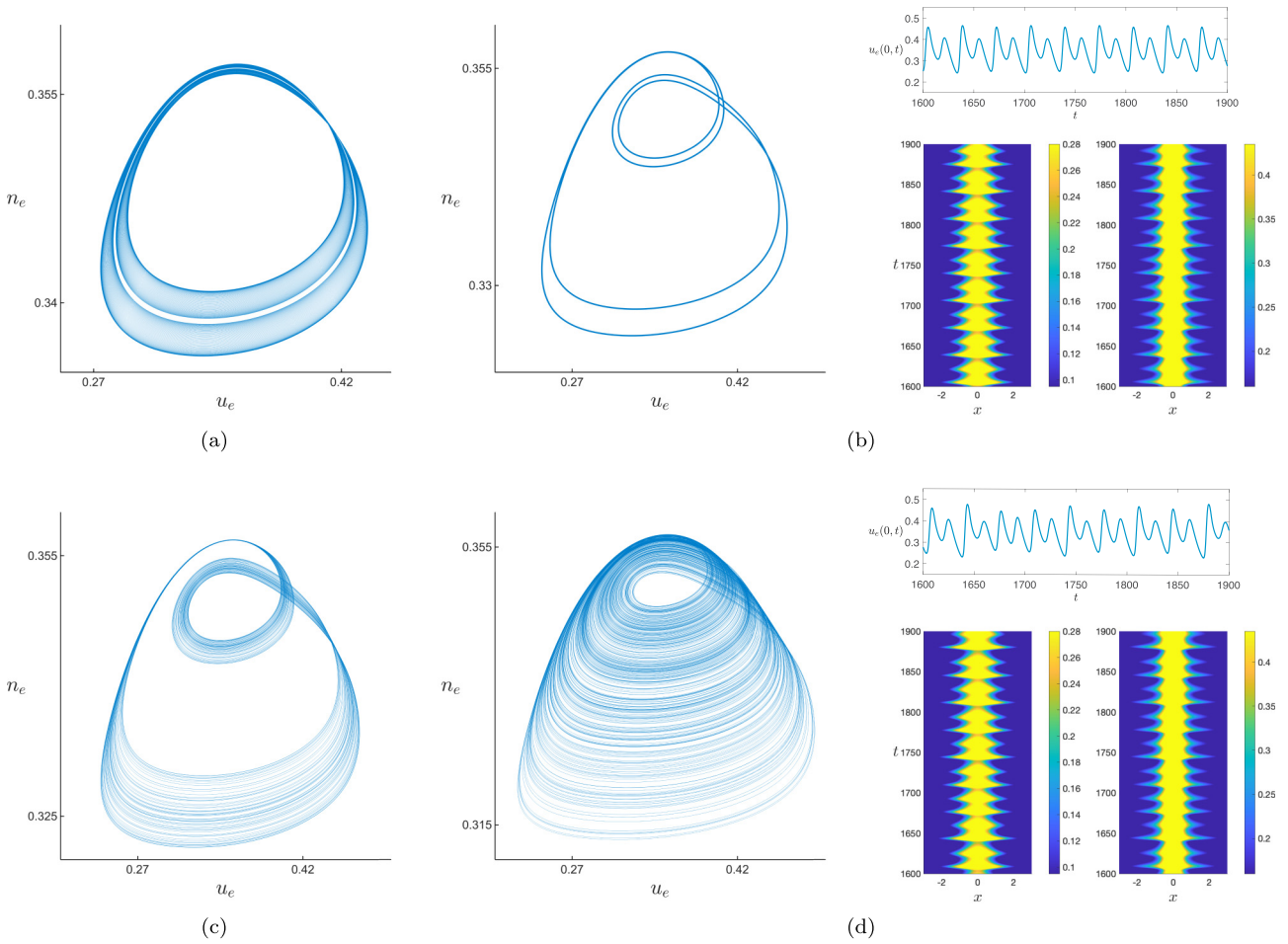

FIG. 8. Rossler band-like chaotic behavior observed in breathers in the AE-I neural field. In each figure, one orbit or trajectory of the AE-I neural field is plotted in the (u_e, n_e, u_i) phase space for one spatial point $x = 0$ (other spatial locations are similar). The u_i axis (not shown) is orthogonal to the figure. (a) At $\beta = 1.76$, the fine light blue orbit starts near an unstable period-1 breather (white ring) and approaches a stable period-2 orbit breather (dark blue). (b) Stable period-4 orbit breather at $\beta = 1.764$, (c) long term behavior at $\beta = 1.76437$. (d) Long-term behavior at $\beta = 1.764585$. Included in panels (b) and (d) are graphs of $u_e(0,t)$ and space-time plots of $u_e(x,t)$ (left) and $u_i(x,t)$ (right) for comparison.

Solving for

$$\psi_1(x) = \left(\frac{\alpha}{\lambda+\alpha}\right)\varphi_1(x),$$
$$\psi_2(x) = \left(\frac{\alpha}{\lambda+\alpha}\right)\varphi_2(x),$$

the compatibility equation determining both the eigenvalues and special nonlocal values $\boldsymbol{\phi}$ of the eigenfunctions at the common threshold points $x = \pm a$ is given by

$$(\mathbf{M}_{\mathrm{SYM}} - \mathbf{I})\boldsymbol{\phi} = \left(\lambda + \frac{\alpha\beta}{\lambda+\alpha}\right)\boldsymbol{\phi}, \tag{46}$$

where

$$\mathbf{M}_{\mathrm{SYM}} = \begin{bmatrix} \mathcal{M}_{\mathrm{loc}}(0) & \mathcal{M}_{\mathrm{loc}}(2a) & \mathcal{M}_{\mathrm{lay}}(0) & \mathcal{M}_{\mathrm{lay}}(2a) \\ \mathcal{M}_{\mathrm{loc}}(2a) & \mathcal{M}_{\mathrm{loc}}(0) & \mathcal{M}_{\mathrm{lay}}(2a) & \mathcal{M}_{\mathrm{lay}}(0) \\ \mathcal{M}_{\mathrm{lay}}(0) & \mathcal{M}_{\mathrm{lay}}(2a) & \mathcal{M}_{\mathrm{loc}}(0) & \mathcal{M}_{\mathrm{loc}}(2a) \\ \mathcal{M}_{\mathrm{lay}}(2a) & \mathcal{M}_{\mathrm{lay}}(0) & \mathcal{M}_{\mathrm{loc}}(2a) & \mathcal{M}_{\mathrm{loc}}(0) \end{bmatrix},$$

$$\mathcal{M}_j(x) = \frac{w_j(x)}{|U'(a)|}, \qquad \boldsymbol{\phi} = \begin{pmatrix} \varphi_1(+a) \\ \varphi_1(-a) \\ \varphi_2(+a) \\ \varphi_2(-a) \end{pmatrix}.$$

The following similarity transform yields:

$$\widetilde{\mathbf{Q}}^{-1}\mathbf{M}_{\mathrm{SYM}}\widetilde{\mathbf{Q}} = \mathbf{\Lambda}_{\mathrm{SYM}},$$

where

$$\mathbf{\Lambda}_{\mathrm{SYM}} = \begin{bmatrix} \mathcal{M}_+^{\oplus} & 0 & 0 & 0 \\ 0 & \mathcal{M}_-^{\oplus} & 0 & 0 \\ 0 & 0 & \mathcal{M}_+^{\ominus} & 0 \\ 0 & 0 & 0 & \mathcal{M}_-^{\ominus} \end{bmatrix},$$

$$\widetilde{\mathbf{Q}} = \begin{bmatrix} 1 & 1 & 1 & 1 \\ 1 & 1 & -1 & -1 \\ 1 & -1 & 1 & -1 \\ 1 & -1 & -1 & 1 \end{bmatrix},$$

where

$$\mathcal{M}^{\oplus}_{+} = \mathcal{M}^{\oplus}_{\rm loc}(a;a) + \mathcal{M}^{\oplus}_{\rm lay}(a;a),$$
$$\mathcal{M}^{\oplus}_{-} = \mathcal{M}^{\oplus}_{\rm loc}(a;a) - \mathcal{M}^{\oplus}_{\rm lay}(a;a),$$
$$\mathcal{M}^{\ominus}_{+} = \mathcal{M}^{\ominus}_{\rm loc}(a;a) + \mathcal{M}^{\ominus}_{\rm lay}(a;a),$$
$$\mathcal{M}^{\ominus}_{-} = \mathcal{M}^{\ominus}_{\rm loc}(a;a) - \mathcal{M}^{\ominus}_{\rm lay}(a;a),$$

and $\mathcal{M}^{\circledpm}_{l}(a;a) = \mathcal{M}_l(0) \pm \mathcal{M}_l(2a)$, where $l \in \{\text{loc, lay}\}$.

Compatibility equation (46) can be rewritten as

$$(\mathbf{M}_{\rm SYM} - \mu(\lambda)\mathbf{I})\boldsymbol{\phi} = 0, \tag{47}$$

where $\mu(\lambda) = (1 + \lambda + \frac{\alpha\beta}{\lambda+\alpha})$. Nontrivial solutions $\boldsymbol{\phi}$ to Eq. (47) exist yielding eigenfunctions if $\det(\mathbf{M}_{\rm SYM} - \mu(\lambda)\mathbf{I}) = 0$. Solving for μ and then λ in terms of μ we obtain

$$\lambda^{\circledpm}_{\pm} = -\Gamma \pm \sqrt{\Gamma^2 - \Delta}, \qquad \Gamma = \tfrac{1}{2}\big(1 + \alpha - \mu^{\circledpm}_{\pm}\big),$$
$$\mu^{\circledpm}_{\pm} = \mathcal{M}^{\circledpm}_{\rm loc}(a;a) \pm \mathcal{M}^{\circledpm}_{\rm lay}(a;a), \qquad \Delta = \alpha\big(1 + \beta - \mu^{\circledpm}_{\pm}\big).$$

There are four spatial eigenmodes corresponding to the four permutations of $\mu^{\circledpm}_{\pm}$ expressed succinctly as

$$\boldsymbol{\varphi}^{\circledpm}_{\pm}(x) = \begin{pmatrix}\varphi_1\\ \varphi_2\\ \psi_1\\ \psi_2\end{pmatrix} = \begin{pmatrix}1\\ \pm 1\\ \frac{\alpha}{\lambda^{\circledpm}_{\pm}+\alpha}\\ \frac{\pm\alpha}{\lambda^{\circledpm}_{\pm}+\alpha}\end{pmatrix}\big(\mathcal{M}^{\circledpm}_{\rm loc}(x;a) \pm \mathcal{M}^{\circledpm}_{\rm lay}(x;a)\big),$$

$$\mathcal{M}^{\circledpm}_{l}(x;a) = \Omega^{\circledpm}_{l}(x;a)/|U'(a)|,$$
$$\Omega^{\circledpm}_{l}(x;a) = w_l(x-a) \pm w_l(x+a).$$

Graphs of $\mathcal{M}^{\circledpm}_{loc}(x;a) \pm \mathcal{M}^{\circledpm}_{lay}(x;a)$ in Fig. 9 reveal the spatial structure of the four different eigenmodes $\mu^{\circledpm}_{\pm}$.

At a Hopf bifurcation point, the Hopf frequency is

$$\omega_H = \mathrm{Im}\{\lambda^{\circledpm}_{\pm}\} = \sqrt{\alpha(\beta - \alpha)}.$$

Condition for Hopf bifurcation of the $\mu^{\circledpm}_{\pm}$ mode

In the absence of any input ($I = 0$), the difference mode $\mu^{\ominus}_{+}$ has one persistent 0 eigenvalue, reflecting the translation invariance of the stationary bump, and a second real eigenvalue. Only the other three eigenmodes can undergo Hopf bifurcation. In the presence of an input inhomogeneity where $I(x) \neq 0$, the eigenvalues are nonzero generically, and it is possible for all four eigenmodes to have complex eigenvalues and destabilize in a Hopf bifurcation.

Below we describe a condition for determining which mode $\mu^{\circledpm}_{\pm}$ destabilizes first, assuming all eigenmodes are complex, by identifying a dominate eigenvalue that has the larger real part of two pairs of complex eigenvalues. The opposite case occurs when the inequality is switched.

In-phase mode $\mu^{\circledpm}_{+}$ dominates antiphase mode $\mu^{\circledpm}_{-}$ if

$$w_{\rm lay}(0) \pm w_{\rm lay}(2a) > 0.$$

Sum mode $\mu^{\oplus}_{\pm}$ dominates difference mode $\mu^{\ominus}_{\pm}$ when

$$w_{\rm loc}(2a) \pm w_{\rm lay}(2a) > 0.$$

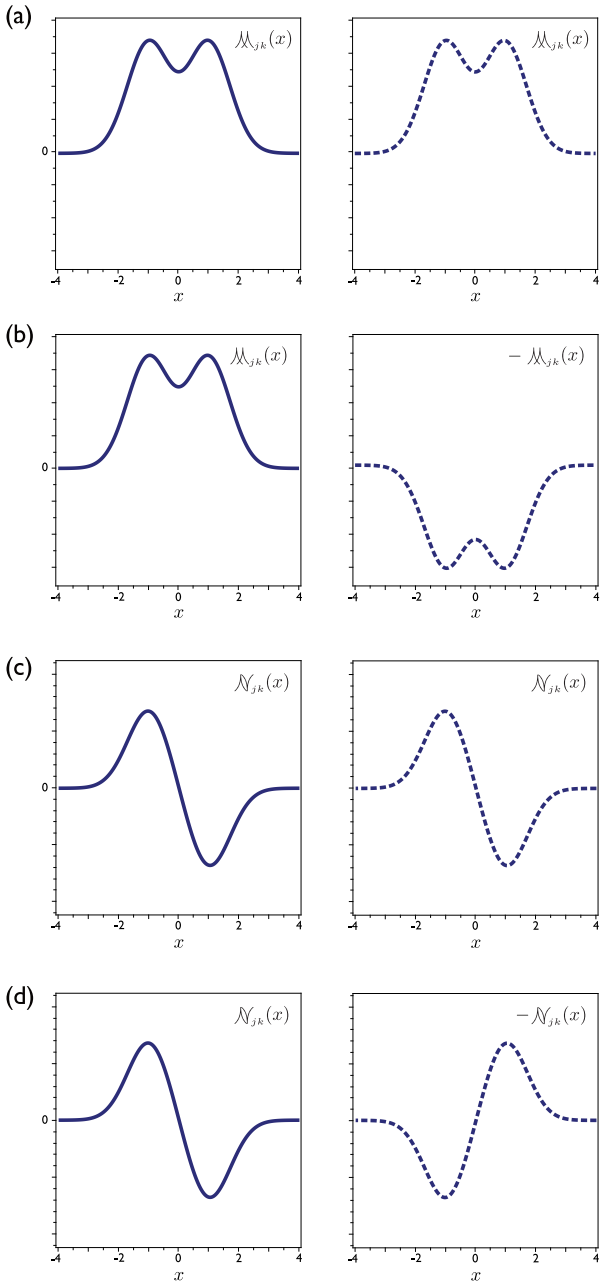

FIG. 9. Structure of the eigenmodes ($(\varphi_1(x), \varphi_2(x))$ only) associated with $\mu^{\circledpm}_{\pm}$ depends on terms $\mathcal{M}_{jk}(x)$ in the sum ($\oplus$) mode and $\mathcal{N}_{jk}(x)$ in the difference ($\ominus$) mode. (a) Sum mode $\mu^{\oplus}_{+}$ leads to *in-phase* breathers, (b) sum mode $\mu^{\oplus}_{-}$ leads to antiphase breathers, (c) difference mode $\mu^{\ominus}_{+}$ leads to *in-phase* sloshers, (d) difference mode $\mu^{\ominus}_{-}$ leads to *antiphase* sloshers.

Sum mode $\mu^{\oplus}_{\pm}$ dominates difference mode $\mu^{\ominus}_{\mp}$ when

$$w_{\rm loc}(2a) \pm w_{\rm lay}(0) > 0,$$

extending the case of $w_{\rm loc}(2a)$ in the AA neural field. Note that the case $-w_{\rm lay}(x) > +w_{\rm lay}(x)$ occurs only when $w_{\rm lay}(x) < 0$. Figure 10 illustrates in-phase and antiphase breathers and sloshers bifurcating from eigenmodes $\mu^{\circledpm}_{\pm}$.

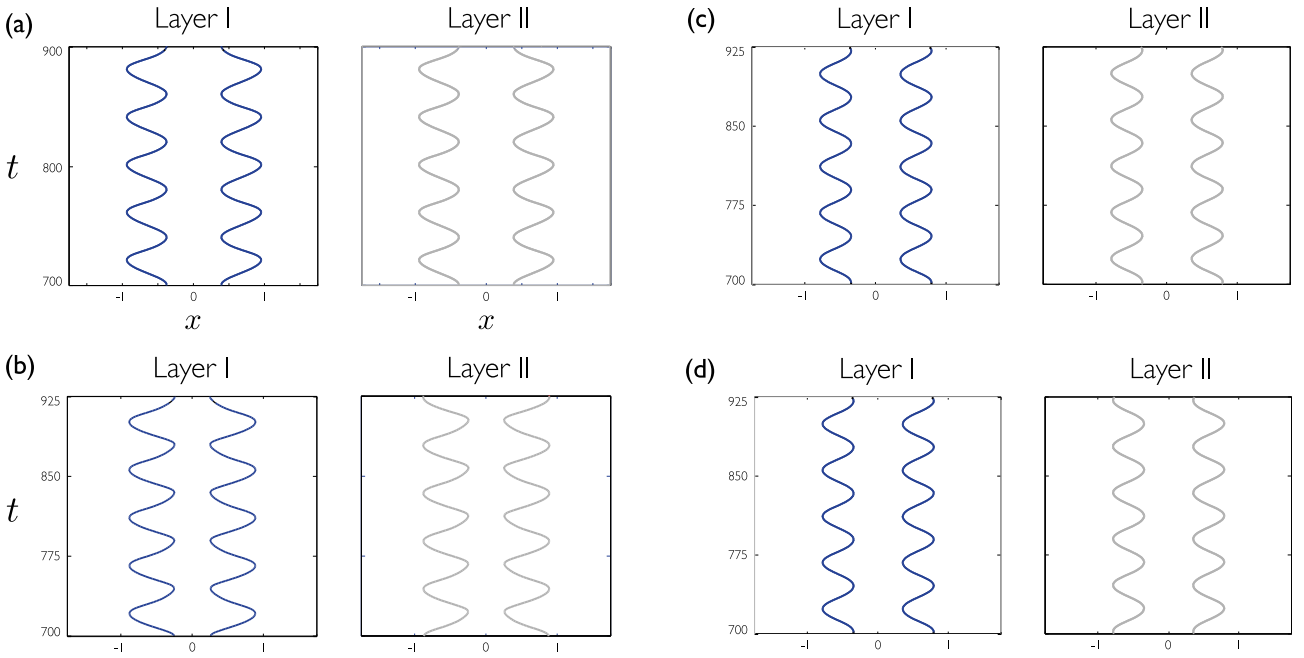

FIG. 10. Graphs of *in-phase* and *antiphase* breathers and sloshers in an interacting pair of symmetric AE/AI/AA neural fields due to destabilization of the $\mu_{\pm}^{\oplus}$ eigenmodes (depicted in Fig. 9) in a Hopf bifurcation. Destabilization of (a) sum mode $\mu_{+}^{\oplus}$ leads to *in-phase* breathers, (b) sum mode $\mu_{-}^{\oplus}$ leads to *antiphase* breathers, (c) difference mode $\mu_{+}^{\ominus}$ leads to *in-phase* sloshers, and (d) difference mode $\mu_{-}^{\ominus}$ leads to *antiphase* sloshers. Curves indicate the threshold contours of activity variables u_1 and u_2.

Case II: Asymmetric case

A stationary bump solution to neural field equation (7) with different widths a_1 and a_2 in each population is expressed as $(u_1, u_2, n_1, n_2) = (U_1(x), U_2(x), N_1(x), N_2(x))$, where

$$\begin{aligned}(1+\beta)U_1(x) &= \left[W_{11}^{\rm loc}(x+a_1) - W_{11}^{\rm loc}(x-a_1)\right] \\ &\quad + \left[W_{12}^{\rm lay}(x+a_2) - W_{12}^{\rm lay}(x-a_2)\right] + I_1(x)\big], \\ (1+\beta)U_2(x) &= \left[W_{22}^{\rm loc}(x+a_2) - W_{22}^{\rm loc}(x-a_2)\right] \\ &\quad + \left[W_{21}^{\rm lay}(x+a_1) - W_{21}^{\rm lay}(x-a_1)\right] + I_2(x), \\ N_1(x) &= U_1(x), \\ N_2(x) &= U_2(x),\end{aligned}$$

where a_1 and a_2 satisfy the threshold condition

$$\begin{aligned}W_{11}^{\rm loc}(2a_1) + W_{12}^{\rm lay}(a_1+a_2) - W_{12}^{\rm lay}(a_1-a_2) + I_1(a_1) &= \widetilde{\theta}_1, \\ W_{22}^{\rm loc}(2a_2) + W_{21}^{\rm lay}(a_2+a_1) - W_{21}^{\rm lay}(a_2-a_1) + I_2(a_2) &= \widetilde{\theta}_2,\end{aligned}$$

where $\widetilde{\theta}_1 = \theta_1(1+\beta)$ and $\widetilde{\theta}_2 = \theta_2(1+\beta)$ provided the threshold behavior is obeyed on $(-\infty, \infty)$.

Perturbations $(\widetilde{\varphi}_1, \widetilde{\varphi}_2, \widetilde{\psi}_1, \widetilde{\psi}_2)(x,t)$ of the stationary bump $(U_1(x), U_2(x), N_1(x), N_2(x))$ evolve according to

$$\begin{aligned}\frac{\partial \widetilde{\varphi}_1}{\partial t} + \widetilde{\varphi}_1 &= \mathcal{N}_{11}^{\rm loc}\,\widetilde{\varphi}_1 + \mathcal{N}_{12}^{\rm lay}\,\widetilde{\varphi}_2 - \beta\widetilde{\psi}_1, \\ \frac{\partial \widetilde{\varphi}_2}{\partial t} + \widetilde{\varphi}_2 &= \mathcal{N}_{22}^{\rm loc}\,\widetilde{\varphi}_2 + \mathcal{N}_{21}^{\rm lay}\,\widetilde{\varphi}_1 - \beta\widetilde{\psi}_2, \\ \frac{1}{\alpha}\frac{\partial \widetilde{\psi}_1}{\partial t} + \widetilde{\psi}_1 &= \widetilde{\varphi}_1, \\ \frac{1}{\alpha}\frac{\partial \widetilde{\psi}_2}{\partial t} + \widetilde{\psi}_2 &= \widetilde{\varphi}_2.\end{aligned} \tag{48}$$

Setting $(\widetilde{\varphi}_1, \widetilde{\varphi}_2, \widetilde{\psi}_1, \widetilde{\psi}_2) = \boldsymbol{\varphi}(x)e^{\lambda t}$ yields the spectral problem for λ and $\boldsymbol{\varphi}(x) = (\varphi_1(x), \varphi_2(x), \psi_1(x), \psi_2(x))^{\rm T}$,

$$\begin{aligned}-\varphi_1 + \mathcal{N}_{11}^{\rm loc}\,\varphi_1 + \mathcal{N}_{12}^{\rm lay}\,\varphi_2 - \beta\psi_1 &= \lambda\varphi_1, \\ -\varphi_2 + \mathcal{N}_{22}^{\rm loc}\,\varphi_2 + \mathcal{N}_{21}^{\rm lay}\,\varphi_1 - \beta\psi_2 &= \lambda\varphi_2, \\ \alpha\varphi_1 - \alpha\psi_1 &= \lambda\psi_1, \\ \alpha\varphi_2 - \alpha\psi_2 &= \lambda\psi_2.\end{aligned} \tag{49}$$

Similarly, the compatibility equation determining the eigenvalues and special nonlocal values of the eigenfunctions at threshold points $\pm a_1$ and $\pm a_2$ is

$$(\mathbf{M}_{\rm ASYM} - \mathbf{I})\boldsymbol{\phi} = \left(\lambda + \frac{\alpha\beta}{\lambda+\alpha}\right)\boldsymbol{\phi}, \tag{50}$$

where $b = a_1 - a_2$ and $c = a_1 + a_2$,

$$\mathbf{M}_{\rm ASYM} = \begin{bmatrix} \mathcal{M}_{11}^{\rm loc}(0) & \mathcal{M}_{11}^{\rm loc}(2a_1) & \mathcal{M}_{12}^{\rm lay}(b) & \mathcal{M}_{12}^{\rm lay}(c) \\ \mathcal{M}_{11}^{\rm loc}(2a_1) & \mathcal{M}_{11}^{\rm loc}(0) & \mathcal{M}_{12}^{\rm lay}(c) & \mathcal{M}_{12}^{\rm lay}(b) \\ \mathcal{M}_{21}^{\rm lay}(b) & \mathcal{M}_{21}^{\rm lay}(c) & \mathcal{M}_{22}^{\rm loc}(0) & \mathcal{M}_{22}^{\rm loc}(2a_2) \\ \mathcal{M}_{21}^{\rm lay}(c) & \mathcal{M}_{21}^{\rm lay}(b) & \mathcal{M}_{22}^{\rm loc}(2a_2) & \mathcal{M}_{22}^{\rm loc}(0) \end{bmatrix},$$

and

$$\mathcal{M}_{jk}^{l}(x) = \frac{w_{jk}^{l}(x)}{|U_k'(a_k)|}, \qquad \boldsymbol{\phi} = \begin{pmatrix} \varphi_1(+a_1) \\ \varphi_1(-a_1) \\ \varphi_2(+a_2) \\ \varphi_2(-a_2) \end{pmatrix}.$$

The following similarity transform yields

$$\mathbf{Q}^{-1}\mathbf{M}_{\mathrm{ASYM}}\mathbf{Q} = \begin{bmatrix} \mathbf{\Lambda}^{\oplus} & 0 \\ 0 & \mathbf{\Lambda}^{\ominus} \end{bmatrix},$$
$$\mathbf{Q} = \begin{bmatrix} 1 & 0 & 1 & 0 \\ 1 & 0 & -1 & 0 \\ 0 & 1 & 0 & 1 \\ 0 & 1 & 0 & -1 \end{bmatrix},$$
$$\mathbf{\Lambda}^{\circledpm} = \begin{bmatrix} \mathcal{M}_{11}^{\circledpm}(a_1;a_1) & \mathcal{M}_{12}^{\circledpm}(a_1;a_2) \\ \mathcal{M}_{21}^{\circledpm}(a_2;a_1) & \mathcal{M}_{22}^{\circledpm}(a_2;a_2) \end{bmatrix},$$

where for $j,k=1,2$ $(k\neq j)$,

$$\mathcal{M}_{jj}^{\circledpm}(a_j;a_j) = \mathcal{M}_{jj}^{\mathrm{loc}}(0) \pm \mathcal{M}_{jj}^{\mathrm{loc}}(2a_j),$$
$$\mathcal{M}_{jk}^{\circledpm}(a_j;a_k) = \mathcal{M}_{jk}^{\mathrm{lay}}(a_j-a_k) \pm \mathcal{M}_{jk}^{\mathrm{lay}}(a_j+a_k).$$

Compatibility equation (50) can be rewritten as

$$(\mathbf{M}_{\mathrm{ASYM}} - \mu(\lambda)\mathbf{I})\boldsymbol{\phi} = 0, \tag{51}$$

where $\mu(\lambda) = 1+\lambda+\frac{\alpha\beta}{\lambda+\alpha}$. For nontrivial values $\boldsymbol{\phi}$ to exist, we require $\mathsf{det}(\mathbf{M}_{\mathrm{ASYM}} - \mu(\lambda)\mathbf{I}) = 0$. Solving for such μ and then solving for λ in terms of μ we obtain

$$\lambda_{\pm}^{\circledpm} = -\Gamma \pm \sqrt{\Gamma^2-\Delta}, \quad \Gamma = \frac{1}{2}\big(1+\alpha-\mu_{\pm}^{\circledpm}\big), \quad \Delta = \alpha\big(1+\beta-\mu_{\pm}^{\circledpm}\big),$$
$$\mu_{\pm}^{\circledpm} = \left[\frac{\mathcal{M}_{11}^{\circledpm}+\mathcal{M}_{22}^{\circledpm}}{2}\right] \pm \sqrt{\left[\frac{\mathcal{M}_{11}^{\circledpm}-\mathcal{M}_{22}^{\circledpm}}{2}\right]^2 + \mathcal{M}_{12}^{\circledpm}\mathcal{M}_{21}^{\circledpm}},$$

where $\mathcal{M}_{jk}^{\circledpm} = \mathcal{M}_{jk}^{\circledpm}(a_j;a_k)$. This defines four pairs of eigenvalues corresponding to the four spatial eigenmodes associated with $\mu_{\pm}^{\circledpm}$. We note here that the condition for $\mu_{\pm}^{\circledpm}$ to be complex-valued is given by

$$\mathcal{M}_{12}^{\circledpm}(a_1;a_2)\,\mathcal{M}_{21}^{\circledpm}(a_2;a_1) < -\left[\frac{\mathcal{M}_{11}^{\circledpm}(a_1;a_1) - \mathcal{M}_{22}^{\circledpm}(a_2;a_2)}{2}\right]^2,$$

which requires $\mathcal{M}_{12}^{\circledpm}(a_1;a_2)$ or $\mathcal{M}_{21}^{\circledpm}(a_2;a_1)$ be negative. Solving Eq. (51) yields the vector of nonlocal values

$$\boldsymbol{\phi} = (\varphi_1(-a_1), \varphi_1(a_1), \varphi_2(a_2), \varphi_2(-a_2)) = (1, \pm 1, \nu_{\pm}^{\circledpm}, \pm\nu_{\pm}^{\circledpm}),$$
$$\nu_{\pm}^{\circledpm} = \frac{\mu_{\pm}^{\circledpm} - \mathcal{M}_{11}^{\circledpm}(a_1;a_1)}{\mathcal{M}_{12}^{\circledpm}(a_1;a_2)} = \frac{\left[\frac{\mathcal{M}_{11}^{\circledpm}-\mathcal{M}_{22}^{\circledpm}}{2}\right] \pm \sqrt{\left[\frac{\mathcal{M}_{11}^{\circledpm}-\mathcal{M}_{22}^{\circledpm}}{2}\right]^2 + \mathcal{M}_{12}^{\circledpm}\mathcal{M}_{21}^{\circledpm}}}{\mathcal{M}_{12}^{\circledpm}}.$$

The spatial eigenfunctions $\boldsymbol{\varphi}(x)$ are given by

$$\boldsymbol{\varphi}_{\pm}^{\circledpm}(x) = \begin{pmatrix} \varphi_1(x) \\ \varphi_2(x) \\ \psi_1(x) \\ \psi_2(x) \end{pmatrix} = \begin{pmatrix} \mathcal{M}_{11}^{\circledpm}(x;a_1) + \nu_{\pm}^{\circledpm}\mathcal{M}_{12}^{\circledpm}(x;a_2) \\ \nu_{\pm}^{\circledpm}\mathcal{M}_{22}^{\circledpm}(x;a_2) + \mathcal{M}_{21}^{\circledpm}(x;a_1) \\ \frac{\alpha}{\lambda^{\circledpm}+\alpha}\varphi_1(x) \\ \frac{\alpha}{\lambda^{\circledpm}+\alpha}\varphi_2(x) \end{pmatrix},$$
$$\mathcal{M}_{jk}^{\circledpm}(x;a_k) = \Omega_{jk}^{\circledpm}(x;a_k)/|U_k'(a_k)|,$$
$$\Omega_{jk}^{\circledpm}(x;a_k) = w_{jk}^{l}(x-a_k) \pm w_{jk}^{l}(x+a_k).$$

At a Hopf bifurcation point the Hopf frequency is

$$\omega_H = \mathsf{Im}\{\lambda_{\pm}^{\circledpm}\} = \sqrt{\alpha(\beta-\alpha)}.$$

E. Interacting pair of EI neural fields

A stationary bump solution to neural field (8) can be expressed as $(u_e,u_i,v_e,v_i) = (U_e(x),U_i(x),V_e(x),V_i(x))$, where the solution is identical in each neural field layer and expressed as

$$\begin{aligned} U_e(x) &= \big[W_{ee}^{\mathrm{loc}}(x+a_e) - W_{ee}^{\mathrm{loc}}(x-a_e)\big] \\ &\quad - \big[W_{ei}^{\mathrm{loc}}(x+a_i) - W_{ei}^{\mathrm{loc}}(x-a_i)\big] \\ &\quad + \big[W_{ee}^{\mathrm{lay}}(x+a_e) - W_{ee}^{\mathrm{lay}}(x-a_e)\big] + I_e(x), \\ U_i(x) &= \big[W_{ie}^{\mathrm{loc}}(x+a_e) - W_{ie}^{\mathrm{loc}}(x-a_e)\big] \\ &\quad - \big[W_{ii}^{\mathrm{loc}}(x+a_i) - W_{ii}^{\mathrm{loc}}(x-a_i)\big] \\ &\quad + \big[W_{ie}^{\mathrm{lay}}(x+a_e) - W_{ie}^{\mathrm{lay}}(x-a_e)\big] + I_i(x), \\ V_e(x) &= U_e(x), \\ V_i(x) &= U_i(x), \end{aligned}$$

where a_e and a_i satisfy the threshold conditions

$$\begin{aligned} &W_{ee}^{\mathrm{loc}}(2a_e) - W_{ei}^{\mathrm{loc}}(a_e+a_i) + W_{ei}^{\mathrm{loc}}(a_e-a_i) \\ &\quad + W_{ee}^{\mathrm{lay}}(2a_e) + I_e(a_e) = \theta_e, \\ &W_{ie}^{\mathrm{loc}}(a_i+a_e) - W_{ie}^{\mathrm{loc}}(a_i-a_e) - W_{ii}^{\mathrm{loc}}(2a_i) \\ &\quad + W_{ie}^{\mathrm{lay}}(a_i+a_e) - W_{ie}^{\mathrm{lay}}(a_i-a_e) + I_i(a_i) = \theta_i. \end{aligned}$$

Perturbations $(\widetilde{\varphi}_e,\widetilde{\varphi}_i,\widetilde{\psi}_e,\widetilde{\psi}_i)(x,t)$ of the stationary bump $(U_e(x),U_i(x),V_e(x),V_i(x))$ evolve according to

$$\frac{\partial\widetilde{\varphi}_e}{\partial t} + \widetilde{\varphi}_e = \mathcal{N}_{ee}^{\mathrm{loc}}\,\widetilde{\varphi}_e - \mathcal{N}_{ei}^{\mathrm{loc}}\,\widetilde{\varphi}_i + \mathcal{N}_{ee}^{\mathrm{lay}}\,\widetilde{\psi}_e,$$
$$\tau\frac{\partial\widetilde{\varphi}_i}{\partial t} + \widetilde{\varphi}_i = \mathcal{N}_{ie}^{\mathrm{loc}}\,\widetilde{\varphi}_e - \mathcal{N}_{ii}^{\mathrm{loc}}\,\widetilde{\varphi}_i + \mathcal{N}_{ie}^{\mathrm{lay}}\,\widetilde{\psi}_e,$$

$$\frac{\partial\widetilde{\psi}_e}{\partial t}+\widetilde{\psi}_e=\mathcal{N}_{ee}^{\rm loc}\,\widetilde{\psi}_e-\mathcal{N}_{ei}^{\rm loc}\,\widetilde{\psi}_i+\mathcal{N}_{ee}^{\rm lay}\,\widetilde{\varphi}_e,$$
$$\tau\frac{\partial\widetilde{\psi}_i}{\partial t}+\widetilde{\psi}_i=\mathcal{N}_{ie}^{\rm loc}\,\widetilde{\psi}_e-\mathcal{N}_{ii}^{\rm loc}\,\widetilde{\psi}_i+\mathcal{N}_{ie}^{\rm lay}\,\widetilde{\varphi}_e. \tag{52}$$

Setting $(\widetilde{\varphi}_e,\widetilde{\varphi}_i,\widetilde{\psi}_e,\widetilde{\psi}_i)=\boldsymbol{\varphi}(x)e^{\lambda t}$ yields the spectral problem for λ and $\boldsymbol{\varphi}(x)=(\varphi_e(x),\varphi_i(x),\psi_e(x),\psi_i(x))^{\rm T}$,

$$\begin{aligned}
-\varphi_e+\mathcal{N}_{ee}^{\rm loc}\,\varphi_e-\mathcal{N}_{ei}^{\rm loc}\,\varphi_i+\mathcal{N}_{ee}^{\rm lay}\,\psi_e&=\lambda\varphi_e,\\
-\frac{1}{\tau}\varphi_i+\frac{1}{\tau}\mathcal{N}_{ie}^{\rm loc}\,\varphi_e-\frac{1}{\tau}\mathcal{N}_{ii}^{\rm loc}\,\varphi_i+\frac{1}{\tau}\mathcal{N}_{ie}^{\rm lay}\,\psi_e&=\lambda\varphi_i,\\
-\psi_e+\mathcal{N}_{ee}^{\rm loc}\,\psi_e-\mathcal{N}_{ei}^{\rm loc}\,\psi_i+\mathcal{N}_{ee}^{\rm lay}\,\varphi_e&=\lambda\psi_e,\\
-\frac{1}{\tau}\psi_i+\frac{1}{\tau}\mathcal{N}_{ie}^{\rm loc}\,\psi_e-\frac{1}{\tau}\mathcal{N}_{ii}^{\rm loc}\,\psi_i+\frac{1}{\tau}\mathcal{N}_{ie}^{\rm lay}\,\varphi_e&=\lambda\psi_i.
\end{aligned}\tag{53}$$

The compatibility equation determining both the eigenvalues and special nonlocal values of the eigenfunctions at threshold points $x=\pm a_e$ and $\pm a_i$ is

$$(\mathbf{M}_{\rm dual}-\mathbf{I}_{\rm dual})\mathbf{\Phi}=\lambda\,\mathbf{\Phi}, \tag{54}$$

where $\mathbf{M}_{\rm dual}$ is an (8×8) matrix represented in block form

$$\mathbf{M}_{\rm dual}=\begin{bmatrix}\mathbf{M}_{\rm EI} & \mathbf{M}_{\rm lay}\\ \mathbf{M}_{\rm lay} & \mathbf{M}_{\rm EI}\end{bmatrix},\qquad \mathbf{\Phi}=\begin{pmatrix}\boldsymbol{\phi}\\ \boldsymbol{\psi}\end{pmatrix},$$

and $\mathbf{\Phi}$ is an (8×1) vector in block form where

$$\boldsymbol{\phi}=\begin{pmatrix}\varphi_e(+a_e)\\ \varphi_e(-a_e)\\ \varphi_i(+a_i)\\ \varphi_i(-a_i)\end{pmatrix},\quad \boldsymbol{\psi}=\begin{pmatrix}\psi_e(+a_e)\\ \psi_e(-a_e)\\ \psi_i(+a_i)\\ \psi_i(-a_i)\end{pmatrix}.$$

$$\mathbf{I}_{\rm dual}=\mathsf{diag}\,(1,\ 1,\ \tau^{-1},\ \tau^{-1},\ 1,\ 1,\ \tau^{-1}\,\tau^{-1}),$$

$$\mathbf{M}_{\rm EI}=\begin{bmatrix}\mathcal{M}_{ee}(0) & \mathcal{M}_{ee}(2a_e) & -\mathcal{M}_{ei}(a_{e-i}) & -\mathcal{M}_{ei}(a_{e+i})\\ \mathcal{M}_{ee}(2a_e) & \mathcal{M}_{ee}(0) & -\mathcal{M}_{ei}(a_{e+i}) & -\mathcal{M}_{ei}(a_{e-i})\\ \frac{1}{\tau}\mathcal{M}_{ie}(a_{e-i}) & \frac{1}{\tau}\mathcal{M}_{ie}(a_{e+i}) & -\frac{1}{\tau}\mathcal{M}_{ii}(0) & -\frac{1}{\tau}\mathcal{M}_{ii}(2a_i)\\ \frac{1}{\tau}\mathcal{M}_{ie}(a_{e+i}) & \frac{1}{\tau}\mathcal{M}_{ie}(a_{e-i}) & -\frac{1}{\tau}\mathcal{M}_{ii}(2a_i) & -\frac{1}{\tau}\mathcal{M}_{ii}(0)\end{bmatrix},$$

$$\mathbf{M}_{\rm lay}=\begin{bmatrix}\mathcal{M}_{ee}^{\rm lay}(0) & \mathcal{M}_{ee}^{\rm lay}(2a_e) & 0 & 0\\ \mathcal{M}_{ee}^{\rm lay}(2a_e) & \mathcal{M}_{ee}^{\rm lay}(0) & 0 & 0\\ \frac{1}{\tau}\mathcal{M}_{ie}^{\rm lay}(a_i-a_e) & \frac{1}{\tau}\mathcal{M}_{ie}^{\rm lay}(a_i+a_e) & 0 & 0\\ \frac{1}{\tau}\mathcal{M}_{ie}^{\rm lay}(a_i+a_e) & \frac{1}{\tau}\mathcal{M}_{ie}^{\rm lay}(a_i-a_e) & 0 & 0\end{bmatrix},$$

where $\mathcal{M}_{jk}^{l}(x)=w_{jk}^{l}(x)/|U'(a_k)|$ and $a_{e\pm i}=a_e\pm a_i$.

$\mathbf{M}_{\rm dual}$ is block diagonalized by a similarity transformation

$$\widetilde{\mathbf{Q}}^{-1}\mathbf{M}_{\rm dual}\widetilde{\mathbf{Q}}=\mathbf{\Lambda}_{\rm dual},\qquad \widetilde{\mathbf{Q}}=\begin{bmatrix}\mathbf{Q} & \mathbf{Q}\\ \mathbf{Q} & -\mathbf{Q}\end{bmatrix},$$

where

$$\mathbf{\Lambda}_{\rm dual}=\begin{bmatrix}\mathbf{\Lambda}_+^{\oplus} & 0 & 0 & 0\\ 0 & \mathbf{\Lambda}_+^{\ominus} & 0 & 0\\ 0 & 0 & \mathbf{\Lambda}_-^{\oplus} & 0\\ 0 & 0 & 0 & \mathbf{\Lambda}_-^{\ominus}\end{bmatrix},$$
$$\mathbf{Q}=\begin{bmatrix}1 & 0 & 1 & 0\\ 1 & 0 & -1 & 0\\ 0 & 1 & 0 & 1\\ 0 & 1 & 0 & -1\end{bmatrix},$$

$$\mathbf{\Lambda}_{\pm}^{\oplus}=\begin{bmatrix}\mathcal{M}_{ee}^{\oplus}(a_e;a_e)\pm\mathcal{M}_{ee}^{\oplus\,\rm lay}(a_e;a_e) & -\mathcal{M}_{ei}^{\oplus}(a_e;a_i)\\ \frac{1}{\tau}\mathcal{M}_{ie}^{\oplus}(a_i;a_e)\pm\frac{1}{\tau}\mathcal{M}_{ie}^{\oplus\,\rm lay}(a_i;a_e) & -\frac{1}{\tau}\mathcal{M}_{ii}^{\oplus}(a_i;a_i)\end{bmatrix},$$

$$\begin{aligned}
\mathcal{M}_{jj}^{\oplus}(a_j;a_j)&=\mathcal{M}_{jj}(0)\pm\mathcal{M}_{jj}(2a_j),\\
\mathcal{M}_{jk}^{\oplus}(a_j;a_k)&=\mathcal{M}_{jk}(a_j-a_k)\pm\mathcal{M}_{jk}(a_j+a_k),\\
\mathcal{M}_{jk}^{\oplus\rm lay}(a_j;a_k)&=\mathcal{M}_{jk}^{\rm lay}(a_j-a_k)\pm\mathcal{M}_{jk}^{\rm lay}(a_j+a_k).
\end{aligned}$$

Nonzero solutions of Eq. (54) exist if $\mathsf{det}(\mathbf{M}_{\rm dual}-\mathbf{I}_{\rm dual}-\lambda\mathrm{I})=0$, generating four pairs of eigenvalues λ corresponding to the four different spatial eigenmodes associated with $\mathbf{\Lambda}_{\pm}^{\oplus}$

$$\lambda_{\pm}^{\oplus}=\left[\frac{\mathcal{M}_{\pm,ee}^{\oplus}-1}{2}-\frac{\mathcal{M}_{ii}^{\oplus}+1}{2\tau}\right]\pm\sqrt{\left[\frac{\mathcal{M}_{\pm,ee}^{\oplus}-1}{2}+\frac{\mathcal{M}_{ii}^{\oplus}+1}{2\tau}\right]^2-\frac{\mathcal{M}_{\pm,ie}^{\oplus}\mathcal{M}_{ei}^{\oplus}}{\tau}},$$

where

$$\mathcal{M}_{\pm,jk}^{\oplus}(a_j;a_k)=\mathcal{M}_{jk}^{\oplus}(a_j;a_k)\pm\mathcal{M}_{jk}^{\oplus\,\rm lay}(a_j;a_k).$$

Each *pair* of eigenvalues is denoted by $\pm$ preceding the root. The associated vector $\mathbf{\Phi}$ of special nonlocal values is $\mathbf{\Phi}_{\pm}^{\oplus}=(\boldsymbol{\phi}^{\oplus},\pm\boldsymbol{\phi}^{\oplus})^{\rm T}$ where $\boldsymbol{\phi}^{\oplus}=(1,(\pm1),\nu_{\pm}^{\oplus},(\pm1)\nu_{\pm}^{\oplus})^{\rm T}$,

$$\nu_{\pm}^{\oplus}=\frac{\lambda_{\pm}^{\oplus}+1-\mathcal{M}_{\pm,ee}^{\oplus}(a_e;a_e)}{-\mathcal{M}_{ei}^{\oplus}(a_e;a_i)},$$

generating the four spatial eigenmodes $\boldsymbol{\varphi}_{\pm}^{\oplus}(x)$, where

$$\boldsymbol{\varphi}_{\pm}^{\oplus}(x)=\begin{pmatrix}\frac{1}{\lambda_{\pm}^{\oplus}+1}\left[\mathcal{M}_{\pm,ee}^{\oplus}(x;a_e)-\nu_{\pm}^{\oplus}\mathcal{M}_{ei}^{\oplus}(x;a_i)\right]\\ \frac{1}{\tau\lambda_{\pm}^{\oplus}+1}\left[\mathcal{M}_{\pm,ie}^{\oplus}(x;a_e)-\nu_{\pm}^{\oplus}\mathcal{M}_{ii}^{\oplus}(x;a_i)\right]\\ \pm\frac{1}{\lambda_{\pm}^{\oplus}+1}\left[\mathcal{M}_{\pm,ee}^{\oplus}(x;a_e)-\nu_{\pm}^{\oplus}\mathcal{M}_{ei}^{\oplus}(x;a_i)\right]\\ \pm\frac{1}{\tau\lambda_{\pm}^{\oplus}+1}\left[\mathcal{M}_{\pm,ie}^{\oplus}(x;a_e)-\nu_{\pm}^{\oplus}\mathcal{M}_{ii}^{\oplus}(x;a_i)\right]\end{pmatrix},$$

$$\begin{aligned}
\mathcal{M}_{\pm,jk}^{\oplus}(x;a_k)&=\left[\Omega_{jk}^{\oplus}(x;a_k)\pm\Omega_{jk}^{\oplus\,\rm lay}(x;a_k)\right]/|U_k'(a_k)|,\\
\mathcal{M}_{jk}^{\oplus}(x;a_k)&=\left[\Omega_{jk}^{\oplus}(x;a_k)\right]/|U_k'(a_k)|,\\
\Omega_{jk}^{\oplus\,l}(x;a_k)&=w_{jk}^{l}(x-a_k)\pm w_{jk}^{l}(x+a_k).
\end{aligned}$$

Although the eigenfunctions are complex-valued, we can see the whether the components of the eigenfunctions associated with the two neural field layers are aligned (+) and in-phase or opposite (−) and antiphase.

At a Hopf bifurcation point the Hopf frequency is

$$\omega_H = \mathrm{Im}\{\lambda_{\pm}^{\oplus}\} = \sqrt{\frac{(1-\mathcal{M}_{\pm,ee}^{\oplus})(\mathcal{M}_{ii}^{\oplus}+1)+\mathcal{M}_{\pm,ie}^{\oplus}\mathcal{M}_{ei}^{\oplus}}{\tau}},$$

where $(\mathcal{M}_{\pm,ee}^{\oplus}-1)=(\mathcal{M}_{ii}^{\oplus}+1)/\tau$ at the bifurcation point.

Condition for Hopf bifurcation of the $\mathbf{\Lambda}_{\pm}^{\oplus}$ mode

In the absence of any input ($I_e = I_i = 0$), the difference (translation) mode $\mu_{+}^{\ominus}$ has one persistent 0 eigenvalue, reflecting the translation invariance of the stationary bump, and a second real eigenvalue. Only the other three eigenmodes can undergo Hopf bifurcation. In the presence of an input inhomogeneity where $I_e(x) \neq 0$ and/or $I_i(x) \neq 0$, the eigenvalues are nonzero generically, and it is possible for all four eigenmodes to have complex eigenvalues and destabilize in a Hopf bifurcation.

Below we describe a condition for determining which mode destabilizes first, assuming all eigenvalues are complex, by identifying a dominate eigenvalue that has the larger real part of two pairs of complex eigenvalues.

Assuming that a stationary bump is stable, that all eigenvalues $\lambda_{+}^{\oplus}$ and $\lambda_{-}^{\oplus}$ are complex, and only one eigenmode destabilizes in a Hopf bifurcation, the condition determining whether the *in-phase* $\mathbf{\Lambda}_{+}^{\oplus}$ or *antiphase* $\mathbf{\Lambda}_{-}^{\oplus}$ eigenmodes destabilize is determined by the pair of eigenvalues whose real part is closer to 0 is as follows; the opposite dominance occurs with the inequality flipped.

In-phase mode $\mathbf{\Lambda}_{+}^{\oplus}$ dominates antiphase mode $\mathbf{\Lambda}_{-}^{\oplus}$ if

$$\mathcal{M}_{ee}^{\mathrm{lay}}(0) \pm \mathcal{M}_{ee}^{\mathrm{lay}}(2a_e) > 0.$$

Sum mode $\mathbf{\Lambda}_{\pm}^{\oplus}$ dominates difference mode $\mathbf{\Lambda}_{\pm}^{\ominus}$ when

$$\mathcal{M}_{ee}(2a_e) \pm \mathcal{M}_{ee}^{\mathrm{lay}}(2a_e) > \frac{\mathcal{M}_{ii}(2a_i)}{\tau}.$$

Sum mode $\mathbf{\Lambda}_{\pm}^{\oplus}$ dominates difference mode $\mathbf{\Lambda}_{\mp}^{\ominus}$ when

$$\mathcal{M}_{ee}(2a_e) \pm \mathcal{M}_{ee}^{\mathrm{lay}}(0) > \frac{\mathcal{M}_{ii}(2a_i)}{\tau}.$$

These conditions extend the single E-I neural field case and also parallel the structure of the conditions in the case of the interacting pair of symmetric AA neural fields.

For physiological reasons we assumed $w_{ee}^{\mathrm{lay}}(x) \geqslant 0$, to represent excitatory long-range synaptic connections [40,41]. Allowing $w_{ee}^{\mathrm{lay}}(x) < 0$ or including inhibitory interlayer connections would introduce additional means to destabilize different modes.

VI. MULTIBUMP SOLUTIONS

Multibump solutions exist in a variety of different forms [12,15,16,19], but we describe one example exhibiting a Hopf bifurcation in the AE/AI/AA neural field and demonstrate the extension to multibump solutions.

AE, AI, and AA neural fields

A stationary two-bump solution is a bounded solution $U^{\mathrm{multi}}(x)$ on $(-\infty,\infty)$ in which there is an even-symmetric pair of bumps centered about the origin (as depicted in Fig. 11), satisfying threshold conditions

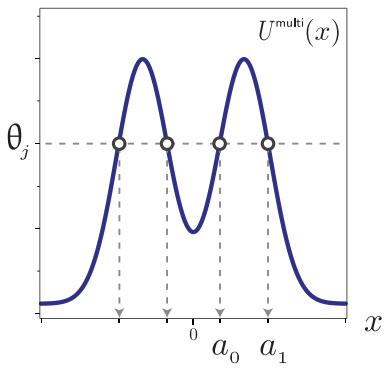

FIG. 11. Multibump solution profile $U^{\mathrm{multi}}(x)$ with threshold points $x = \pm a_0$ and $\pm a_1$ in a single neural field $u(x,t)$.

$$\begin{aligned}
&U^{\mathrm{multi}}(x) > \theta, \quad x \in (-a_1,-a_0)\cup(a_0,a_1),\\
&U^{\mathrm{multi}}(x) = \theta, \quad x = \pm a_0, \pm a_1,\\
&U^{\mathrm{multi}}(x) < \theta, \quad \text{otherwise},\\
&U^{\mathrm{multi}}(x) \to 0, \quad \text{as } x \longrightarrow \pm\infty.
\end{aligned}$$

Such a stationary two-bump solution to neural field (3) is given by $(u(x,t),n(x,t)) = (U^{\mathrm{multi}}(x), N^{\mathrm{multi}}(x))$, where

$$\begin{aligned}
(1+\beta)U^{\mathrm{multi}}(x) &= [W(x+a_1)-W(x+a_0)]\\
&\quad + [W(x-a_0)-W(x-a_1)] + I(x),\\
N^{\mathrm{multi}}(x) &= U^{\mathrm{multi}}(x),
\end{aligned}$$

where a_0 and a_1 satisfy the threshold conditions

$$\begin{aligned}
&W(a_0+a_1)-W(2a_0)-W(a_0-a_1)+I(a_0) = \theta(1+\beta),\\
&W(2a_1)-W(a_0+a_1)+W(a_1-a_0)+I(a_1) = \theta(1+\beta),
\end{aligned}$$

provided $U^{\mathrm{multi}}(x)$ properly obeys the threshold behavior.

Perturbations $(\widetilde{\varphi}(x,t), \widetilde{\psi}(x,t))$ of the stationary two-bump $(U^{\mathrm{multi}}(x), N^{\mathrm{multi}}(x))$ evolve according to

$$\begin{aligned}
\frac{\partial\widetilde{\varphi}}{\partial t} + \widetilde{\varphi} &= \mathcal{N}^{\mathrm{multi}}\widetilde{\varphi} - \beta\widetilde{\psi},\\
\frac{1}{\alpha}\frac{\partial\widetilde{\psi}}{\partial t} + \widetilde{\psi} &= \widetilde{\varphi}.
\end{aligned} \tag{55}$$

Setting $(\widetilde{\varphi},\widetilde{\psi}) = \boldsymbol{\varphi}(x)e^{\lambda t}$ yields the spectral problem for λ and $\boldsymbol{\varphi}(x) = (\varphi(x),\psi(x))^{\mathrm{T}}$,

$$\begin{aligned}
-\varphi + \mathcal{N}^{\mathrm{multi}}\varphi - \beta\psi &= \lambda\varphi,\\
\alpha\varphi - \alpha\psi &= \lambda\psi,
\end{aligned} \tag{56}$$

where, for a two-bump solution, the integral operator

$$\mathcal{N}^{\mathrm{multi}}\varphi = \sum_{l=0}^{1}[\mathcal{M}(x;-a_l)\,\varphi(-a_l) + \mathcal{M}(x;a_l)\,\varphi(a_l)]$$

and $\mathcal{M}(x;\pm a_l) = w(x \mp a_l)/|U^{\mathrm{multi}\,\prime}(\pm a_l)|$.

Solving for ψ leads to the reduced spectral problem

$$-\varphi + \mathcal{N}^{\mathrm{multi}}\varphi = \left(\lambda + \frac{\alpha\beta}{\lambda+\alpha}\right)\varphi. \tag{57}$$

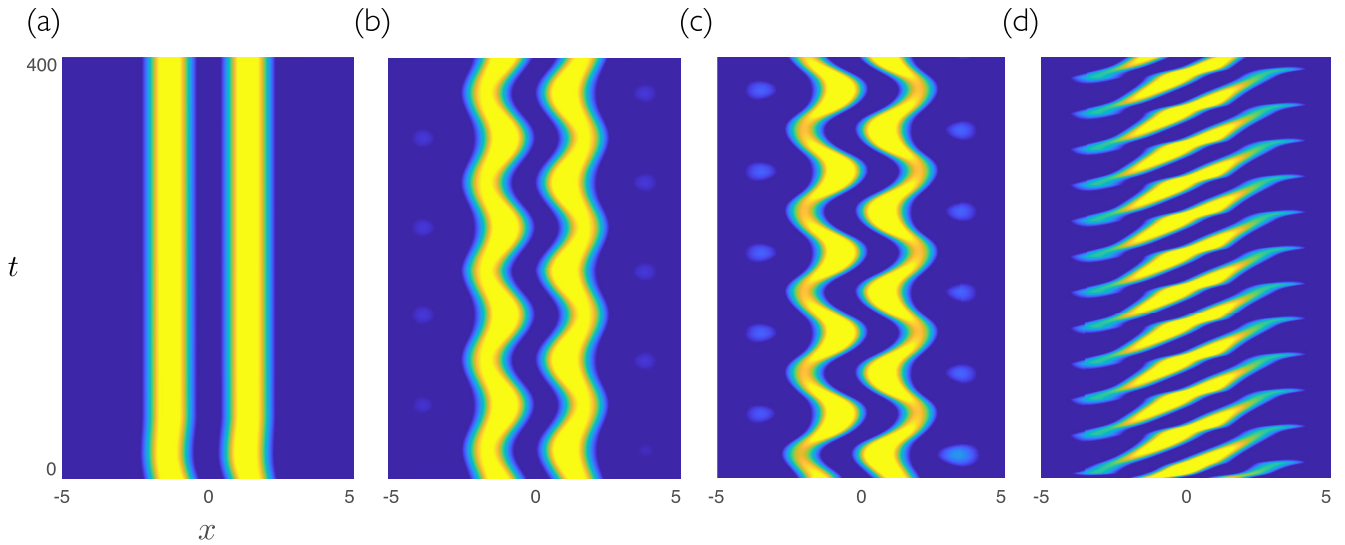

FIG. 12. Multibump solution in the AA neural field. As the negative feedback strength β is increased, a stationary two-bump solution (stable) undergoes a *subcritical* Hopf bifurcation at $\beta \approx 0.151$ with a sharp transition to a stable two-bump slosher as a result of destabilization of the in-phase difference eigenmode $\mu_+^{\ominus}$. A small region of bistability was detected near the bifurcation point. (a) At $\beta = 0.1$, a stable stationary two-bump solution, (b) at $\beta = 0.17$, a stable two-bump slosher, (c) at $\beta = 0.25$, a stable two-bump slosher, (d) at $\beta = 0.5$, a localized periodic traveling wave. Note that the bump locations move side-to-side in-phase but the bump amplitudes oscillate out of phase. Other parameters are $I_0 = 1.5$, $\sigma = 3.5$, $\theta = 0.3$, $\alpha = 0.1$, $\overline{w}_e = 1$, $\overline{w}_i = 4$, $\sigma_e = 1$, $\sigma_i = 2$, and the weight functions are Gaussian. Warm/light colors represent superthreshold values of $u(x,t)$, whereas cool/dark colors are subthreshold.

The compatibility equation for eigenvalues and special nonlocal values of the eigenfunctions at $x = \pm a_0, \pm a_1$ is

$$(\mathbf{M}_{\text{multi}} - \mathbf{I})\boldsymbol{\phi} = \left(\lambda + \frac{\alpha\beta}{\lambda+\alpha}\right)\boldsymbol{\phi}, \tag{58}$$

where $b = a_0 - a_1$ and $c = a_0 + a_1$,

$$\mathbf{M}_{\text{multi}} = \begin{bmatrix} \mathcal{M}_0(0) & \mathcal{M}_0(2a_0) & \mathcal{M}_1(b) & \mathcal{M}_1(c) \\ \mathcal{M}_0(2a_0) & \mathcal{M}_0(0) & \mathcal{M}_1(c) & \mathcal{M}_1(b) \\ \mathcal{M}_0(b) & \mathcal{M}_0(c) & \mathcal{M}_1(0) & \mathcal{M}_1(2a_1) \\ \mathcal{M}_0(c) & \mathcal{M}_0(b) & \mathcal{M}_1(2a_1) & \mathcal{M}_1(0) \end{bmatrix},$$

and

$$\mathcal{M}_k(x) = \frac{w(x)}{|U^{\text{multi}\,\prime}(a_k)|}, \quad \boldsymbol{\phi} = \begin{pmatrix} \varphi(+a_0) \\ \varphi(-a_0) \\ \varphi(+a_1) \\ \varphi(-a_1) \end{pmatrix}.$$

The following similarity transform yields

$$\mathbf{Q}^{-1}\mathbf{M}_{\text{multi}}\mathbf{Q} = \begin{bmatrix} \mathbf{\Lambda}^{\oplus} & 0 \\ 0 & \mathbf{\Lambda}^{\ominus} \end{bmatrix},$$

$$\mathbf{Q} = \begin{bmatrix} 1 & 0 & 1 & 0 \\ 1 & 0 & -1 & 0 \\ 0 & 1 & 0 & 1 \\ 0 & 1 & 0 & -1 \end{bmatrix},$$

$$\mathbf{\Lambda}^{\oplus} = \begin{bmatrix} \mathcal{M}_0^{\oplus}(a_0;a_0) & \mathcal{M}_1^{\oplus}(a_0;a_1) \\ \mathcal{M}_0^{\oplus}(a_1;a_0) & \mathcal{M}_1^{\oplus}(a_1;a_1) \end{bmatrix},$$

where $\mathcal{M}_k^{\oplus}(a_j;a_k) = \mathcal{M}_k(a_j - a_k) \pm \mathcal{M}_k(a_j + a_k)$ for $j,k = 0, 1$. Compatibility equation (58) then becomes

$$(\mathbf{M}_{\text{multi}} - \mu(\lambda)\mathbf{I})\boldsymbol{\phi} = 0, \tag{59}$$

where $\mu(\lambda) = 1 + \lambda + \frac{\alpha\beta}{\lambda+\alpha}$. For nontrivial values $\boldsymbol{\phi}$ to exist, we require $\det(\mathbf{M}_{\text{multi}} - \mu(\lambda)\mathbf{I}) = 0$. Solving for such μ and then solving for λ in terms of μ we obtain

$$\lambda_{\pm}^{\oplus} = -\Gamma \pm \sqrt{\Gamma^2 - \Delta}, \quad \Gamma = \frac{1}{2}\left(1 + \alpha - \mu_{\pm}^{\oplus}\right), \quad \Delta = \alpha\left(1 + \beta - \mu_{\pm}^{\oplus}\right),$$

$$\mu_{\pm}^{\oplus} = \left[\frac{\mathcal{M}_{00}^{\oplus} + \mathcal{M}_{11}^{\oplus}}{2}\right] \pm \sqrt{\left[\frac{\mathcal{M}_{00}^{\oplus} - \mathcal{M}_{11}^{\oplus}}{2}\right]^2 + \mathcal{M}_{01}^{\oplus}\mathcal{M}_{10}^{\oplus}},$$

where $\mathcal{M}_{jk}^{\oplus} = \mathcal{M}_k^{\oplus}(a_j;a_k)$ for $j,k = 0, 1$. This defines four pairs of eigenvalues corresponding to the four spatial eigenmodes associated with $\mu_{\pm}^{\oplus}$. We note here that the condition for $\mu_{\pm}^{\oplus}$ to be complex-valued is given by

$$\mathcal{M}_1^{\oplus}(a_0;a_1)\,\mathcal{M}_0^{\oplus}(a_1;a_0) < -\left[\frac{\mathcal{M}_0^{\oplus}(a_0;a_0) - \mathcal{M}_1^{\oplus}(a_1;a_1)}{2}\right]^2,$$

which requires $\mathcal{M}_1^{\oplus}(a_0;a_1)$ or $\mathcal{M}_0^{\oplus}(a_1;a_0)$ be negative. Solving Eq. (59) for the vector of special nonlocal values $\boldsymbol{\phi} = (\varphi_0(a_0), \varphi_0(-a_0), \varphi_1(a_1), \varphi_1(-a_1)) = (1, \pm 1, \nu_{\pm}^{\oplus}, \pm\nu_{\pm}^{\oplus})$ we obtain

$$\nu_{\pm}^{\oplus} = \frac{\mu_{\pm}^{\oplus} - \mathcal{M}_0^{\oplus}(a_0;a_0)}{\mathcal{M}_1^{\oplus}(a_0;a_1)} = \frac{\left[\frac{\mathcal{M}_{00}^{\oplus} - \mathcal{M}_{11}^{\oplus}}{2}\right] \pm \sqrt{\left[\frac{\mathcal{M}_{00}^{\oplus} - \mathcal{M}_{11}^{\oplus}}{2}\right]^2 + \mathcal{M}_{01}^{\oplus}\mathcal{M}_{10}^{\oplus}}}{\mathcal{M}_{01}^{\oplus}}.$$

The spatial eigenfunctions $\boldsymbol{\varphi}(x)$ are given by

$$\boldsymbol{\varphi}^{\oplus}(x) = \begin{pmatrix}\varphi\\ \psi\end{pmatrix} = \begin{pmatrix}1\\ \frac{\alpha}{\lambda+\alpha}\end{pmatrix}\left(\mathcal{M}_0^{\oplus}(x;a_0) + \nu_{\pm}^{\oplus}\mathcal{M}_1^{\oplus}(x;a_1)\right),$$

$$\mathcal{M}_k^{\oplus}(x;a_k) = \Omega^{\oplus}(x;a_k)/|U^{\text{multi}\,\prime}(a_k)|,$$

$$\Omega^{\oplus}(x;a_k) = w(x-a_k) \pm w(x+a_k).$$

At a Hopf bifurcation point the Hopf frequency is

$$\omega_H = \text{Im}\{\lambda_{\pm}^{\oplus}\} = \sqrt{\alpha(\beta-\alpha)}.$$

The eigenfunctions, in the case that $\nu_{\pm}^{\oplus} = \pm 1$, resemble the pattern illustrated in Fig. 9 for bumps in two different interacting layers, except in this case it would be based around the two-bump solution in a single layer. See Fig. 12 for an example of a stationary two-bump solution that undergoes a Hopf bifurcation resulting from destabilization of the $\mu_{+}^{\ominus}$ eigenmode.

VII. DISCUSSION

In this paper we have discussed a family of elementary neural fields whose activity is mediated by synaptic excitation and inhibition and modulated by a linear adaptation or a negative feedback gating variable and an input homogeneity on one-dimensional domain $(-\infty, \infty)$. (The two-dimensional case is treated separately as there are many significant differences in the model equations, structure of solutions and their bifurcation.) For each neural field model, the linear stability and Hopf bifurcation of stationary bump solutions was analyzed and presented in a notation that facilitates direct comparison of the structure and the dependency on the model parameters across this family of neural fields on one-dimensional domains. We also obtain conditions that clarify which eigenmode destabilizes in the bifurcation and how its spatial structure relates to the network parameters.

To facilitate the existence and stability analysis of stationary bumps across this family of neural fields, a general vectorized neural field model to analyze any configuration of N interacting neural fields with M linear gating variables was established to analyze the general case. Included in its analysis was the construction of the eigenfunctions associated with different eigenmodes of the linearization to investigate their spatial structure and the role it plays in bifurcations when these modes destabilize.

Using the vectorized neural field framework and making further symmetry assumptions on the synaptic weight functions, input inhomogeneities, and stationary bump solutions, we were able to show that for any neural of field of this form with even-symmetric weight functions and input inhomogeneities, the linearization about an even-symmetric stationary bump yields two broad classes of eigenfunctions that either exhibit even or odd spatial symmetry.

Hopf bifurcation of these classes of even and odd eigenmodes was investigated across the family of neural fields demonstrating that Hopf instability of these two broad classes of eigenmodes can lead to different patterns of expanding-and-contracting *breather-type* solutions and side-to-side *slosher-type* solutions, respectively, which may additionally have *in-phase* and *antiphase* structure in the oscillation depending on the relative signs of the eigenfunctions in different neural fields. Secondary bifurcations were also shown to exist leading to novel forms of activity patterns, including a secondary bifurcation from a limit cycle (slosher) to a torus leading to a slosher with a variable amplitude pattern, a period-doubling bifurcation of an expanding-contracting breather leading to a breather whose activity is modulated in a side-to-side sloshing fashion, and a period doubling cascade on a limit cycle (breather) leading to Rossler band-like nonlinear dynamics in a projection of the solution in phase space. A novel pattern of a spatially localized traveling periodic wave solution was found to emerge in the AA neural field during a transition in two cases from either a stationary slosher or multibump slosher as a parameter is varied and the superthreshold activity pattern widens.

In the case of interacting pairs of symmetrically coupled neural fields that support bumps, it was shown that both in-phase and antiphase breather-type and slosher-type solutions occur, where in-phase and antiphase are in reference to the spatiotemporal dynamics in the different layers with respect to a universal coordinate system. In the case of *in-phase* breathers and sloshers, the activity bump in the two layers are synchronous in time and identical in space. In the *antiphase* breather case the oscillations in each population are out of phase by half a period in time so one breather expands while the other contracts, sharing a common center at all times. In the *antiphase* slosher case the activity bumps in each population displace in opposite directions and oscillate side-to-side half a period out of phase in time. Depending on the number of neural fields in a model, one can imagine mixtures of in-phase and antiphase elements depending on the synaptic interactions mediating the activity in the populations.

Evidence of a *Hopf-Hopf bifurcation* with a nonlinear mode interaction was sought between the breather and slosher eigenmodes in the presence of an input homogeneity as the analog to the *drift-Hopf bifurcation* found in the input-free case [51] which produces a tongue of traveling breather solutions that issues from the codimension 2 bifurcation point between a region of traveling bumps and a region of stationary breathers connected to the drift and Hopf bifurcations, respectively. Such a mode interaction was not explicitly identified in numerical simulations of the AE/AI/AA neural field after a considerable search over a variety of regions of parameter space where the two types of Hopf bifurcation curves are known to intersect and both bifurcations are supercritical. The Hopf bifurcations in the AE/AI/AA neural field were determined to be supercritical (where stability of the stationary bump is transferred to the periodic solution) using both numerical simulations and the relevant coefficient at third order of the normal form or amplitude equation calculated in Ref. [39] which controls the direction of the bifurcation. The E-I neural field was also investigated to a lesser extent to identify such a mode interaction also without success.

Finally, the analysis was extended to the case of multibump solutions. Hopf bifurcation of the multibump solutions was investigated and shown to give rise to Hopf bifurcations leading to stable sloshing multibumps. We mention that such sloshing multibump activity patterns have been observed in spiking

networks with both periodic and without periodic boundary conditions in Ref. [71]. Hopf bifurcations of stationary multibumps also exist in the E-I neural field, though there are more threshold points to track with two neuronal populations. The multibump slosher was also found to transition to the novel pattern of a localized traveling periodic wave solution as a parameter is varied.

While this work serves to highlight a family of elementary neural fields, the main implication is to understand and categorize how network interactions and symmetry lead to the underlying spatiotemporal structure of spatially coherent time-periodic oscillations arising from Hopf bifurcation which may occur more universally in a wide range of more complex and biologically relevant neural field models, given the universality of bifurcations in nonlinear dynamical systems. It is also important to understand how modeling choices could also lead to symmetry breaking or preclude certain types of bifurcations. Although the Heaviside nonlinearity serves as an analytically tractable edge case, it could be used to predict where bifurcations occur, and one could subsequently use numerical continuation [52] to explore related regions in parameter space in models with smooth nonlinearity f where such bifurcations may be more robust. Finally the comprehensive set of existence and stability results categorized and consolidated in this paper may serve to support a wide variety of applications of bumps and breathers in these or related neural field models.

It may be possible to observe stationary and oscillatory bumps either in *in vitro* or *in vivo* experimental preparations using optogenetics and voltage sensitive dyes. Optogenetics could be used to generate the input inhomogeneity by continually stimulating neurons in a local patch of tissue and observing the activity across a layer of the cortex with populations of neurons that form approximately homogeneous and isotropic (distance-dependent) short-range synaptic connections. Different pharmacological conditions in *in vitro* slice preparations could be used to modify the properties of the network to observe the changes in the spatiotemporal behavior. Two densely interconnected areas with reciprocal and topographic connections, e.g., somatosensory cortices S1 and S2 [72], could be investigated by stimulating local patches of tissue in one or both regions and monitoring the activity in both. While it would be difficult to predict when such solutions should occur, our work suggests that one could expect at least two characteristic forms of *localized* spatiotemporal activity patterns as a steady-state response to a persistent localized input inhomogeneity in the form of a stationary activity bump of steady persistent activity or stationary activity bump exhibiting spatiotemporal oscillations in the activity. We have also found the localized oscillations can emit an outward propagating circular wave, ring waves, and target patterns in response to an input in the AE neural field [18] and in some cases with inhibition when the network supports such waves in the absence of an input, indicating other types of responses one might observe that are not localized in space. Such waves perhaps may be observed, for example, in disinhibited cortical slice preparations that support wave propagation.

[1] H. Wilson and J. D. Cowan, A mathematical theory of the functional dynamics of cortical and thalamic nervous tissue, Biol. Cybern. **13**, 55 (1973).

[2] S.-I. Amari, Dynamics of pattern formation in lateral-inhibition type neural fields, Biol. Cybern. **27**, 77 (1977).

[3] D. Pelinovsky, A. Shadrin, and V. Yakhno, Formation of pulsed sources in neuro-like media, in *Proceedings of the RNNS/IEEE Symposium on Neuroinformatics and Neurocomputers* (IEEE, New York, 1992), pp. 521–528.

[4] D. E. Pelinovsky and V. G. Yakhno, Generation of collective-activity structures in a homogeneous neuron-like medium I: Bifurcation analysis of static structures, Int. J. Bifurcation Chaos **06**, 81 (1996).

[5] D. E. Pelinovsky and V. G. Yakhno, Generation of collective-activity structures in a homogeneous neuron-like medium II: Dynamics of propagating and pulsating structures, Int. J. Bifurcation Chaos **06**, 89 (1996).

[6] D. J. Pinto, Computational, experimental, and analytic explorations of neuronal circuits in the cerebral cortex, Ph.D. thesis, University of Pittsburgh, 1997.

[7] R. Ben-Yishai, D. Hansel, and H. Sompolinsky, Traveling waves and the processing of weakly tuned inputs in a cortical network module, J. Comput. Neurosci. **4**, 57 (1997).

[8] D. Hansel and H. Sompolinsky, Modeling feature selectivity in local cortical circuits, in *Methods in Neuronal Modeling: From Ions to Networks*, edited by C. Koch and I. Segev, 2nd ed. (MIT Press, Cambridge, MA, 1998), pp. 499–567.

[9] G. B. Ermentrout, Neural networks as spatio-temporal pattern-forming systems, Rep. Prog. Phys. **61**, 353 (1998).

[10] D. J. Pinto and G. B. Ermentrout, Spatially structured activity in synaptically coupled neuronal networks: I. Traveling fronts and pulses, SIAM J. Appl. Math. **62**, 206 (2001).

[11] D. J. Pinto and G. B. Ermentrout, Spatially structured activity in synaptically coupled neuronal networks: II. Lateral inhibition and standing pulses, SIAM J. Appl. Math. **62**, 226 (2001).

[12] C. Laing, W. C. Troy, B. S. Gutkin, and G. B. Ermentrout, Multiple bumps in a neuronal model of working memory, SIAM J. Appl. Math. **63**, 62 (2002).

[13] X. Xie, R. Hahnloser, and H. Seung, Double-ring network model of the head-direction system, Phys. Rev. E **66**, 041902 (2002).

[14] P. C. Bressloff, S. E. Folias, A. Prat, and Y.-X. Li, Oscillatory waves in inhomogeneous neural media, Phys. Rev. Lett. **91**, 178101 (2003).

[15] C. Laing and W. C. Troy, PDE methods for nonlocal models, SIAM J. Appl. Dyn. Syst. **2**, 487 (2003).

[16] C. Laing and W. C. Troy, Two-bump solutions of Amari-type models of neuronal pattern formation, Physica D **178**, 190 (2003).

[17] L. Zhang, On stability of traveling wave solutions in synaptically coupled neuronal networks, Differ. Integr. Equations **16**, 513 (2003).

[18] S. E. Folias and P. C. Bressloff, Breathing pulses in an excitatory neural network, SIAM J. Appl. Dyn. Syst. **3**, 378 (2004).

[19] J. E. Rubin and W. C. Troy, Sustained spatial patterns of activity in neuronal populations without recurrent excitation, SIAM J. Appl. Math. **64**, 1609 (2004).
[20] J. Jalics, Slow waves in mutually inhibitory neuronal networks, Physica D **192**, 95 (2004).
[21] S. Coombes and M. Owen, Evans functions for integral neural field equations with heaviside firing rate function, SIAM J. Appl. Dyn. Syst. **3**, 574 (2004).
[22] A. Hutt, Effects of nonlocal feedback on traveling fronts in neural fields subject to transmission delay, Phys. Rev. E **70**, 052902 (2004).
[23] S. E. Folias and P. C. Bressloff, Stimulus-locked traveling waves and breathers in an excitatory neural network, SIAM J. Appl. Math. **65**, 2067 (2005).
[24] P. Blomquist, J. Wyller, and G. Einevoll, Localized activity patterns in two-population neuronal networks, Physica D **206**, 180 (2005).
[25] S. E. Folias and P. C. Bressloff, Breathers in two-dimensional neural media, Phys. Rev. Lett. **95**, 208107 (2005).
[26] K. A. Richardson, S. J. Schiff, and B. J. Gluckman, Control of traveling waves in the mammalian cortex, Phys. Rev. Lett. **94**, 028103 (2005).
[27] C. R. Laing and S. Coombes, The importance of different timings of excitatory and inhibitory pathways in neural field models, Network **17**, 151 (2006).
[28] C. C. Chow and S. Coombes, Existence and wandering of bumps in a spiking neural network model, SIAM J. Appl. Dyn. Syst. **5**, 552 (2006).
[29] W. C. Troy and V. Shusterman, Patterns and features of families of traveling waves in large-scale neuronal networks, SIAM J. Appl. Dyn. Syst. **6**, 263 (2007).
[30] W. C. Troy, Traveling waves and synchrony in an excitable large-scale neuronal network with asymmetric connections, SIAM J. Appl. Dyn. Syst. **7**, 1247 (2008).
[31] D. Pinto and W. C. Troy (unpublished).
[32] V. Shusterman and W. C. Troy, From baseline to epileptiform activity: A path to synchronized rhythmicity in large-scale neural networks, Phys. Rev. E **77**, 061911 (2008).
[33] G. Deco, V. K. Jirsa, P. A. Robinson, M. Breakspear, and K. Friston, The dynamic brain: From spiking neurons to neural masses and cortical fields, PLoS Comput. Biol. **4**, e1000092 (2008).
[34] Z. P. Kilpatrick, S. E. Folias, and P. C. Bressloff, Traveling pulses and wave propagation failure in inhomogeneous neural media, SIAM J. Appl. Dyn. Syst. **7**, 161 (2008).
[35] Z. P. Kilpatrick and P. C. Bressloff, Effects of synaptic depression and adaptation on spatiotemporal dynamics of an excitatory neuronal network, Physica D **239**, 547 (2010).
[36] Z. P. Kilpatrick and P. C. Bressloff, Stability of bumps in piecewise smooth neural fields with nonlinear adaptation, Physica D **239**, 1048 (2010).
[37] P. C. Bressloff, Spatiotemporal dynamics of continuum neural fields, J. Phys. A: Math. Theor. **45**, 033001 (2012).
[38] P. C. Bressloff and M. A. Webber, Neural field model of binocular rivalry waves, J. Comput. Neurosci. **32**, 233 (2012).
[39] S. E. Folias, Nonlinear analysis of breathing pulses in a synaptically coupled neural network, SIAM J. Appl. Dyn. Syst. **10**, 744 (2011).
[40] S. E. Folias and G. B. Ermentrout, New patterns of activity in a pair of interacting excitatory-inhibitory neural fields, Phys. Rev. Lett. **107**, 228103 (2011).
[41] S. E. Folias and G. B. Ermentrout, Bifurcations of stationary solutions in an interacting pair of E-I neural fields, SIAM J. Appl. Dyn. Syst. **11**, 895 (2012).
[42] G. Faye, J. Rankin, and P. Chossat, Localized states in an unbounded neural field equation with smooth firing rate function: A multi-parameter analysis, J. Math. Biol. **66**, 1303 (2013).
[43] H. G. E. Meijer and S. Coombes, Travelling waves in a neural field model with refractoriness, J. Math. Biol. **68**, 1249 (2014).
[44] G. Faye, Existence and stability of traveling pulses in a neural field equation with synaptic depression, SIAM J. Appl. Dyn. Syst. **12**, 2032 (2013).
[45] G. Faye and J. Touboul, Pulsatile localized dynamics in delayed neural field equations in arbitrary dimension, SIAM J. Appl. Math. **74**, 1657 (2014).
[46] G. B. Ermentrout, S. E. Folias, and Z. P. Kilpatrick, Spatiotemporal pattern formation in neural fields with linear adaptation, in *Neural Fields*, edited by S. Coombes, P. Beim Graben, R. Potthast, and J. Wright (Springer, Heidelberg, 2014), pp. 119–151.
[47] H. Meijer and S. Coombes, Travelling waves in models of neural tissue: From localised structures to periodic waves, EPJ Nonlin. Biomed. Phys. **2**, 3 (2014).
[48] P. C. Bressloff, *Waves in Neural Media*, Lecture Notes on Mathematical Modeling in the Life Sciences (Springer Verlag, New York, NY, 2014).
[49] Z. P. Kilpatrick, Coupling layers regularizes wave propagation in stochastic neural fields, Phys. Rev. E **89**, 022706 (2014).
[50] C. R. Laing, Waves in spatially-disordered neural fields: A case study in uncertainty quantification, in *Uncertainty in Biology a Computational Modeling Approach*, edited by L. Geris and D. Gomez-Cabrero (Springer International Publishing, Heidelberg, 2016), pp. 367–391.
[51] S. E. Folias, Traveling waves and breathers in an excitatory-inhibitory neural field, Phys. Rev. E **95**, 032210 (2017).
[52] W. G. van Harten, Numerical continuation schemes for 1D patterns in neural fields, Master's thesis, University of Twente, 2021.
[53] J.-Y. Wu, L. Guan, and Y. Tsau, Propagating activation during oscillations and evoked responses in neocortical slices, J. Neurosci. **19**, 5005 (1999).
[54] J.-Y. Wu, X. Huang, and C. Zhang, Propagating waves of activity in the neocortex: What they are, what they do, Neuroscientist **14**, 487 (2008).
[55] Y. Xiao, X.-Y. Huang, S. Van Wert, E. Barreto, J.-Y. Wu, B. J. Gluckman, and S. J. Schiff, The role of inhibition in oscillatory wave dynamics in the cortex, Eur. J. Neurosci. **36**, 2201 (2012).
[56] W. Xu, X. Huang, K. Takagaki, and J.-Y. Wu, Compression and reflection of visually evoked cortical waves, Neuron **55**, 119 (2007).
[57] Z. Yang, D. J. Heeger, R. Blake, and E. Seidemann, Long-range traveling waves of activity triggered by local dichoptic stimulation in V1 of behaving monkeys, J. Neurophysiol. **113**, 277 (2015).
[58] J. W. Yang, S. An, J. J. Sun, and V. Reyes-Puerta, Thalamic network oscillations synchronize ontogenetic columns

in the newborn rat barrel cortex, Cereb. Cortex **23**, 1299 (2013).

[59] K. Takagaki, C. Zhang, J.-Y. Wu, and M. T. Lippert, Cross-modal propagation of sensory-evoked and spontaneous activity in the rat neocortex, Neurosci. Lett. **431**, 191 (2008).

[60] T. P. Zanos, P. J. Mineault, K. T. Nasiotis, and D. Guitton, A sensorimotor role for traveling waves in primate visual cortex, Neuron **85**, 615 (2015).

[61] H. Zhang and J. Jacobs, Traveling theta waves in the human hippocampus, J. Neurosci. **35**, 12477 (2015).

[62] T. Berger, A. Borgdorff, S. Crochet, F. B. Neubauer, S. Lefort, B. Fauvet, I. Ferezou, A. Carleton, H. R. Lüscher, and C. C. H. Petersen, Combined voltage and Calcium epifluorescence imaging *in vitro* and *in vivo* reveals subthreshold and suprathreshold dynamics of mouse barrel cortex, J. Neurophysiol. **97**, 3751 (2007).

[63] Y. Chagnac-Amitai and B. W. Connors, Horizontal spread of synchronized activity in neocortex and its control by gaba-mediated inhibition, J. Neurophysiol. **61**, 747 (1989).

[64] R. B. Langdon and M. Sur, Components of field potentials evoked by white matter stimulation in isolated slices of primary visual cortex: Spatial distributions and synaptic order, J. Neurophysiol. **64**, 1484 (1990).

[65] I. Nauhaus, L. Busse, D. L. Ringach, and M. Carandini, Robustness of traveling waves in ongoing activity of visual cortex, J. Neurosci. **32**, 3088 (2012).

[66] D. J. Pinto, S. Patrick, W. Huang, and B. Connors, Initiation, propagation, and termination of epileptiform activity in rodent neocortex *in vitro* involve distinct mechanisms, J. Neurosci. **25**, 8131 (2005).

[67] L. Muller and A. Destexhe, Propagating waves in thalamus, cortex and the thalamocortical system: Experiments and models, J. Phys. Paris **106**, 222 (2012).

[68] T. Sato, I. Nauhaus, and M. Carandini, Traveling waves in visual cortex, Neuron **75**, 218 (2012).

[69] A. Benucci, R. A. Frazor, and M. Carandini, Standing waves and traveling waves distinguish two circuits in visual cortex, Neuron **55**, 103 (2007).

[70] T. Kato, *Perturbation Theory for Linear Operators*, Classics in Mathematics (Springer Verlag, New York, NY, 1966).

[71] R. Rosenbaum and B. Doiron, Balanced networks of spiking neurons with spatially dependent recurrent connections, Phys. Rev. X **4**, 021039 (2014).

[72] G. Minamisawa, S. E. Kwon, M. Chevée, S. P. Brown, and D. H. O'Connor, A non-canonical feedback circuit for rapid interactions between somatosensory cortices, Cell Rep. **23**, 2718 (2018).